

**UNIVERSIDADE FEDERAL DE SÃO CARLOS
CENTRO DE CIÊNCIAS EXATAS E DE TECNOLOGIA
PROGRAMA DE PÓS-GRADUAÇÃO EM CIÊNCIA E
ENGENHARIA DE MATERIAIS**

**REFILL FRICTION STIR SPOT WELDING:
EVALUATION OF THE WELDING OF AA2198-T8 SHEETS AND
PRELIMINARY TOOL WEAR INVESTIGATION**

Camila Caroline de Castro

São Carlos – SP
2019

**UNIVERSIDADE FEDERAL DE SÃO CARLOS
CENTRO DE CIÊNCIAS EXATAS E DE TECNOLOGIA
PROGRAMA DE PÓS-GRADUAÇÃO EM CIÊNCIA E
ENGENHARIA DE MATERIAIS**

**REFILL FRICTION STIR SPOT WELDING:
EVALUATION OF THE WELDING OF AA2198-T8 SHEETS AND
PRELIMINARY TOOL WEAR INVESTIGATION**

Camila Caroline de Castro

Dissertation presented to
Programa de Pós-Graduação em Ciência e
Engenharia de Materiais to obtain the
MASTER OF SCIENCE DEGREE IN
MATERIALS SCIENCE AND ENGINEERING

Supervisor: Dr. Nelson Guedes de Alcântara

Co-supervisor: Dr. Athos Henrique Plaine

Grant Agency: CNPq (Process no. 134520/2017-3)

São Carlos – SP

2019

To Koda and my beloved family.

RESUME

Bachelor degree in Materials Engineering (2013) from UFSCar



UNIVERSIDADE FEDERAL DE SÃO CARLOS

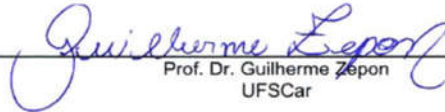
Centro de Ciências Exatas e de Tecnologia
Programa de Pós-Graduação em Ciência e Engenharia de Materiais

Folha de Aprovação

Assinaturas dos membros da comissão examinadora que avaliou e aprovou a Defesa de Dissertação de Mestrado da candidata Camila Caroline de Castro, realizada em 26/04/2019:



Prof. Dr. Nelson Guedes de Alcântara
UFSCar



Prof. Dr. Guilherme Zépon
UFSCar



Prof. Dr. Celso Roberto Ribeiro
LEMM

AGRADECIMENTOS

Meus primeiros e mais sinceros agradecimentos à minha família. Aos meus pais Sueli e José Luiz, que sempre acreditaram incondicionalmente em mim, por todos os sacrifícios feitos para que eu chegasse até aqui. Agradeço aos meus irmãos, José Pedro, Luiz Gustavo e Nathalia (sim, você entra aqui), por todo o apoio e por estarem sempre tão perto mesmo tão longe.

Ao Koda, por sua presença(zinha) em cada segundo da minha vida e por ser minha maior inspiração.

Gostaria de agradecer ao Prof. Nelson Guedes de Alcântara, pela orientação e apoio durante esta jornada, e especialmente por me incentivar tanto a ir cada vez mais longe.

Agradeço ao meu co-orientador e amigo Dr. Athos Henrique Plaine pelas contribuições valiosas no desenvolvimento deste trabalho. Começamos nossas jornadas como colegas de estágio no HZG, e foi um grande prazer contar com o seu apoio durante o mestrado e vê-lo chegar tão longe.

Gostaria de agradecer ao Helmholtz Zentrum Geesthacht pela oportunidade de desenvolver este trabalho, em especial ao Dr. Jorge Fernandez dos Santos.

A todos os meus queridos amigos, aqueles que perto ou distantes tornaram essa jornada mais fácil.

Um agradecimento especial ao André Neves não apenas pelo companheirismo, carinho, serenidade e incentivo, mas também por todas as contribuições científicas para este trabalho. Ouso dizer que eu quase não teria conseguido sem você.

Ao DEMa e PPGCEM por todo suporte dado, em especial aos secretários sempre tão prestativos.

Gostaria também de agradecer ao CNPq (processo no. 134520/2017-3) pela bolsa de estudos concedida

O presente trabalho foi realizado com apoio da Coordenação de Aperfeiçoamento de Pessoal de Nível Superior - Brasil (CAPES) - Código de Financiamento 001.

ABSTRACT

Refill Friction Stir Spot Welding (RFSSW) is an innovative method for joining similar and dissimilar lightweight metallic materials or thermoplastics. This technique has the advantage of issuing energy savings, producing welds with suitable mechanical properties and having the possibility of industrial scalability with the use of robots and automation. The use of aluminum alloys is widespread in aircraft industry. However, some of these alloys present poor weldability with conventional methods, an issue which can be overcome with the use of friction-based processes such as RFSSW. Furthermore, the substitution of riveting (today used as joining method for these alloys) can cause a reduction of aircraft weight, saving energy and potentially reducing costs. This work presents the evaluation of overlapped joints performed on AA2198-T8 1.6 and 3.2 mm-thick sheets produced by RFSSW. The optimization and correlation between process parameters and weld performance was studied by employing design of experiment (Taguchi) and analysis of variance (ANOVA) by measuring the welds' response to the variation of welding time, plunge depth and rotational speed in order to verify the technical feasibility of the process. Moreover, the stir zone area was quantified and a positive correlation of this area was found with lap shear strength (*LSS*) performance. Finally, a preliminary study of the tool wear effects on the welds' properties and microstructure was performed. Although results show a trend in reduction of lap shear strength along the 2350 studied joints, all the tested welds presented good mechanical properties, which greatly exceed the minimum standardized requirements for aircraft industry. However, more studies need to be carried out in order to determine the wear effects on the tool which affect the welds' properties and tool lifecycle and might influence the economic and technical feasibility of using this technique in large scale industrial setups.

Key words: Refill Friction Stir Spot Welding; AA2198; Taguchi method; Tool wear

RESUMO

SOLDAGEM POR FRICÇÃO A PONTO COM PREENCHIMENTO: AVALIAÇÃO DA SOLDAGEM DE CHAPAS DE ALUMÍNIO AA2198-T8 E INVESTIGAÇÃO PRELIMINAR DO DESGASTE DA FERRAMENTA

Soldagem por fricção a ponto com preenchimento (RFSSW) é uma técnica inovadora para soldagem de materiais similares e dissimilares aplicada em ligas leves e termoplásticos. Suas principais vantagens estão relacionadas à economia de energia, produção de soldas com propriedades mecânicas adequadas, facilidade de automatização do processo, redução do peso e adequação para soldagem de ligas de alumínio. Este trabalho apresenta a avaliação de juntas sobrepostas por RFSSW de chapas de AA2198-T8 nas espessuras de 1.6 e 3.2 mm. A otimização e correlação entre os parâmetros de processo e o desempenho das soldas foi estudada por meio da metodologia Taguchi e análise de variância (ANOVA) considerando-se a resposta das propriedades das juntas às variações de velocidade de rotação da ferramenta, tempo de soldagem e profundidade de penetração a fim de se verificar a viabilidade técnica do processo. Também foi avaliada a variação área da zona de mistura com o desempenho mecânico das juntas, identificando-se uma correlação positiva entre essas variáveis. Por fim, um estudo preliminar dos efeitos do desgaste da ferramenta foi realizado considerando-se as alterações nas propriedades e microestrutura das juntas. Embora os resultados indiquem uma tendência à redução da resistência ao cisalhamento ao longo das 2350 soldas produzidas, os ensaios realizados durante o estudo revelaram soldas com desempenho mecânico satisfatório, excedendo os requisitos mínimos normatizados para a união de estruturas aeronáuticas. A avaliação preliminar sobre o desgaste da ferramenta de RFSSW indica a necessidade de estudos complementares para a determinação dos efeitos sobre a ferramenta que afetam sua vida útil e as propriedades das juntas, além de fatores que influenciam a viabilidade técnica e econômica da tecnologia em larga escala.

Palavras-chave: Soldagem por fricção a ponto com preenchimento; AA2198; metodologia Taguchi; Desgaste da ferramenta

PUBLICATIONS

PEER-REVIEWED PAPERS

de Castro, C. C., Plaine, A. H., de Alcântara, N. G., & dos Santos, J. F. (2018). "Taguchi approach for the optimization of refill friction stir spot welding parameters for AA2198-T8 aluminum alloy". *The International Journal of Advanced Manufacturing Technology*, 99(5-8), 1927-1936. DOI: 10.1007/s00170-018-2609-2

de Castro, C. C., Plaine, A. H., Dias, G. P., de Alcântara, N. G., & dos Santos, J. F. (2018). "Investigation of geometrical features on mechanical properties of AA2198 refill friction stir spot welds". *Journal of Manufacturing Processes*, 36, 330-339. DOI: 10.1016/j.jmapro.2018.10.027

de Castro, C. C., Plaine, A. H., de Alcântara, N. G., & dos Santos, J. F. (2018). "Estudo dos Parâmetros do Processo de Soldagem a Ponto por Fricção de Chapa Fina da Liga de Alumínio AA2198-T8". *Soldagem & Inspeção*. DOI: 10.1590/0104-9224/SI2303.08

ABSTRACTS PUBLISHED IN CONFERENCE PROCEEDINGS

de Castro, C. C., Plaine, A. H., de Alcântara, N. G., & dos Santos, J. F.. "Otimização do processo de soldagem a ponto por fricção da liga de alumínio AA2198-T8". 23th Congresso Brasileiro de Engenharia e Ciência dos Materiais. Brazil. 2018.

LIST OF CONTENTS

APPROVAL SHEET	i
AGRADECIMENTOS	iii
ABSTRACT	v
RESUMO	vii
PUBLICATIONS	ix
LIST OF CONTENTS	xi
LIST OF TABLES	xiii
LIST OF FIGURES	xv
SYMBOLS AND ABBREVIATIONS	xix
1 INTRODUCTION AND RATIONALE	1
2 OBJECTIVES	5
3 LITERATURE REVIEW	7
3.1 Aluminum alloys	7
3.1.1 Aluminum alloys for aerospace applications	7
3.1.2 Al-Cu-Li alloys	8
3.1.3 Weldability of Al-Cu-Li aluminum alloys	9
3.2 Refill Friction Stir Spot Welding	10
3.2.1 Overview	10
3.2.2 3-piece tool and variants of RFSSW process	12
3.2.3 Microstructural features of RFSSW joints	14
3.2.4 Tool wear	15
4 MATERIALS AND METHODS	17
4.1 Flowchart	17
4.1.1 Effects of welding parameters on welds' features	17
4.1.2 Tool wear evaluation	17
4.2 Design of Experiments	18
4.2.1 Definition of the processing window	18
4.2.2 Taguchi Approach	19
4.2.3 Analysis of variance (ANOVA)	19
4.3 Production of specimens	20
4.4 Mechanical testing	22
4.5 Micro and macrostructural analysis	24

4.6	Tool wear evaluation.....	25
4.6.1	Tool material.....	25
4.6.2	Characterization of pin and sleeve's profile	25
4.6.3	Tool cleaning procedure	26
4.6.4	Weight measurement of pin and sleeve	27
5	RESULTS AND DISCUSSION	29
5.1	Microstructural development of RFSSW joints	29
5.2	RFSSW: Optimization of AA2198-T8 1.6 mm-thick sheets.....	33
5.2.1	Selection of parameters.....	33
5.2.2	Taguchi analysis.....	34
5.2.3	Analysis of variance – ANOVA.....	39
5.3	Effect of stir zone size in welds' resistance.....	41
5.3.1	Correlation between LSS and SZA for 1.6 and 3.2 mm-thick sheets.....	41
5.3.2	Statistical analysis of process parameters' influence on stir zone area	44
5.3.3	Effects of <i>RS</i> and <i>PD</i> on stir zone development.....	48
5.4	Tool wear investigation	52
5.4.1	Lap shear strength along the welding cycles.....	52
5.4.2	Wear effects on tool dimension	58
5.4.2.1	Pin wear	58
5.4.2.2	Sleeve wear.....	60
5.4.3	Effects of tool wear in welds' microstructural features	69
6	CONCLUSIONS	73
7	SUGGESTIONS FOR FUTURE WORK	77
8	REFERENCES	79
	APPENDIX A.....	85
	APPENDIX B.....	87
	APPENDIX C.....	91
	APPENDIX D.....	93
	APPENDIX E.....	95

LIST OF TABLES

Table 4.1 – Chemical composition of AA2198 in %wt. Adapted from Rioja et al. [5].....	21
Table 4.2 – RFSSW parameters and their levels	22
Table 4.3 – Chemical requirements (%wt) for H13 tool steel according to ASTM A681 [43]	25
Table 5.1 – Experimental conditions for the Taguchi analysis (rotational speed, welding time and plunge depth), mean of experimental results for lap shear strength test (LSS) and calculated signal-to-noise ratio (SNR) for each welding condition	35
Table 5.2 – Response table for means and signal-to-noise ratio (SNR) for rotational speed (<i>RS</i>), welding time (<i>WT</i>) and plunge depth (<i>PD</i>) based on LSS response	36
Table 5.3 – Optimum welding condition predicted by Taguchi method (<i>C10</i>) and mean of experimental results for lap shear strength test (LSS)	38
Table 5.4 – Analysis of variance (ANOVA) and individual influence of parameters – rotational speed (<i>RS</i>), welding time (<i>WT</i>) and plunge depth (<i>PD</i>) – in LSS in terms of means and SNR.....	40
Table 5.5 – Experimental conditions (rotational speed, welding time and plunge depth), mean of experimental results for lap shear strength test (LSS) and stir zone area (SZA) for each welding condition	42
Table 5.6 – Response table of means for rotational speed (<i>RS</i>), welding time (<i>WT</i>) and plunge depth (<i>PD</i>) based on SZA response for 1.6 mm and 3.2 sheets	44
Table 5.7 – Pin weight measurement at the different points of evaluation and their weight reduction relatively to the as-received pin condition (in mass and percentage).....	60
Table 5.8 – Sleeve weight measurement at the different points of evaluation, weight reduction relatively to the as-received pin condition (in mass and percentage), and average rate of weight loss in each stage.....	63
Table 5.9 – Mean of experimental results for lap shear strength test (<i>LSS</i>) and stir zone area (<i>SZA</i>) for selected points of measurement along welding cycles.....	70

LIST OF FIGURES

Figure 1.1 – Greenhouse emissions contribution by sector. Adapted from Strocker [1].	1
Figure 1.2 – CO ₂ emissions contribution by sector. Adapted from OICA [2].	2
Figure 3.1 – Cross-section of AA7075 friction-based welds: (a) FSSW (b) RFSSW [32].	11
Figure 3.2 – (a) RFSSW tool assembly of the 3-piece tool (b) parts of the tool: pin, sleeve and clamping ring	12
Figure 3.3 – Variants of RFSSW: (a) pin plunge and (b) sleeve plunge	13
Figure 3.4 – Cross-section of a representative weld produced by RFSSW indicating the stir zone (SZ), thermo-mechanically affected zone (TMAZ), heat affected zone (HAZ) and base material (BM).	14
Figure 4.1 – Flowchart of the experimental activities performed for the study of the welding parameters effects and optimization for 1.6 and 3.2 mm-thick sheets	17
Figure 4.2 – Flowchart of the experimental activities performed for the tool wear evaluation	18
Figure 4.3 – Schematic representation of friction lap shear specimens. Dimensions in mm. Adapted from ISO 14273 [41].	21
Figure 4.4 – Refill Friction Stir Spot welding RPS 100 (Hams & Wende) machine, developed by HZG and RIFTEC GmbH	22
Figure 4.5 – (a) Zwick/Roell machine adapted for lap shear testing and (b) lap shear specimen configuration	23
Figure 4.6 – Tool measurement: (a) Mahr Multiscope 250 used on the experiment and (b) sleeve and pin measured plane indicated by red arrows	26
Figure 5.1 – Representative macrograph of overlapped AA2198-T8 sheets welded by RFSSW indicating different microstructures: stir zone (SZ), thermo-mechanically affected zone (TMAZ) and heat affected zone (HAZ). Red markings indicate important microstructural features: A (shown in higher magnification on Figure 5.2) shows the SZ-TMAZ interface region, while B indicates the hook region between the sheets and C shows bonding ligament caused by the welding process.	29
Figure 5.2 – Region marked as A in Figure 5.1 in higher magnification indicating the transition between SZ and TMAZ and sleeve penetration path	30

Figure 5.3 – Higher magnification of the region marked as (b) in Figure 5.2 indicating recrystallized grains in TMAZ (dashed white line) and elongated grains with sub-boundaries (red contour) found in TMAZ	31
Figure 5.4 – Region marked as (c) in Figure 5.1 in higher magnification indicating recrystallized grains in SZ	32
Figure 5.5 – Selection of upper and lower parameters for the basis of Taguchi analysis: plots of lap shear strength values along different levels of rotational speed (<i>RS</i>), welding time (<i>WT</i>) and plunge depth (<i>PD</i>).....	33
Figure 5.6 – Main effect plots of means and signal-to-noise ratio (<i>SNR</i>) for rotational speed (<i>RS</i>), welding time (<i>WT</i>) and plunge depth (<i>PD</i>) based on <i>LSS</i> response.....	37
Figure 5.7 – Means of experimental results for lap shear strength test (<i>LSS</i>) for L9 orthogonal array welding conditions (<i>C1a</i> to <i>C9a</i>) and Taguchi predicted optimum condition (<i>C10a</i>)	39
Figure 5.8 – Influence of individual parameters – rotational speed (<i>RS</i>), welding time (<i>WT</i>) and plunge depth (<i>PD</i>) – on the variance of <i>LSS</i> in terms of means (in teal) and <i>SNR</i> (in orange) given by ANOVA.....	40
Figure 5.9 – Plots of stir zone area (<i>SZA</i>) and lap shear strength mean (<i>LSS</i>) values for Taguchi array welding conditions	43
Figure 5.10 – Main effect plots of means for rotational speed (<i>RS</i>), welding time (<i>WT</i>) and plunge depth (<i>PD</i>) based on <i>SZA</i> and <i>LSS</i> for the thickness of 1.6 mm	45
Figure 5.11 – Main effect plots of means for rotational speed (<i>RS</i>), welding time (<i>WT</i>) and plunge depth (<i>PD</i>) based on <i>SZA</i> and <i>LSS</i> for the thickness of 3.2 mm	46
Figure 5.12 – Influence of individual parameters – rotational speed (<i>RS</i>), welding time (<i>WT</i>) and plunge depth (<i>PD</i>) – on the variance of <i>SZA</i> given by ANOVA for different sheet thicknesses: 1.6 mm (in teal) and 3.2 mm (in orange).....	48
Figure 5.13 – Macrograph of a typical cross-section of a 3.2 mm-thick sheets joint with indication of geometrical variables of SZ. In green, portion of SZ determined by <i>PD</i> and sleeve diameter (D_{sleeve}). In red, SZ's region associated with metallurgical phenomena and ruled by rotational speed <i>RS</i> , <i>WT</i> and <i>PD</i>	49
Figure 5.14 – Influence of individual parameters – rotational speed (<i>RS</i>), welding time (<i>WT</i>) and plunge depth (<i>PD</i>) – on the variance of <i>h</i> (in teal) and <i>w</i> (in orange) given by ANOVA	50

Figure 5.15 – Joints' strength behavior along welding cycles: <i>LSS</i> mean values measured between intervals along the welds, showing three different stages of the investigation and points of tool profile measurement (black-crossed points)	53
Figure 5.16 – <i>LSS</i> mean values with associate standard deviation and linear fit along the first stage of evaluation	54
Figure 5.17 – <i>LSS</i> mean values with associate standard deviation for first and second stages of evaluation	56
Figure 5.18 – Standard deviation of each <i>LSS</i> mean value	56
Figure 5.19 – <i>LSS</i> mean values with associate standard deviation highlighting the third stage of evaluation.....	57
Figure 5.20 – Visual aspect of the pin along welding cycles: (a) as-received pin condition (b) after 1350, (c) 2000 and (d) 2350 welds performed.	58
Figure 5.21 – Pin's profile along welding cycles: (a) as-received pin condition (b) after 1350, (c) 2000 and (d) 2350 welds performed.	59
Figure 5.22 – Visual aspect of the sleeve along welding cycles: (a) as-received pin condition (b) after 1350, (c) 2000 and (d) 2350 welds performed.	61
Figure 5.23 – Sleeve's profile along welding cycles: (a) as-received pin condition (b) after 1350, (c) 2000 and (d) 2350 welds performed.	61
Figure 5.24 – Effects of wear on the sleeve: (a) sleeve profile and (b) visual aspect of the sleeve after 1350 welding cycles.....	63
Figure 5.25 – (a) Visual aspect of sleeve after the first stage of evaluation showing the presence of aluminum adhered to H13 surface and trapped between the threads. (b) Detailed view of the sleeve's aluminum-covered region end (left) and start of the aluminum-free region (right).....	64
Figure 5.26 – Effects of wear on the sleeve: (a) sleeve profile and (b) visual aspect of the sleeve after 2000 welding cycles.....	65
Figure 5.27 – Schematic representation of clamping ring indicating the region in frictional contact with sleeve matching the plastic deformed region of sleeve after 2000 performed welds.....	66
Figure 5.28 – Presence of flash in a typical weld indicating the increasing of a slack between clamping ring's inner surface and sleeve's outer surface.	67
Figure 5.29 – Trapped aluminum on the clamping ring inner surface	67
Figure 5.30 – Effects of wear on the sleeve: (a) sleeve profile and (b) visual aspect of the sleeve after 1350 welding cycles.....	68

Figure 5.31 – Plots of lap shear strength (*LSS*) and stir zone area (*SZA*) means of experimental results for selected points of measurement along welding cycles 70

Figure 5.32 – Microhardness maps ($HV_{0.2}$) of selected welds: (a) initial welding, after (b) 80, (c) 220, (d) 600, (e) 1000, and (f) 1300 welding cycles..... 72

SYMBOLS AND ABBREVIATIONS

%I	Percentage of influence
AA	Aluminum alloy
ANOVA	Analysis of variance
AWS	American Welding Society
BM	Base material
CCDM	Center for Characterization and Development of Materials
DEMa	Department of Materials Engineering
DOE	Design of experiments
D_{sleeve}	Sleeve external diameter
FSpW	Friction Spot Welding
FSSW	Friction Stir Spot Welding
FSW	Friction Stir Welding
h	Height dimension of stir zone
H	Hook height
HAZ	Heat affected zone
HZG	Helmholtz-Zentrum Geesthacht
IADS	International Alloy Designation System
IPCC	Intergovernmental Panel on Climate Change
LSS	Lap shear strength
LSW	Laser Spot Welding
MS	ANOVA's mean square
OICA	International Organization of Motor Vehicle Manufacturers
OM	Optical Microscopy
PD	Plunge depth
PP	Pin plunge
Q_{app}	Heat input
RFSSW	Refill Friction Stir Spot Welding
ReX	Dynamic recrystallization
RS	Rotational Speed
RSW	Resistance Spot Welding

SNR	Signal-to-noise ratio
SP	Sleeve plunge
SS	ANOVA's sum of squares
SZ	Stir zone
SZA	Stir zone area
T	Torque
TMAZ	Thermo-Mechanically Affected Zone
WT	Welding time
wt.	Weight percentage
Δ	Difference between maximum and minimum response given by Taguchi method
Δh	Increment of SZ area associated with height dimension due to metallurgical phenomena
Δw	Increment of SZ area associated with width dimension due to metallurgical phenomena

1 INTRODUCTION AND RATIONALE

Human influence on the climate system is patent and growing. Studies show the 2 °C-increase in overall mean temperature since the Industrial Revolution period indicates the urgency of actions in order to mitigate greenhouse gas emissions as CO₂, CH₄, N₂O, CF₄ among others [1]. Against this background, the reduction of the environmental impact of technology on Earth is a growing-in-importance issue. A report of the Intergovernmental Panel on Climate Change (IPCC) presented in 2014 indicates that the Transport sector is responsible for 14% of the total greenhouse gas emissions (Figure 1.1), while studies from the International Organization of Motor Vehicle Manufacturers (OICA) assigns to vehicles 22% of the CO₂ emissions, 16% of which refers to Road Transports whereas 6% is associated to Non-Road transports (Figure 1.2) [2]. Materials selection can be an effective way to reduce CO₂ emissions of the transport sector, since the use of lightweight materials such as aluminum and its alloys for structural purposes reduces the total weight of the vehicle, which leads to a decrease in fuel consumption. The use of welding processes for spot joints instead of mechanical fastening techniques is also a source of saving structural weight, since they do not require any material additions such as rivets. Besides, solid state friction-based welding procedures are considered “green technologies” and energy efficient, since they consume considerable less energy when compared to conventional fusion welding [3].

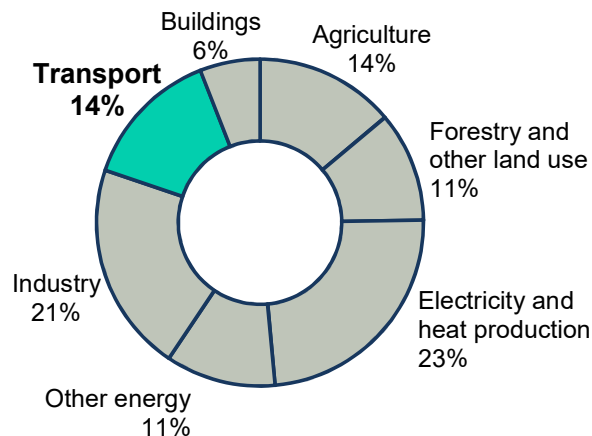


Figure 1.1 – Greenhouse emissions contribution by sector. Adapted from Strocker [1].

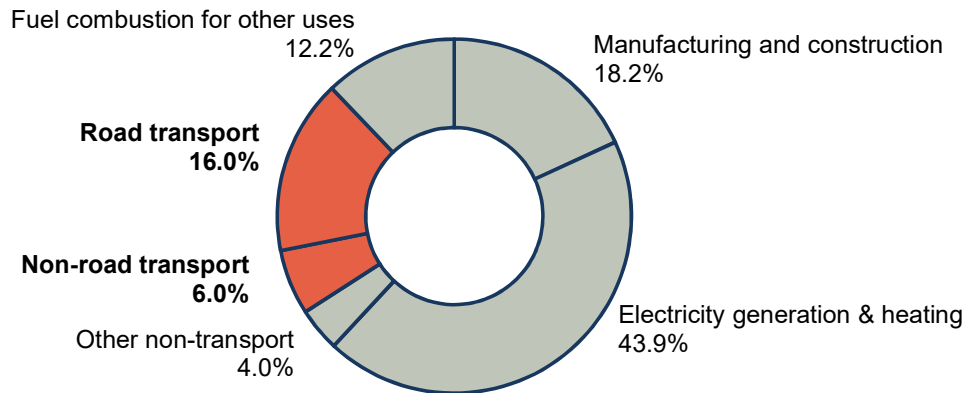


Figure 1.2 – CO2 emissions contribution by sector. Adapted from OICA [2].

Aluminum-based alloys development has been increasing over the time as the aircraft industry evolves. Lightweight aluminum alloys are widely used for the reduction of structure weight and fuel consumption because of their specific properties, such as strength and low density [4, 5]. The Al-Li class of alloys presents significant improvement in required properties for structural performance: reduction in density, stiffness increase, increasing in corrosion resistance and also increasing in fracture toughness and fatigue growth resistance [5]. Small additions of Li on aluminum alloys produce considerable modifications on the materials' properties because of its very low density (0.534 g/cm^3). AA2198 is a 3rd generation Al-Cu-Li alloy developed by Reynolds/MacCook in 2005 aiming aircraft applications. In this alloy, additions of 1% in weight of Li provide a decrease of 3% in density. Furthermore, Li additions to aluminum alloys enables the modification of mechanical properties, such as Young's modulus (1% of Li provides 6% increase in Young's modulus), increasing fatigue crack growth resistance and increasing hardness through the formation of hardening precipitates [5].

Mechanical fastening is widely employed for the assembly of lightweight aircraft and automotive structures. However, the use of rivets for spot-joining represents an increment in weight of the structure, which may implicate on environmental and economical issues since lighter structures may lead to cost saving: as an example, the cost saving over the lifetime for the reduced fuel

consumption is around 17.4 €/kg¹ for a typical car [6, 7]. Refill friction stir spot welding (RFSSW) – also known as Friction Spot Welding (FSpW) – offers opportunities for the replacement of mechanical fastening in aircraft and automotive lightweight structures since no material is added for the joint. Besides, RFSSW is an interesting alternative for the joining of aluminum parts in aeronautic and automotive industries since it is a solid-state technique and avoids defects associated with conventional fusion-based welding processes, such as Resistance Spot Welding (*RSW*) and Laser Spot Welding (*LSW*).

Although RFSSW appears as an interesting alternative for replacing mechanical fastening and fusion-based processes for assemblies in automotive and aircraft industries, there are still some challenges to overcome aiming large scale application. One of them is related to tool wear, which may affect the quality of the joints, once the lap shear strength of the welds decreases along the welding cycles as showed by Montag et al. [8] while the variability increases, as detected in works performed at Helmholtz-Zentrum Geesthacht (HZG) [9]. The determination of tool lifecycle regarding specific requirements for the welds such those listed on AWS D17.2 [10], is another factor to be considered for the correct pricing and analysis of the economical feasibility of the technique.

The refill friction stir spot welding of aluminum alloys in-depth studies becomes necessary in order to ensure the reliability and reproducibility of the process and enable industrial applications. In this work, the influence of process parameters (rotational speed, welding time and plunge depth) in AA2198-T8 joints' mechanical performance and microstructural features was investigated. Furthermore, the effects of the wear along a number of welding cycles in joints' features and tool profile were also analyzed.

¹ Original information dated 2001. Values updated considering dollar and oil barrel quotation of the first trimester of 2018.

2 OBJECTIVES

The purpose of this study is to establish a correlation between joint performance and process inputs in order to determine the optimum set of parameters – tool rotational speed, welding time and plunge depth – for the welding of AA2198-T8 1.6 mm-thick sheets, through lap shear strength testing and macrostructural analysis of the welds.

This work also aims to investigate the interrelation between mechanical properties and welds' microstructural features resulting from RFSSW process on AA2198-T8 1.6 and 3.2 mm-thick sheets using different welding conditions. Additionally, it is intended to evaluate and establish a comparison of the individual influence of rotational speed, plunge depth and welding time on microstructural development based on geometrical features of stir zone and the concept of heat input, using image analysis techniques and statistical methods.

Furthermore, the mechanical strength behavior of the AA2198 joints along the welding cycles is investigated in order to verify the effects of tool wear in welds resistance. It is intended to identify the different effects of wear on tool dimensions and associate this damage to changes in joints' macro and microstructural features and mechanical properties.

3 LITERATURE REVIEW

3.1 Aluminum alloys

3.1.1 Aluminum alloys for aerospace applications

Since the genesis of aviation, in 1903, structural weight has been a major point of concern for the structural design. For ensuring a low weight, the first airframes build until 1927 were wooden structures. From then on, aluminum-based alloys became the dominant material for the purpose due to the development of cladding and anodizing technologies [11]. Aircraft industry evolution made the continuous evolution of aluminum-based alloys with increased specific properties (strength/weight) possible: the first Al alloy used in aircrafts had specific yield strength of 43 MPa/g/cm³, whereas nowadays there are alloys – such as 7055-T7751 – with specific compressive strength up to 229 MPa/g/cm³, more than five times stronger [5].

Over the time, other issues became points of concern on aerospace design aiming durability and damage tolerance. Residual strength and fatigue crack growth became a relevant issue in 1954, when three jet airplanes crashed due to premature fatigue failure of pressurized fuselage concentrations at windows and hatches [5, 11]. Besides, as thicker structures began to be used as a demand for the construction of larger planes, usual alloys were found to be susceptible to stress corrosion cracking. For increasing this type of corrosion resistance, tempering processes involving artificially aging were developed at 60's [11].

Decades later, aluminum alloys development aiming weight reduction came on focus again, but this time, aiming fuel costs reduction. In context of reducing the density of these alloys, Li additions to aluminum alloys would have the greatest influence for the purpose.

3.1.2 Al-Cu-Li alloys

Because of its lower-than-water density (0.534 g/cm^3) and high solubility in aluminum – up to 4% wt. –, lithium has been added to Al-Cu systems in order to reduce the alloy's density and enhance mechanical properties, aiming higher values for specific properties for aeronautic applications. Additions of 1% wt. of Li decrease the alloy density by around 3%, which it is very significant and particularly interesting for application that requires structural weight reduction, such as aircrafts. Furthermore, the use of Li as an alloying element enhances the elastic modulus – by 6% for each 1% Li added (up to the solubility limit of 4%). The addition of lithium is also advantageous because it enables the formation of hardening precipitates, whilst it leads to higher fatigue crack growth resistance [5].

The history of the so-called first generation of age-hardened Al-Li alloy dates from 1950's. AA2020 plates were used in Navy's RA-5C Vigilante aircraft for two decades until it was discontinued because of ductility and production problems. No corrosion or crack issues were reported after a period of 20 years of use, although it presented issues related to ductility and anisotropy [5, 12, 13]. Focused in weight saving of structures by the use of materials with even lower density, the 2nd generation of Al-Li products consists on alloys with Li concentrations above 2%, such as 2090, 2091, 8090 and 8091, which led to a great density reduction (7-10% wt), higher elastic modulus (10-15%) and higher life in fatigue. However, the increasing of Li percentage led to negative performance attributes such as lower plane stress – KC –, lower short-transverse fracture toughness and higher anisotropy of tensile properties [5]. Because of these issues, the 2nd generation of aluminum with higher lithium concentration did not find wide use in aeronautic industry [14]. Intense research and development in the 80's resulted in the modern 3rd new generation of aluminum-lithium, developed to overcome the limitations found in previous Al-Li products. Reduced additions of Li (from 0.75 to 1.8% wt.) led to both optimization of alloying composition and thermal-mechanical processing, with characteristics of weight-saving and damage-tolerance. Alloys 2195, 2196,

2297, 2397, 2198, 2099, 2199, 2050, 2060 and C99N are referred as 3rd generation products [5].

2198 is an Al-Cu-Li-Mg based alloy with Li concentration of 1% wt., resulting in a low density alloy, 2.7 g/cm³ that has been considered for wings components and fuselage box aeronautic applications. This alloy was developed to replace 2024 and 2524 in aircraft products aiming to enhance damage tolerance.

Ageing of AA2198

Al-Cu-Li alloys are ageing-hardening alloys, since the addition of lithium to Al-Cu systems enables the formation of strengthening precipitates responsible for their interesting mechanical properties [5, 15, 16]. To achieve these microstructural features, a supersaturated solid solution is first produced as a result of solution treatment, in order to guarantee the input of a maximum amount of precipitation hardening solutes – Cu, Li, Mg and Ag – dissolved into the matrix [16].

The excellent performance of artificially-aged (T8) 2198 alloys are reported to be mainly associated to the precipitation of $T1$ (Al₂CuLi), δ' (Al₃Li) and θ' (Al₂Cu) intermetallic phases, finely dispersed in the matrix [5, 15, 16]. Additionally to strengthening improvements, the presence of $T1$ precipitates are reported to enhance toughness control, while δ' is also related to increase fatigue properties [5].

3.1.3 Weldability of Al-Cu-Li aluminum alloys

The welding of Al-Cu-Li alloys by fusion-based joining techniques is subject of many metallurgical problems which result in hydrogen porosity, hot cracking and stress corrosion cracking [13, 17]. Furthermore, the heating of the material until melting point causes a large area of heat affected zone (HAZ), that reduces the strength and resistance to fatigue [14]. The obstacles for the welding of high-strength aluminum alloys are listed below:

- High solubility for hydrogen on molten aluminum causes porosity on the weld;
- Due to high solidification shrinkage, cracks may occur on aluminum welds;
- High coefficient of thermal expansion of aluminum may lead to weld cracking or distortion due to residual stress;
- High heat input is necessary during the welding because of the high thermal conductivity of aluminum, in order to avoid distortion or cracking of the weld [14];
- Presence of oxide inclusions that results from the spontaneous stable surface passive layer formed on aluminum surface [18];
- Properties degradation can occur because of the difference of oxide melting temperatures and thermal conductivity, which leads to higher heat input and alloy elements evaporation [6].

To minimize these problems associated to traditional welding methods, new solid-state joining techniques have been developed since 90's, such as friction stir welding (FSW) and refill friction stir spot welding.

3.2 Refill Friction Stir Spot Welding

3.2.1 Overview

The spot weld of two or more aluminum workpieces by using commercially available fusion procedures is problematic because of the spontaneous formation of the passive oxide layer on sheets surface, characteristic of aluminum and its alloys when exposed to oxygen. The presence of this oxide layer causes high electrical resistance between workpieces' surfaces to be joined, what leads to the inclusion of aluminum oxide through the molten material layers formed between the sheets, resulting in spot-joints with insufficient strength required for many applications [18].

Refill Friction Stir Spot Welding (RFSSW) or Friction Spot Welding (FSpW) is a solid-state joining technique developed and patented by Helmholtz-

Zentrum Geesthacht (former GKSS-Forschungszentrum Geesthacht GmbH) in 2000 as an alternative for producing overlapped joints of lightweight materials such as aluminum, magnesium and thermoplastics [6]. The feasibility of the technology has been studied for several authors, and the suitability has been demonstrated for aluminum [19–25], magnesium [26, 27] and dissimilar welds e.g. aluminum and titanium sheets [28, 29].

Friction-based processes for spot welding production were developed aiming to meet aircraft and automotive industries demand. They appear like an attractive alternative to mechanical fastening for joining of two or more workpieces since weight penalties, difficulties in automation and corrosion issues such as crevice are minimized [26, 30]. Friction stir spot welding (FSSW) was developed by Mazda Motor Corporation, as an adaptation of FSW, and was first used in 2003 for the assembly of pieces of the vehicle RX-8 replacing resistance spot welding (RSW) process [31]. RFSSW is a similar process developed in order to refill the residual key-hole left in FSSW, which may lead to corrosion and mechanical issues. Typical cross-sections of both FSSW and RFSSW (Figure 3.1) illustrate the difference between the processes, where the refilled residual key-hole can be observed.

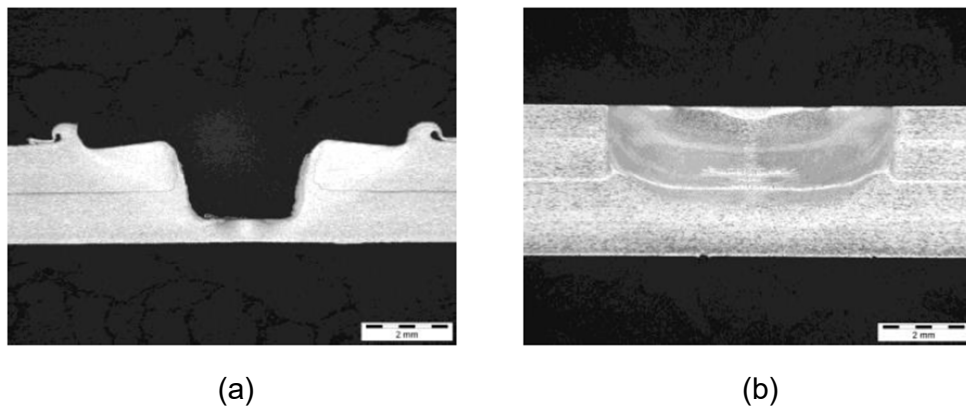


Figure 3.1 – Cross-section of AA7075 friction-based welds: (a) FSSW (b) RFSSW [32]

The friction of the tool against the workpiece is responsible for the heat input into the material and the generation of sufficient conditions for the high deformation of and decreasing in its viscosity without reaching the melting point of the alloy. The combination of plasticization of the material and temperature enables the mixture between the material of sheets and recrystallization of the

region, resulting in the weld. In comparison to fusion spot welding techniques, this friction-based process offers environmental and economical benefits due to energy savings over 90% [32].

3.2.2 3-piece tool and variants of RFSSW process

The refill of the residual key-hole left in welds performed by the Mazda's process is enabled by the design of the non-consumable 3-piece tool – the pin, sleeve and clamping ring (Figure 3.2). The device is responsible for the improvement of the welds produced by FSSW since it enables the creation of a cavity to accommodate the displaced plasticized material due to the tool plunge for subsequently push back into the sheet. The pin and the sleeve are the rotational and axial-movable parts of the system, whilst the clamping ring is responsible for holding the sheets together in order to avoid the plasticized material loss during the movement of the two other components [30].

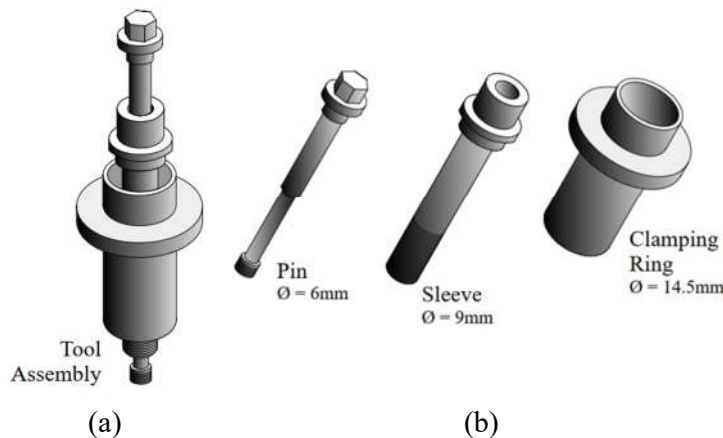


Figure 3.2 – (a) RFSSW tool assembly of the 3-piece tool (b) parts of the tool: pin, sleeve and clamping ring

The principles of RFSSW technique is represented in Figure 3.3. The process is divided in four stages, and there are two variants of the process: pin and sleeve plunge. The first stage of the pin plunge variant (PP) (Figure 3.3a) consists in the clamping of the sheets together towards a backing plate and the head of the device, while the pin and sleeve start to rotate and reaches the upper surface of the workpiece. In the sequence, pin is forced against the sheet

material generating sufficient frictional heat to plasticize and displace the material while the sleeve is moved in the opposite axial direction, creating a cavity between pin and clamping ring surface for the accommodation of the displaced material. When the set plunge and time are reached, both pin and sleeve are moved back to the original position simultaneously, forcing the imprisoned plasticized material to refill the key-hole left by the pin. Finally, the tool assembly is removed from the surface of the sheet, resulting in a refill friction spot weld [18].

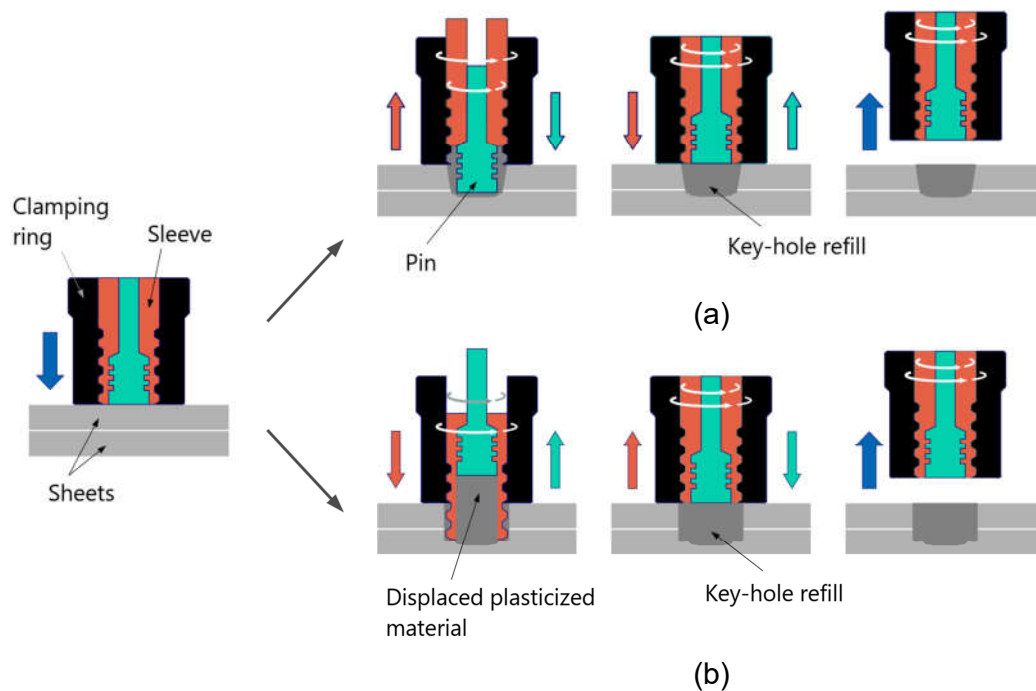


Figure 3.3 – Variants of RFSSW: (a) pin plunge and (b) sleeve plunge

The sleeve plunge variant (SP) (Figure 3.3b) works similarly to the procedure presented in (a) for the PP, except that, in this case, the sleeve part of the tool is plunged into the material instead of the pin. This variant is widely applied for performing RFSSW because it results in larger welds than the ones produced by PP, leading to stronger joints. PP, however, is easier to execute once it requires less power associated with lower frictional forces [22].

Besides of the plunge variants of the process in which the mechanisms of joining are related to the mixture of the sheets' material to be welded, the feasibility of RFSSW for the joint of dissimilar materials with different chemical

and physical features, such as aluminum/titanium, have been studied and showed similar or superior mechanical performance compared to other dissimilar joints produced with traditional fusion-based techniques [28, 29, 33]. The conventional joining of these kinds of dissimilar materials by fusion welding methods is still a challenge due to the formation of excessive brittle intermetallic compounds. RFSSW is a viable technique for this application since sufficient heat input can be generated by the frictional heat related to the plunging of the upper sheet, which enables the interdiffusion of atoms at sheets' interface and result in the formation of the thinnest possible brittle intermetallic layer but ensuring the sufficient number of atoms to consolidate the joint [28].

3.2.3 Microstructural features of RFSSW joints

Welds produced by refill friction stir spot process show different microstructural regions along the workpiece, as a result of a combination between the base material microstructure, heat and displacement rates associated with the movement of the tool [3]. Authors [20, 22, 24, 27] refer to the three different regions of the weld as the stir zone (SZ), thermo-mechanically affected zone (TMAZ) and heat affected zone (HAZ). These zones are indicated in Figure 3.4 on the cross-section macrograph of a weld produced by the sleeve plunge variant of RFSSW.

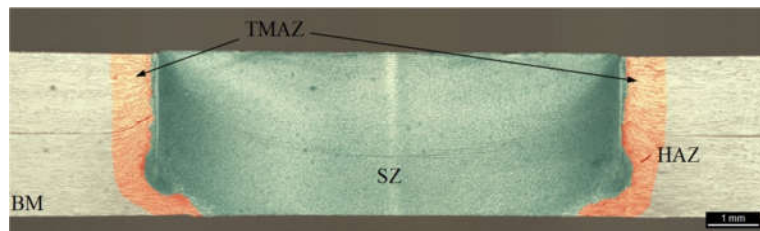


Figure 3.4 – Cross-section of a representative weld produced by RFSSW indicating the stir zone (SZ), thermo-mechanically affected zone (TMAZ), heat affected zone (HAZ) and base material (BM)

The SZ is the portion of material which experiences high deformation rates and mixture of material enabled by the plasticization due to the heat input generated by the friction of the tool against the sheets. This combination of high

deformation and temperature leads to the dynamic recrystallization phenomenon which results in a region with fine and equiaxed grains [24].

The region comprised between SZ and HAZ is the so-called TMAZ. This zone is distinguished by long-and-forward-bent grains resulted from the influence of moderate temperature and the deformation caused by the retraction of the tool back to the sheet surface. Recrystallized grains may be found along the grains boundaries when a parameter selection leads to enough heat input to reach the thermodynamic conditions to enable the phenomenon [24, 34].

The HAZ is a region distant of the influence of the tool activity, i.e., is a deformation-free zone, adjacent to the base material. It is affected, however, by the effects of the rising in temperature due to the thermal conductivity through the sheets, that enables the recovery of rolled microstructure and a slight grain growth [22, 25].

3.2.4 Tool wear

Tool wear is a major issue for friction-based welding processes and is determinant for the quality and pricing of the welds. For the adequate performance of these processes, the tool must be dimensional stable and present the designed features, besides enough mechanical resistance to avoid fracture [35]. Thus, wear in solid-state joining techniques, such as FSW, FSSW and RFSSW, is mainly determined by the tool design features, as well as the adequate tool material selection in face of the workpiece alloy [35, 36]. While FSSW pins made of tool steel are reported adequate for joining lightweight materials such as aluminum and magnesium alloys with little or no wear along the welds [37–39], the welding of materials with higher melting point requires tools made of harder and with higher thermal and wear resistance materials such as WC-Co, TiC and polycrystalline boron nitride, since the process temperatures are above 1000 °C [38].

Although there are studies on tool wear for the FSW [36] and FSSW [38] processes, the issue still demands a proper evaluation for RFSSW. Alcântara identifies in his analysis about the application of RFSSW in the automotive industry [40] that the weld quality and good reproducibility are issues that

requires attention aspiring to large scale applications of the process. Studies on the selection of new materials for the tool, design and the evaluation of tool wear and its life cycle are important issues to be studied in order to accomplish industrial aims [40].

4 MATERIALS AND METHODS

4.1 Flowchart

4.1.1 Effects of welding parameters on welds' features

The analysis of the effects of rotational speed, welding time and plunge depth and optimization of the parameters for the welding of 1.6 and 3.2 mm-thick AA2198-T8 sheets to be developed in this study is overviewed on the flowchart presented on Figure 4.1

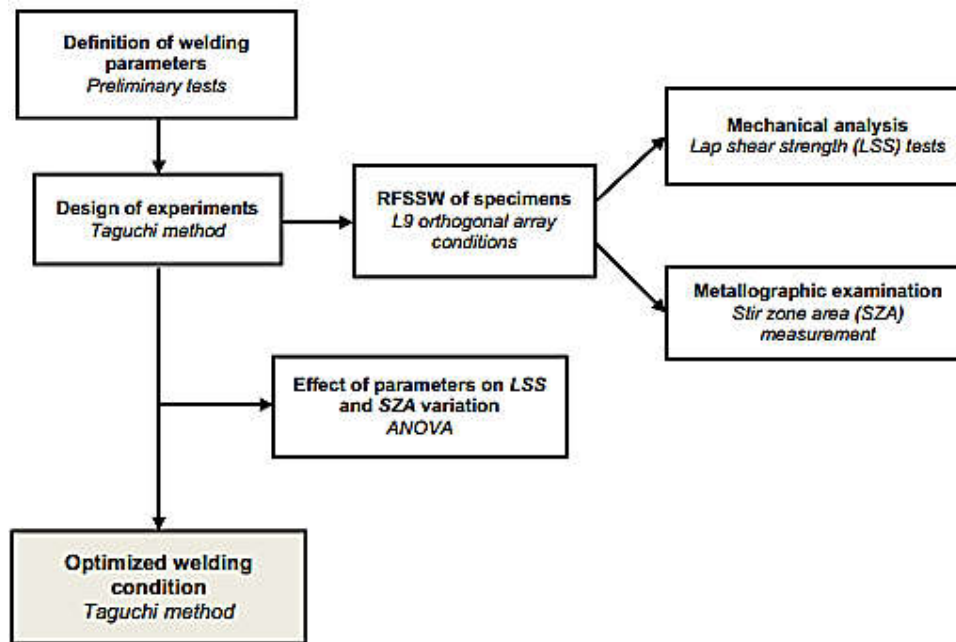


Figure 4.1 – Flowchart of the experimental activities performed for the study of the welding parameters effects and optimization for 1.6 and 3.2 mm-thick sheets

4.1.2 Tool wear evaluation

Tool wear evaluation was based on the analysis for the determination of the range of parameters previously performed for the optimization of welding

parameters study. The experimental stages for the analysis are presented on Figure 4.2.

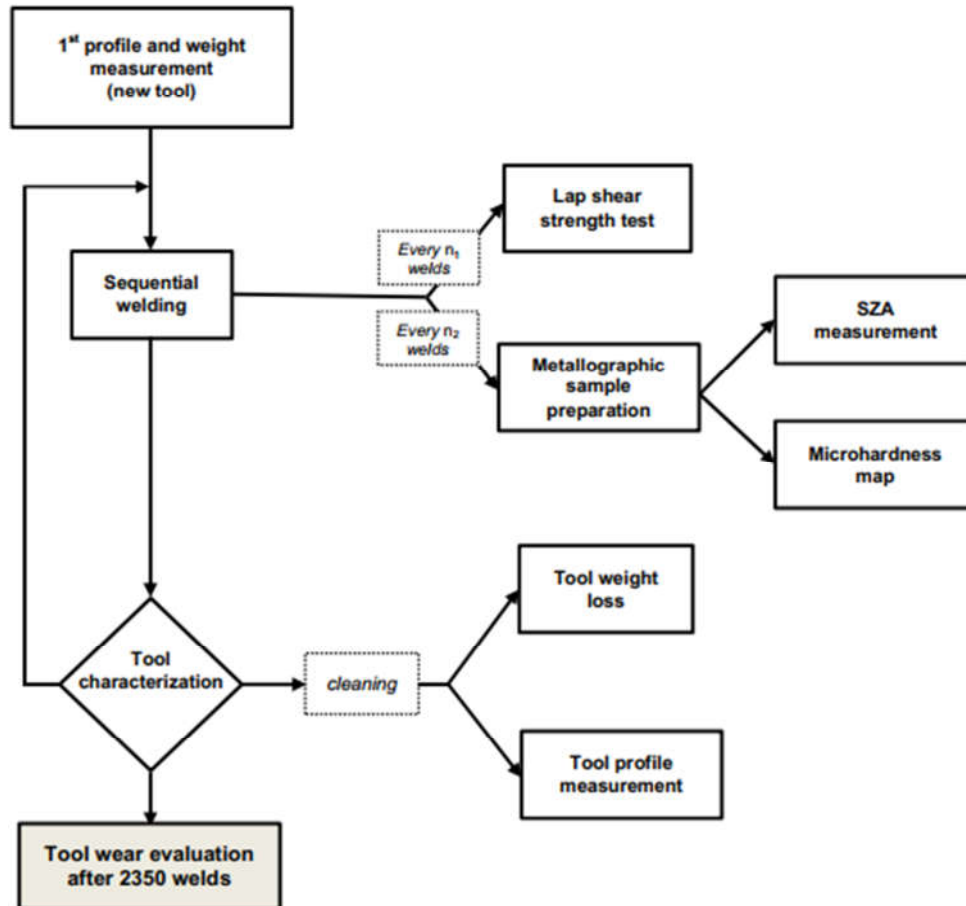


Figure 4.2 – Flowchart of the experimental activities performed for the tool wear evaluation

4.2 Design of Experiments

4.2.1 Definition of the processing window

Preliminary studies were performed to define maximum and minimum levels for the three factors of RFSSW - rotational speed (RS), plunge depth (PD) and welding time (WT). Several welds were produced for the determination of the process parameters and its levels aiming the production of

sound joints. The criteria for the definition of were based on visual aspects (absence of severe volumetric defects of the welds, such as lack of filling/mixing, porosity and cracks), followed by mechanical resistance of lap joints and review of previous works on friction-based processes [20–22]. Parameters producing joints with no defects and higher mechanical strength among the conditions were considered appropriate for the study and used for the production and analysis of the welds.

4.2.2 Taguchi Approach

Taguchi analysis was carried out in order to determinate the effects of the variation of welding parameters (control factors) on the joint's strength and stir zone's cross section area. This design of experiment (DOE) method based on orthogonal array were selected since it allows identifying the main effects of each factor with high efficiency through the smallest fractional factorial plain among DOE methods, although the interaction between the factors is not taken into account. A L9 orthogonal array was employed, resulting in nine experiments – three factors (*RS*, *WT* and *PD*) with three levels each. Lap shear strength (*LSS*) was taken as the mechanical performance metric for the Taguchi analysis. Statistical study was generated by MINITAB® 18 software.

The signal-to-noise ratio (SNR) analysis is a logarithmic function used to optimize process parameters in order to minimize the variability. The appropriate SNR function is selected depending on the expected response: smaller-the-better, nominal-the-better and larger-the-better, the function used in this study since Taguchi approach response aims the best *LSS*. SNR can be calculated as [41]

$$SNR = -10 \log \left[\frac{1}{n} \sum_{i=1}^n \frac{1}{y_i^2} \right] \quad (1)$$

4.2.3 Analysis of variance (ANOVA)

Analysis of variance (ANOVA) is a widely used technique to analyze results of experiments and determine the percentage of contribution of each

parameter (factor). By testing the equality of several means, the statistical significance of the process parameter can be demonstrated.

ANOVA was performed considering three factors: *RS*, *WT* and *PD*, and the results and the statistical study was generated by MINITAB® 18 software. To understand the effects of each parameter on variance, sum of squares (*SS*), degree of freedom (*df*), mean of squares (*MS*), F-value and p-value are calculated and displayed in a typical ANOVA table [41].

Sum of squares (*SS*) is the sum of deviations for the mean, and is calculated considering *n* values of y_i and the mean value \bar{y} described in Equation 2.

$$SS = \sum_{i=1}^n (y_i - \bar{y})^2 \quad (2)$$

Degree of freedom (*df*) is defined as the number of levels for each factor minus 1.

The mean of squares (*MS*) of each factor is calculated based on the ratio between sum of squares and degrees of freedom, according to Equation 3.

$$MS = \frac{SS}{df} \quad (3)$$

F-value is the ratio between the effects of mean of squares and mean of squares error (Equation 4). This value is used to indicate the significance of the effect of each factor on the response variable.

$$F = \frac{MS_{effect}}{MS_{error}} \quad (4)$$

Finally, *p* is a value associated with the degree of confidence at which the factor is significant.

4.3 Production of specimens

The material used for this work is the AA2198-T8 Al-Cu-Li alloy, whose nominal chemical composition is listed in Table 4.1. The 1.6 and 3.2 mm-thick sheets were supplied by Airbus, heat treated under T8 condition (solution heat treatment, cold work and artificial aging). For the mechanical analysis of 1.6 mm

sheets, 126 mm (length) x 35 mm (width) workpieces were cut (schematically presented in Figure 4.3) and welded with an overlap of 46 mm in accordance to the ISO 14273 [42] that standardizes specimen dimensions and procedure for shear-testing spot welds. Furthermore, welds of both 1.6 and 3.2 mm sheets were produced for macro and micrographic analysis purposes. Before welding, all the workpiece surfaces were cleaned with acetone.

Table 4.1 – Chemical composition of AA2198 in %wt. Adapted from Rioja et al. [5]

	Cu	Li	Mg	Ag	Zr	Al
Material as received	3.40	1.01	0.33	0.22	0.11	Balance
Nominal	3.20	1.00	0.50	0.40	0.11	Balance

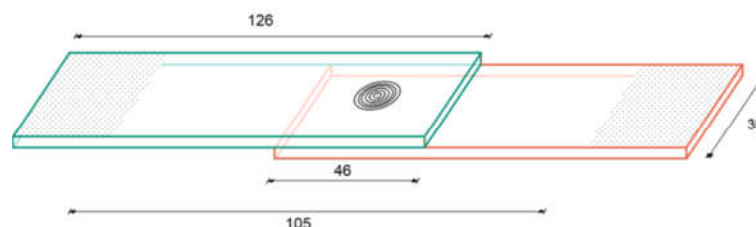


Figure 4.3 – Schematic representation of friction lap shear specimens. Dimensions in mm. Adapted from ISO 14273 [41]

The welds were produced at HZG in a RPS 100 (Harms & Wende) machine, which was developed by the HZG in partnership with the company RIFTEC GmbH (Figure 4.4). Process information - such as the plunge depth, rotational speed, torque, axial load, welding time and the position of pin and sleeve – are recorded by a system monitor. Up to 15 kN forces in vertical axes can be employed during the welding, with a maximum rotational speed of 3300 rpm. The process is performed by 3-piece-tool system – pin, sleeve and clamping ring –, made of H13 tool steel. The system assembly indicating the diameter of the parts is presented in Figure 3.2.



Figure 4.4 – Refill Friction Stir Spot welding RPS 100 (Hams & Wende) machine, developed by HZG and RIFTEC GmbH

The sleeve plunge variant of RFSSW was selected for this evaluation, and the specimens were produced using a clamping force of 14.6 kN. The factors (*RS*, *WT* and *PD*) and their levels set for the study are presented in Table 4.2.

Table 4.2 – RFSSW parameters and their levels

Sheet	Level	RS [rpm]	WT [s]	PD [mm]
1.6 mm	L1	1100	3	2.1
	L2	1300	4	2.6
	L3	1500	5	2.8
3.2 mm	L1	1500	4	3.7
	L2	2000	7	4.2
	L3	2500	10	4.7

4.4 Mechanical testing

Mechanical testing was made to determinate the properties of the joints in order to enables the evaluation of the technology for structural applications,

LSS was based on ISO 14273 standard [41] for both procedure and specimens geometry, since there is no specific standard for lap shear testing of

refill friction spot welds. The tests were carried out in a Zwick-Roell 1478 testing machine, with a load capacity of 200 kN and constant displacement velocity of 1 mm/s. Each experiment was performed in triplicates.

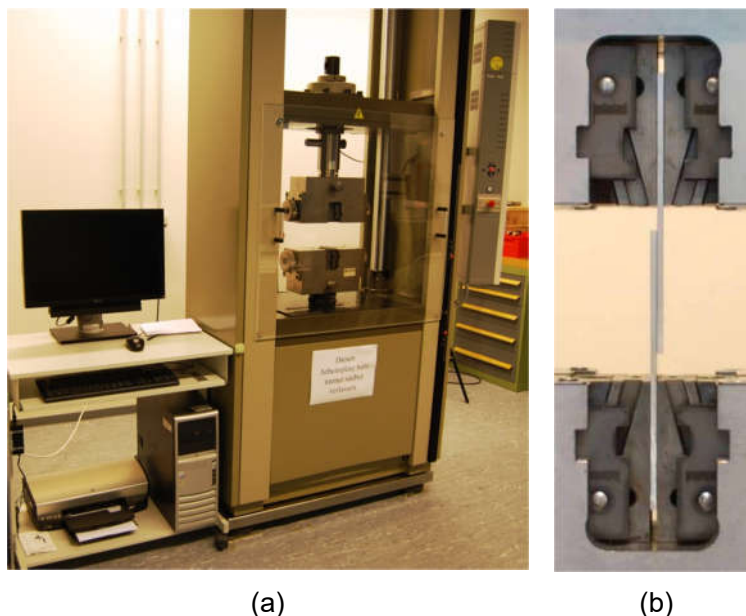


Figure 4.5 – (a) Zwick/Roell machine adapted for lap shear testing and (b) lap shear specimen configuration

Microhardness mapping is a useful technique for the understanding of mechanical and microstructural (e.g. inclusions due to tool wear) properties changes along the welding cycles of the tool wear evaluation. The procedure provides a map of colors proportional to the quantified microhardness on each point, resulting in an overview of the property variation along the weld. A precisely determined area of the sample can be analyzed based on the set of intervals of indentations (measurements) along the X and Y axis. Because of the symmetry on the welding, the maps were developed for one half of the sample, with the distance between each indentation of 0.15 mm and a load of 200 gf for 10 s.

4.5 Micro and macrostructural analysis

Optical Microscopy (OM) characterization of joints' cross-section of the samples allows the evaluation of the welding zones, the presence of defects, and other macrostructural features that can be present on the welds considering the process parameters. Besides, OM analysis along mechanical testing results enabling the explanation of metallurgical phenomena and may help understanding the effects of tool wear on the quality of the welds.

The procedure for sample preparation is described below:

- Low-velocity specimen cutting: the samples were cut on a plan close to the weld's cross-section using a Struers Discotom-6 diamond abrasive wheel cutter
- Embedding of the samples with a soft-transparent resin (Buehler's Epoxicure system)
- Manual grinding of the samples using Buehler's Silicon Carbide grinding paper P-80 until it the center of the weld cross-section (symmetry plan) was reached with subsequent grinding with finer sand papers(grit 320 to 4000)
- Polishing in two steps: first, polishing with 3 μ m diamond suspension, followed by OPS solution polishing (colloidal silica suspension)
- Chemical etching by immersion in Keller's reagent (2 mL HF (48% vol.), 3 mL HCl (concentrated), 5 mL HNO₃ (concentrated) and 190 mL distilled H₂O).

Micro and macrographies were acquired using a Leica DFC 296 camera attached to a Leica IRM optical microscope.

Measurement of welds' stir zone area and other geometrical features were performed with the ImageJ 1.51k image analysis software. To measure the stir zone area, macrographs were treated in order to enhance the contrast between the regions to be observed based on differences of shape and size of the grains. Then, binary images were build (only black and white pixels)

isolating the stir zone region and the counting of these black pixels resulted in the area measurement.

4.6 Tool wear evaluation

2350 sequential welds were performed in AA2198-T8 1.6 mm-thick sheets considering the intermediate levels of rotational speed, welding time and plunge depth defined in Table 4.2 – 1300 rpm, 4 s and 2.6 mm. Samples for macrographic analysis and hardness mapping were welded each 200 welding cycles. Furthermore, lap shear strength test coupons were prepared in triplicates in determinate intervals. All joints were performed with an initial tool temperature of 30 °C, measured with a thermocouple.

4.6.1 Tool material

Tool material used in this study is a H13 tool steel, whose composition according to ASTM A618 requirements is presented in Table 4.3.

Table 4.3 – Chemical requirements (%wt) for H13 tool steel according to ASTM A681 [43]

	C	Mn	P	S	Si	Cr	V	Mo	Fe
Min	0.32	0.20	-	-	0.80	4.75	0.80	1.10	Balance
Max	0.45	0.60	0.03	0.03	1.25	5.50	1.20	1.75	

This material is largely used for hot work and cold work tooling applications, when properties such as high thermal fatigue crack resistance, toughness and high dimensional stability in heat treatment are required. H13 is also attractive for tooling construction since it provides good hardenability and consequently wear resistance especially when compared with common alloy steels [43, 44].

4.6.2 Characterization of pin and sleeve's profile

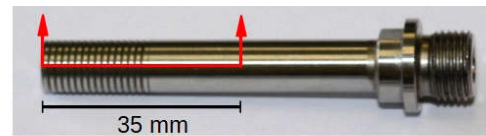
In order to evaluate the wear of tool along the welding cycles, a region at the tip of pin and sleeve were measured using a Mahr Multiscope 250 (Figure

4.6), an optical measurement technique, equipped with KMess software. Tool measurement took place in four different moments:

- Before welding: profile of the as-received tool;
- After 1350 welds;
- After 2000 welds;
- Final measurement: after 2350 welds



(a)



(b)

Figure 4.6 – Tool measurement: (a) Mahr Multiscope 250 used on the experiment and (b) sleeve and pin measured plane indicated by red arrows

4.6.3 Tool cleaning procedure

All the three parts of the tool were cleaned before the measurements, in order to remove all the aluminum trapped in the parts and ensure a proper examination. The tool was immersed in a solution of 0.04 g/mL NaOH, for 3 h at room temperature. In order to avoid saturation of the solution due to the aluminum dissolution, the solution was replaced every 30 minutes.

4.6.4 Weight measurement of pin and sleeve

An analytical balance was used to measure pin and sleeve for quantifying the tool material weight loss caused by wear, at the same points of profile measurement. The variation of mass was determined by the comparison with the mass of the as-received tool before welding.

5 RESULTS AND DISCUSSION

5.1 Microstructural development of RFSSW joints

A representative cross-section of overlapped 3.2 mm-thick AA2198-T8 sheets welded by RFSSW is presented in Figure 5.1. Different microstructures are observed, resulting in three distinctive zones: stir zone (SZ), thermo-mechanically affected zone (TMAZ) and heat affected zone (HAZ), in addition to the base material (BM) – the original microstructure of the material which is not affected neither by temperature or deformation as a result of the process. This is the typical microstructure produced by the RFSSW of aluminum alloy sheets, which is also reported in previous works [20, 34].

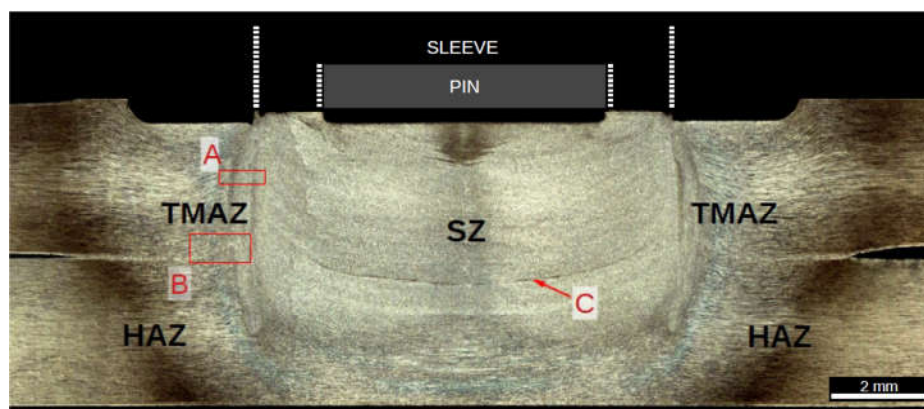


Figure 5.1 – Representative macrograph of overlapped AA2198-T8 sheets welded by RFSSW indicating different microstructures: stir zone (SZ), thermo-mechanically affected zone (TMAZ) and heat affected zone (HAZ). Red markings indicate important microstructural features: A (shown in higher magnification on Figure 5.2) shows the SZ-TMAZ interface region, while B indicates the hook region between the sheets and C shows bonding ligament caused by the welding process.

Figure 5.2 shows the transition between TMAZ and SZ (schematically remarked as A in the cross-section macrograph previously presented) in higher magnification. Long-and-bent-forwards grains are observed on the left side of the image, in the region identified as TMAZ, as a result of the influence of rising-in-temperature and deformation caused by the retraction of the sleeve towards the sheet's upper surface (third stage of Figure 3.3b).

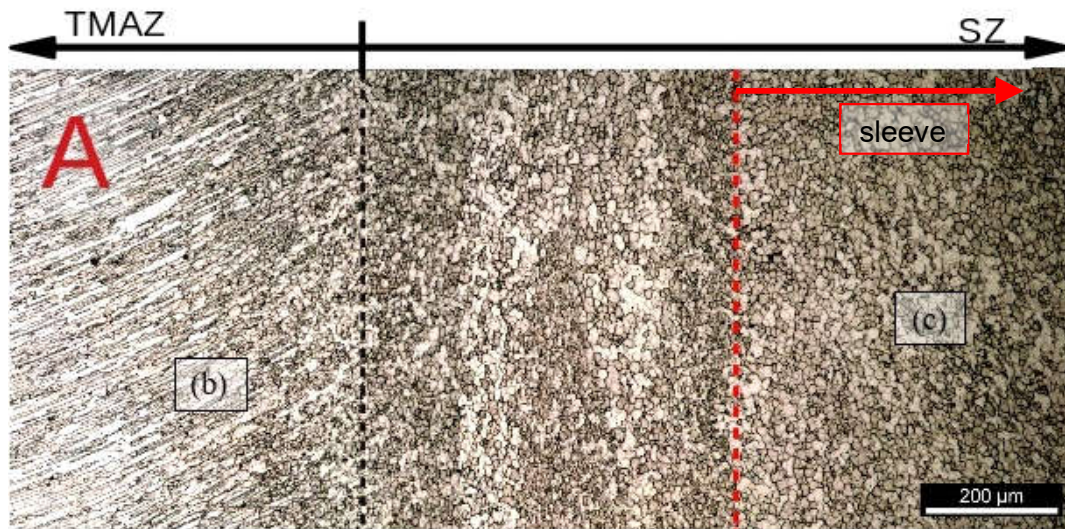


Figure 5.2 – Region marked as A in Figure 5.1 in higher magnification indicating the transition between SZ and TMAZ and sleeve penetration path

TMAZ mostly does not go through the dynamic recrystallization phenomenon (ReX) since there is no sufficient strain rate to induce this transformation. Nonetheless, Figure 5.3 details a portion of TMAZ alongside the SZ interface (identified as (b) in Figure 5.2), in which elongated grains with sub-boundaries (indicated by the red contour and arrows) and strings of fine grains (marked with white dashed contour) as an indicative of ReX on the referred region. These traces of dynamic recrystallization on TMAZ were also found and described by Shen et al. [24].

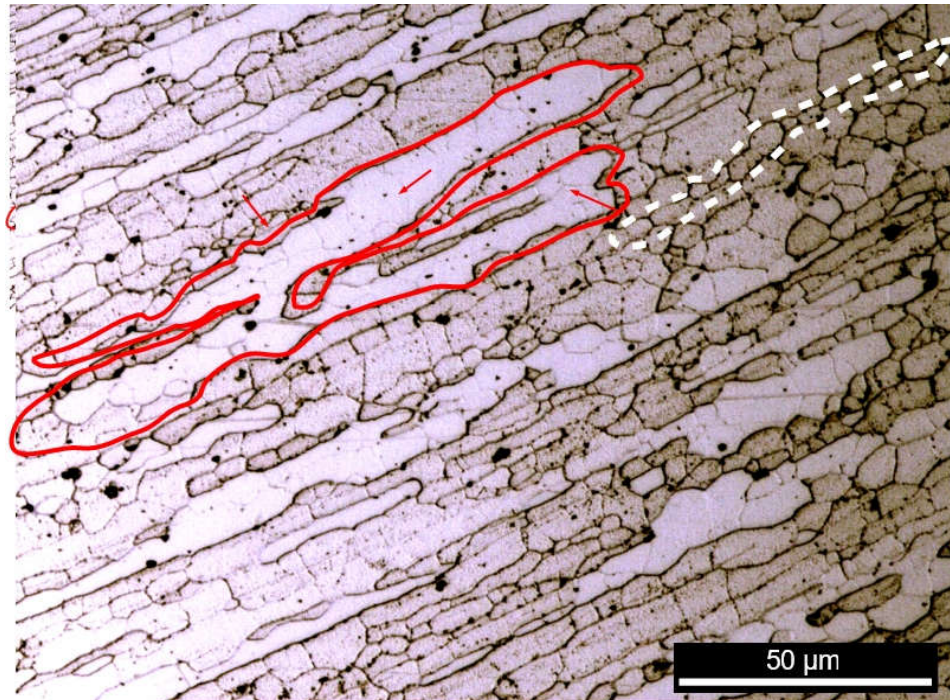


Figure 5.3 – Higher magnification of the region marked as (b) in Figure 5.2 indicating recrystallized grains in TMAZ (dashed white line) and elongated grains with sub-boundaries (red contour) found in TMAZ

Fine-and-equiaxed grained microstructure, which defines the SZ, is observed in Figure 5.4. According to several authors [20, 22, 24, 30], this typical microstructure results from dynamic recrystallization process. Two patterns of grains can be distinguished according to the shape, size and texture of grains. The portion of SZ surrounded by the center of the weld nugget and limited by the sleeve path penetration (right side of the image) is presented in Figure 5.4. The observation in high-magnification of the region shows recrystallized-and-equiaxed grains with average size of 6 to 8 μm oriented according to the plasticized flow, i.e., grains with shear texture [24, 45], which results from the material flow caused by the movement of the sleeve during the refilling stage of the process [34].

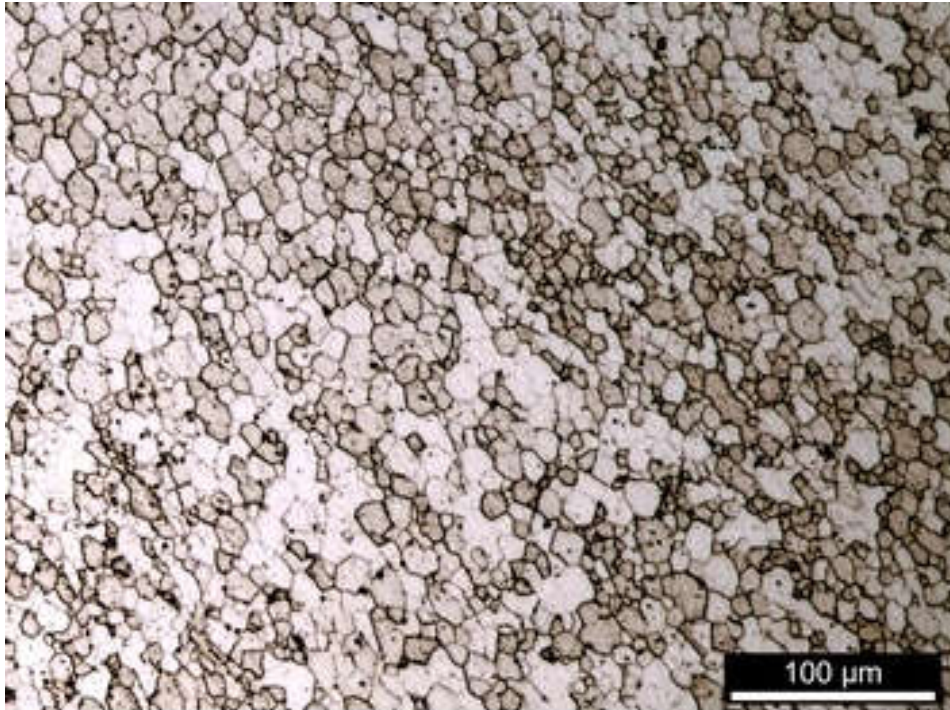


Figure 5.4 – Region marked as (c) in Figure 5.1 in higher magnification indicating recrystallized grains in SZ

The second region of SZ is comprised between sleeve's outer surface and TMAZ interface, roughly 560 μm wider than the sleeve external diameter, as observed in Figure 5.2. In comparison with the nugget microstructure, the shear texture pattern is absent and this region presents a more refined structure (grains with 4 μm average size), developed by the combination of the highest deformation and temperature – caused by the sleeve plunge and retraction associated to the fast rotation of the tool – at the region adjacent to the outer surface of the sleeve. Regardless of these finest grains at the region, larger grains (7 μm) are observed in an area between TMAZ and ReX grains adjacent to sleeve penetration path. Shen et al. [24] associate the presence of these larger grains with RFSSW's plunge stage: the penetration of the sleeve towards the sheets interface generates heat, causing recrystallization and plasticizing of the bottom sheet material. Due to material flow, the plasticized material is displaced upwards to the region of the sleeve outer interface. Hence part of the SZ material is extruded to the region between sleeve and TMAZ, which remains

similar in shape and size as formerly in stir zone. Analogous occurrences of this phenomenon were also described by Reimman et al. [34] in a study of keyhole repairs of AA2198 using RFSSW.

5.2 RFSSW: Optimization of AA2198-T8 1.6 mm-thick sheets

5.2.1 Selection of parameters

Based on literature results and previous experience of usual ranges for process parameters used on RFSSW processes for aluminum alloys, a set of parameters was used in order to obtain the first welded joints. After visual investigation and identification of some set of parameters which could yield sound welds (near defect-free, four levels of each factor (*RS*, *WT* and *PD*) were defined for the analysis. Some of these welds were evaluated regarding their performance in *LSS* test. The results for different conditions for the welding of AA2198-T8 1.6 mm sheets are presented in Figure 5.5. For each plot, two factors were kept constant while the parameter to be observed varies along the selected levels.

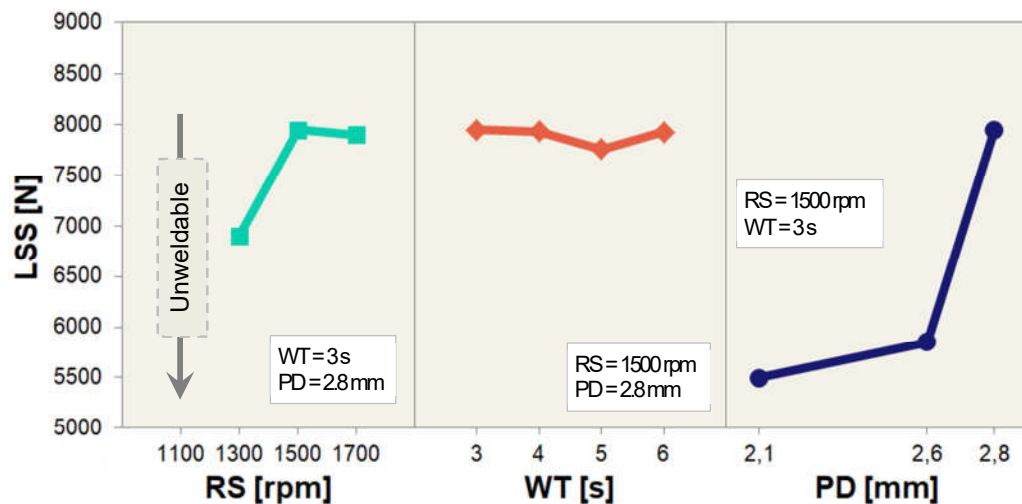


Figure 5.5 – Selection of upper and lower parameters for the basis of Taguchi analysis: plots of lap shear strength values along different levels of rotational speed (*RS*), welding time (*WT*) and plunge depth (*PD*)

Lower and upper levels were defined as 1100 rpm and 1500 rpm for *RS*. The combination of parameters 1100 rpm/3 s/2.8 mm did not welded successfully the sheets due to its association of low heat input and high tool-penetration rate. However, *RS* lower limit was still picked as 1100 rpm for the Taguchi analysis since it provides enough heat input for plasticizing the material for smaller penetration rates – longer welding times and smaller plunge depths. On the other end, the upper limit for the experiment was set as 1500 rpm since it produces welds with the best mechanical resistance in terms of *LSS* (as observed in Figure 5.5). *LSS* starts to decrease from 1500 rpm to 1700 rpm, what may be related to a progressively lower heat input in welds along the increasing of *RS* from that greatest value on. Authors such as Campanelli et al. [26] associate this turning point in terms of *RS* to a decrease in heat input related to the reduction in material viscosity due to higher temperature and shear rates. As material viscosity is reduced, the torque associated to heat input is also reduced, leading to a lower heat input.

The observation of the plots for *WT* in Figure 5.5 indicates the smallest variance in *LSS* of all factors, in addition to a not very significant *LSS* variation along the levels. For this reason, the experimental window was set in order to prioritize industrial requirements associated to production rates, i.e., levels 3 s, 4 s and 5 s were selected for the Taguchi analysis.

PD limits were selected considering sheets' overlapped geometry – resulting in joints of 3.2 mm –, a minimum plunge in the lower sheet of 0.3 mm and maximum of 1.2 mm. Thus, the levels of *PD* were defined as 2.1 mm, 2.6 mm and 2.8 mm.

5.2.2 Taguchi analysis

The L9 orthogonal array given by the Taguchi a is presented in Table 5.1, in which the set of parameters (*RS*, *WT* and *PD*) for nine experiments are listed along with the *LSS* means – obtained from mechanical testing performed in triplicates – and the signal-to-noise ratio (*SNR*) calculated considering the-larger-the-better Taguchi approach.

Table 5.1 – Experimental conditions for the Taguchi analysis (rotational speed, welding time and plunge depth), mean of experimental results for lap shear strength test (LSS) and calculated signal-to-noise ratio (SNR) for each welding condition

WELDING CONDITION	RS [rpm]	WT [s]	PD [mm]	LSS [N]	SNR
C1a	1100	3	2.1	4877 ± 78	73.76
C2a	1100	4	2.6	5733 ± 270	75.17
C3a	1100	5	2.8	7685 ± 420	77.71
C4a	1300	3	2.6	5799 ± 110	75.27
C5a	1300	4	2.8	6996 ± 747	76.90
C6a	1300	5	2.1	5650 ± 505	75.04
C7a	1500	3	2.8	7947 ± 349	78.00
C8a	1500	4	2.1	7426 ± 724	77.42
C9a	1500	5	2.6	7498 ± 237	77.50

According to Table 5.1, the highest value of *LSS* and *SNR* (7947 N and 78.00) are found for the *C7a* condition (1500 rpm, 3 s, 2.8 mm), which corresponds to the highest levels of *RS* and *PD*. On the other hand, the condition associated to the lowest *LSS* and *SNR* (4877 N and 73.76) are *C1a* (1100 rpm, 3 s and 2.1 mm), with a set of parameters combining the lowest levels of the experiments for each factor. All the conditions analyzed in the experiment, however, are able to produce welds that exceeds the minimum *LSS* required by AWS D17.2² [10] considering the AA2198 spot-welding of 1.6 mm sheets for aerospace applications. According to the standard and material properties, the minimum spot weld resistance required for aircraft structures is 3180 N, reached even by the worst *C1a* condition. Nonetheless, it should be noted that this is a particular requirement for lap shear strength, and other aspects of joints' mechanical performance must be studied and taken in consideration.

² As of 2019, specific requirements for friction-based spot welds for aerospace applications have not yet been standardized. For this reason, AWS D17.2 (*Specification for Resistance Welding for Aerospace Applications*) has been adopted as a reference for several authors [20, 25, 28].

Table 5.2 lists the outputs of the Taguchi analysis in terms of *LSS* means and *SNR* for *RS*, *WT* and *PD*, while Figure 5.6 shows the main effect plots of these responses. Since the Taguchi method provides the responses of each level individually, the analysis indicates that *PD* is the most influential factor on *LSS* means and *SNR* considering the selected range of parameters. The variation (*delta* - δ) between maximum and minimum means and *SNR* is associated to the effectiveness parameters variation (*RS*, *WT* and *PD*) – the greater the difference, the more effective the variation of the factor on joint's *LSS*. Delta values were found to be similar to *RS* and *PD* in both terms of means (1525 N versus 1558 N) and *SNR* (2.13 versus 2.09). Contrarily, *WT* is related to the lowest effectiveness of levels variation on weld's strength: its delta values (737 N and 1.07) are significantly smaller than the other two observed factors.

Table 5.2 – Response table for means and signal-to-noise ratio (SNR) for rotational speed (*RS*), welding time (*WT*) and plunge depth (*PD*) based on *LSS* response

Level	RS [rpm]		WT [s]		PD [mm]	
	Means	SNR	Means	SNR	Means	SNR
L1	6098	75.55	6208	75.68	5984	75.41
L2	6148	75.74	6718	76.49	6343	75.98
L3	7624	77.64	6944	76.75	7543	77.54
Delta (δ)	1525	2.09	737	1.07	1558	2.13
Ranking	2		3		1	

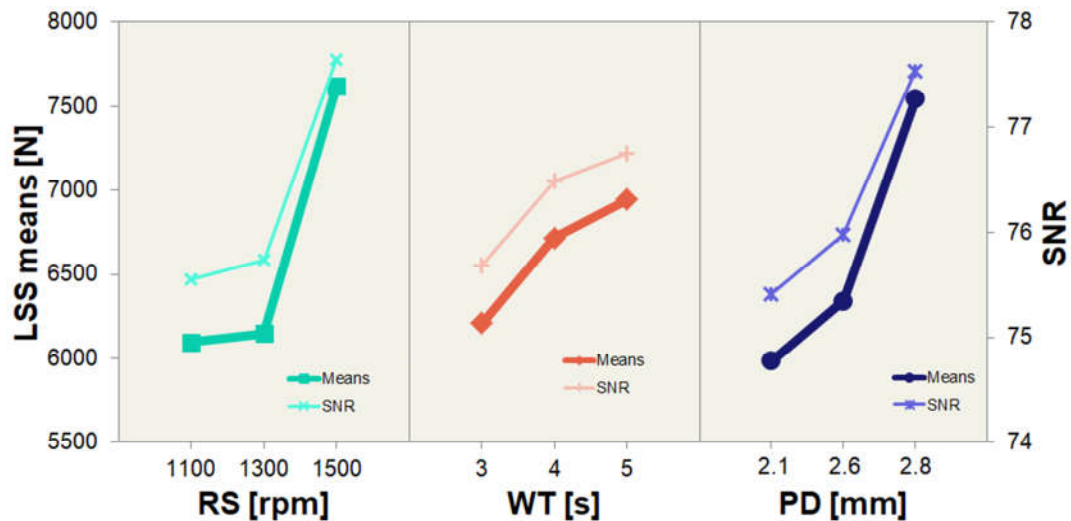


Figure 5.6 – Main effect plots of means and signal-to-noise ratio (SNR) for rotational speed (RS), welding time (WT) and plunge depth (PD) based on LSS response

Discrepancies on each plot's behavior presented in Figure 5.6 are also an indicative of the factor's effectiveness associated to the variance of levels. It is noted that in all cases the increment-in-level results in a positive contribution to welds' resistance. The trends presented by *RS* and *PD* plots are similar: the second portion of the curve is considerably steeper than the first one, indicating that small increments-in-levels between 2 and 3 are expected to result in greater influence on *LSS* than the same additions between levels 1 and 2. Unlike *RS* and *PD*, *WT* shows a decreasing in the slope angle at the second part of the plot (between levels 2 and 3).

Taguchi is also a widely used approach for the optimization of process parameters. The optimum welding condition predicted by the method for the RFSSW of AA2198 1.6 mm-thick sheets is presented in Table 5.3. Considering the selected window of parameters and aiming to the highest lap shear strength of the welds, the best welding condition would be found by the combination of the highest levels of each factor – 1500 rpm, 5 s and 2.8 mm. This new set of parameters – named *C10a* – was welded and lap-shear tested in triplicates.

Table 5.3 – Optimum welding condition predicted by Taguchi method (*C10*) and mean of experimental results for lap shear strength test (*LSS*)

WELDING CONDITION	RS [rpm]	WT [s]	PD [mm]	LSS [N]
<i>C10a</i>	1500	5	2.8	7759 ± 428

Figure 5.7 presents the plots of *LSS* means for all conditions considered in this study – the L9 experimental array conditions and the optimized combination of parameters predicted by the Taguchi approach. It is possible to note that the condition indicated by the method was not very accurate in terms of providing the set of parameters to enable the welding of the most resistant joint: among all conditions, *C7a* (1500 rpm, 3 s, 2.8 mm) is the one with the highest *LSS* (7947 N), while the optimized *C10a* condition (1500 rpm, 5 s, 2.8 mm) presented a slightly lower *LSS* (7759 N). In terms of parameters, *C7a* and *C10a* were produced with identical *RS* and *PD* levels (1500 rpm and 2.8 mm), differing only on welding time levels – *C7a* is produced with three-seconds-long welding time, and *C10a* with a *WT* of 5 s. As discussed before, the variation in *WT* parameters range produces an almost insignificant influence on *LSS*, and this could be the reason for the similar *LSS* values – especially considering the standard deviation – presented by this two *RS*-and-*PD*-identical conditions.

Finally, although the Taguchi method predicts *C10a* as the optimum welding condition for AA2298-T8 1.6-mm-thick overlapped sheets, the joint analysis of *LSS* results and economical and industrial aspects indicate that the best set of parameters is reached by *C7a*. Considering that *LSS* values of the two conditions are very similar, the selection of a set with shorter welding time is more convenient for industrial applications since it leads to higher production rates.

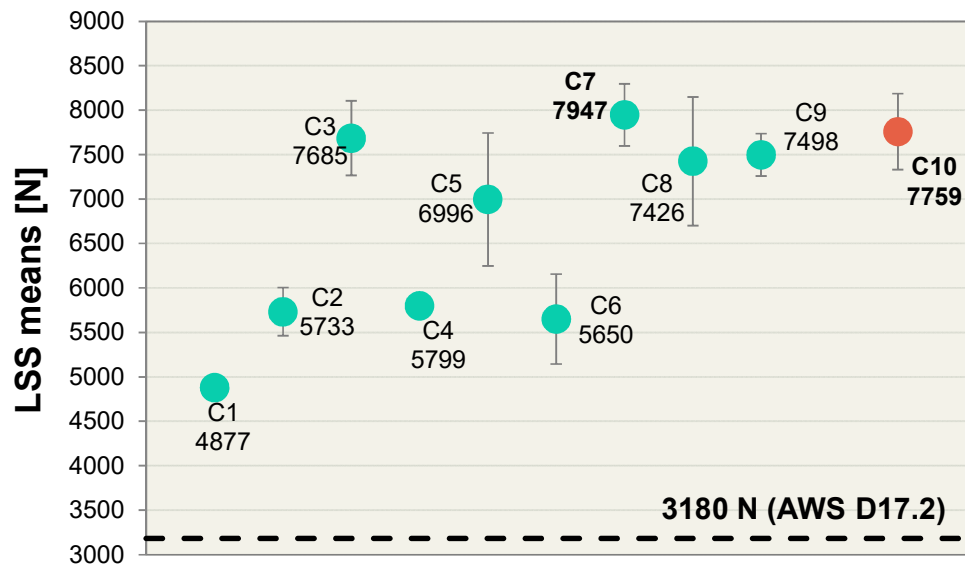


Figure 5.7 – Means of experimental results for lap shear strength test (*LSS*) for L9 orthogonal array welding conditions (*C1a* to *C9a*) and Taguchi predicted optimum condition (*C10a*)

5.2.3 Analysis of variance – ANOVA

Analysis of variance (ANOVA) of factors – *RS*, *WT* and *PD* – indicates the influence (%) of individual parameters on the lap shear strength performance of the welds. For this study, the individual influence of the factors was analyzed, and the interaction between the variables was not taken into consideration. Table 5.4 indicates the outputs of the analysis, and Figure 5.8 graphically presents the influence of each parameter on *LSS* variance. These results point to *RS* and *PD* being the ultimate influence factors on *LSS* – altogether, they correspond to 86% of contribution percentage. Individually, it is not correct to affirm that *RS* is the most relevant factor in *LSS* variation (46% in terms of *means* and 44% in terms of *SNR*) over *PD* (1% of 40% for both *means* and *SNR*) since the analysis error (5% and 6% in terms of *means* and *SNR*, respectively) must be considered, resulting in an overlap of *RS* and *PD* percentage of contribution. The relevance of effect of *RS* variation on *LSS* is also verified in studies reported by Plaine et al. [28] on dissimilar RFFSW of AA6168 and Ti-6Al-V 1.5-mm-thick sheets, and similar AA7975 0.8-mm-thick

sheets presented by Kubit et al. [19]. Furthermore, studies performed by Campanelli et al. [26] indicate that in welds produced by the RFSSW of AZ31B-H24 Mg alloy with 2 mm-thick sheets the variation of *PD* levels leads to the highest percentage of influence on *LSS* variance.



Figure 5.8 – Influence of individual parameters – rotational speed (*RS*), welding time (*WT*) and plunge depth (*PD*) – on the variance of *LSS* in terms of means (in teal) and *SNR* (in orange) given by ANOVA

Table 5.4 – Analysis of variance (ANOVA) and individual influence of parameters – rotational speed (*RS*), welding time (*WT*) and plunge depth (*PD*) – in *LSS* in terms of means and *SNR*

	Factor	df	SS	MS	F value	%I
Means	RS	2	4505750	2252875	8.33	46%
	WT	2	854534	427267	1.58	9%
	PD	2	3995684	1997842	7.39	40%
	Error	2	540734	270367	-	5%
SNR	RS	2	8.036	4.018	7.41	44%
	WT	2	1.882	0.941	1.73	10%
	PD	2	7.304	3.6521	6.73	40%
	Error	2	1.085	0.5425	-	6%

df degrees of freedom, SS sum of squares, MS mean square, %I percentage of influence

On the other hand, the presented ANOVA results indicate that *WT* variation is not able to produce any relevant effect on *LSS* considering the

selected range of parameters, in both terms of *means* (9%) and *SNR* (10%). The irrelevance of *WT* is especially verified when compared along ANOVA's error (5% and 6%) in face of *RS* and *PD*'s 86% and 84% percentage of influence. These findings are in accordance with the presented by Campanelli et al. [26] about the RFSSW of thin Mg alloy sheets, which shows that *WT*'s percentage of influence (4.38% and 6.55% in terms of *means* and *SNR*, respectively) is significantly smaller than error's (16.58% and 17.87%), leading to the conclusion that welding time shows no statistical influence on *LSS* of these welds considering the process window used for this evaluation.

It is noteworthy that Taguchi analysis and ANOVA shows convergent conclusions. For the parameters and levels used in this study, both statistical analysis indicate the great-and-similar relevance of *RS* and *PD* in joint's mechanical performance, whilst *PD* levels variation is pointed as almost irrelevant for *LSS*.

5.3 Effect of stir zone size in welds' resistance

5.3.1 Correlation between *LSS* and *SZA* for 1.6 and 3.2 mm-thick sheets

Amancio et al. [22] indicate the correlation of welds' mechanical performance of a friction spot joint to metallurgical transformations occurred during the processing – which can be quantified in terms of the stir zone area measurement – and other geometric features such as defects (incomplete refill, voids to name some) and hook angle [46].

Based on the welding parameters of 1.6 mm-thick sheets and their *LSS* performance previously studied on Section 5.2, *SZA* of these welds' cross-sections were measured and plotted against their *LSS* values. Furthermore, *SZA* of 3.2 mm sheets were also investigated based on the welding parameters and *LSS* results presented by Pieta et al. [20] on the optimization of process parameters for the welding of these sheets also based on the Taguchi method. The welding parameters used for the production of both 1.6 and 3.2 mm-thick sheets' cross-sections are previously presented in Table 4.2, and the welding

conditions, *LSS* and *SZA* mean values are listed in Table 5.5. The plots of *LSS* and *SZA* along the welding conditions are also presented in Figure 5.9. The macrographies for each welding condition analyzed in this study can be found on Appendix A (1.6 mm-thick sheets) and Appendix B (3.2 mm-thick sheets).

Table 5.5 – Experimental conditions (rotational speed, welding time and plunge depth), mean of experimental results for lap shear strength test (*LSS*) and stir zone area (*SZA*) for each welding condition

THICKNESS	WELDING CONDITION	RS [rpm]	WT [s]	PD [mm]	LSS [N]	SZA [mm²]
1.6 mm	C1a	1100	3	2.1	4877	21.68
	C2a	1100	4	2.6	5733	25.13
	C3a	1100	5	2.8	7685	28.08
	C4a	1300	3	2.6	5799	27.59
	C5a	1300	4	2.8	6996	28.27
	C6a	1300	5	2.1	5650	23.80
	C7a	1500	3	2.8	7947	29.18
	C8a	1500	4	2.1	7426	24.51
	C9a	1500	5	2.6	7498	26.86
3.2 mm (*)	C1b	1500	4	3.7	10980	37.28
	C2b	1500	7	4.2	13710	40.52
	C3b	1500	10	4.7	14710	49.30
	C4b	2000	4	4.2	12560	41.38
	C5b	2000	7	4.7	14460	47.75
	C6b	2000	10	3.7	13610	40.70
	C7b	2500	4	4.7	12730	45.24
	C8b	2500	7	3.7	10740	36.87
	C9b	2500	10	4.2	13550	37.69

(*) *Welding conditions and LSS mean values adapted from Pieta et al., “Optimization of Friction Spot Welding Process Parameters for AA2198-T8 Sheets” [20]*

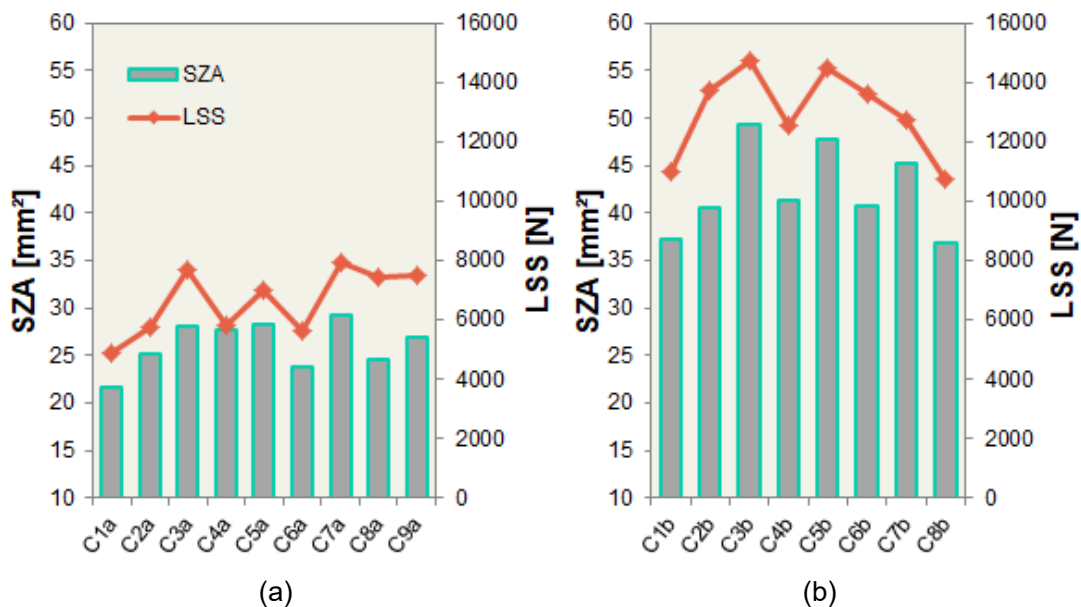


Figure 5.9 – Plots of stir zone area (SZA) and lap shear strength mean (*LSS*) values for Taguchi array welding conditions

All welding conditions for 3.2 mm-thick sheets studied by Pieta et al. [20] and listed in Table 5.5 exceed the minimum lap shear strength (5180 N) required for aeronautic applications according to AWS D17.2 [10] standard. This is also true for all conditions analyzed for the joining of 1.6 mm sheets, as discussed before.

A similar behavior between SZA and *LSS* can be clearly observed for both 1.6 and 3.2 mm-thick sheets, as presented in Figure 5.9. The conditions related to greatest values of SZA (29.18 mm² and 49.30 mm² for *C7a* and *C3b* conditions) match those ones associated to the greatest *LSS* values (7947 N and 14719 N for *C7a* and *C3b* conditions) for the two sets of experiments. Likewise, the smallest SZA measurements (21.68 mm² and 36.87 mm² for *C1a* and *C8b* conditions) are found in welds produced by the same combination of parameters that also leads to the lowest *LSS* values (4877 N and 10740 N for *C7a* and *C3b* conditions).

It is worth mentioning that the stir zone size is not the only factor that determines the *LSS* of joints: other aspects such as the hook effect, geometric defects (such as bonding ligament, voids, incomplete refill and lack of mixing) and heat input should always be considered. These other effects, however, may

have a smaller effect on *LSS* than *SZA*, as demonstrated by Castro et. al [47] about the geometrical feature's effects in AA2198 welds' lap shear strength. The authors point that there is no obvious correlation between the lap shear strength and the hook effect – determined by the “hook height” (*H*) feature – considering the analyzed joints, what may indicate a minor influence of *H* on *LSS*.

5.3.2 Statistical analysis of process parameters' influence on stir zone area

Similarly to the employed approach for the analysis of the effects produced by the variation of process parameters on *LSS* of welds produced from AA2198 1.6 mm-thick sheets, statistical techniques such as the Taguchi method and analysis of variance (ANOVA) can be useful resources for the investigation of welding parameters influence on joints' *SZA*. The response table of means given by the Taguchi analysis for *RS*, *WT* and *PD* considering *SZA* response for welds produced by sheets with 1.6 and 3.2 mm of thickness is presented in Table 5.6.

Table 5.6 – Response table of means for rotational speed (*RS*), welding time (*WT*) and plunge depth (*PD*) based on *SZA* response for 1.6 mm and 3.2 sheets

Level	RS [rpm]		WT [s]		PD [mm]	
	1.6mm	3.2mm	1.6mm	3.2mm	1.6mm	3.2mm
L1	24.96	42.37	26.15	41.3	23.33	38.28
L2	26.55	43.28	25.97	41.71	26.52	39.86
L3	26.85	39.93	26.25	42.56	28.51	47.43
Delta (δ)	1.89	3.35	0.28	1.26	5.18	9.15
Ranking	2		3		1	

Based on the highest listed values given by the Taguchi of 1.6 mm-thick sheets welds, the best response for each factor aiming highest values of *SZA* are reached when combining the highest levels of each parameters, L3 – i.e., *RS* = 1500 rpm, *WT* = 5 s and *PD* = 2.8 mm as defined in Table 4.2. Figure 5.10 presents the main effect plots of means for *RS*, *WT* and *PD* for *SZA*

(identified as thicker-and-darker lines) and the previously discussed in Section 5.2.2 *LSS* response (lighter lines). The best welding condition indicated by the statistical method when aiming maximized *SZA* responses matches the set of parameters pointed as the optimized process condition, *C10a*, for the best mechanical performance of the welds in terms of *LSS*. Furthermore, the condition expected to produce welds with smallest *SZA* according to the analysis is the same as the one related to the lowest *LSS* – *C1a*. Alongside the comparison of experimental *SZA* and *LSS*, Taguchi statistical analysis indication of best and worst performing welding parameters for *SZA* and *LSS* come again as evidence of a strong-and-positive relation between welds' stir zone size and resistance.

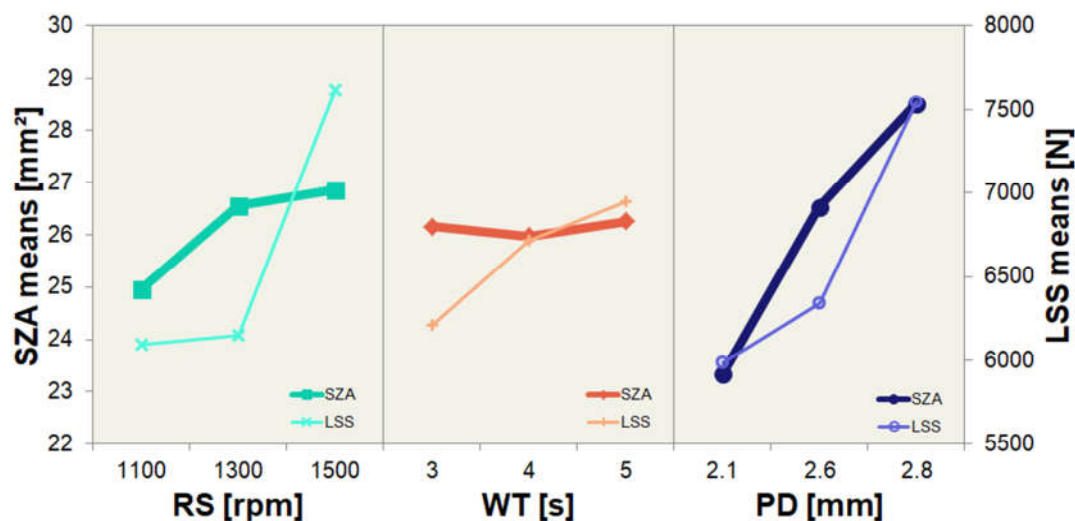


Figure 5.10 – Main effect plots of means for rotational speed (*RS*), welding time (*WT*) and plunge depth (*PD*) based on *SZA* and *LSS* for the thickness of 1.6 mm

It is observed in Figure 5.10 that the crescent variation of the levels for each factor for 1.6 mm-thick sheets produces a positive response on the stir zone increasing-in-area, except for *WT* between 3 and 4 s. Indeed, this is the parameter with the lowest response on the variation of levels: the delta-value of the analysis (Table 5.6) indicates that the variation of the levels among the studied interval produces a variation in *SZA* of 0.28 mm². On the opposite, *PD* is the most affected factor due to the progressive variation of its levels: delta-

values presented in Table 5.6 point that the variation from 2.1 of 2.8 mm produces a positive effect of increasing SZA in up to 5.18 mm².

Based on *LSS* results presented by Pieta et al. [20] on 3.2 mm-thick sheets (Table 5.5), the main effect plots for *LSS* and *SZA* responses were analyzed by the Taguchi method and are shown in Figure 5.11. Likewise verified for the thinnest sheet, the prediction of parameters – *RS*, *WT* and *PD* – aiming the highest *LSS* matches the best welding condition for largest *SZA* considering the selected process window: 2000 rpm, 10 s and 4.7 mm. For the thickest sheets, however, the optimized welding condition does not correspond to the combination of the highest levels of each parameter since the greatest *LSS* and *SZA* are found for the highest levels of both *WT* and *PD* combined with the intermediate *RS* level.

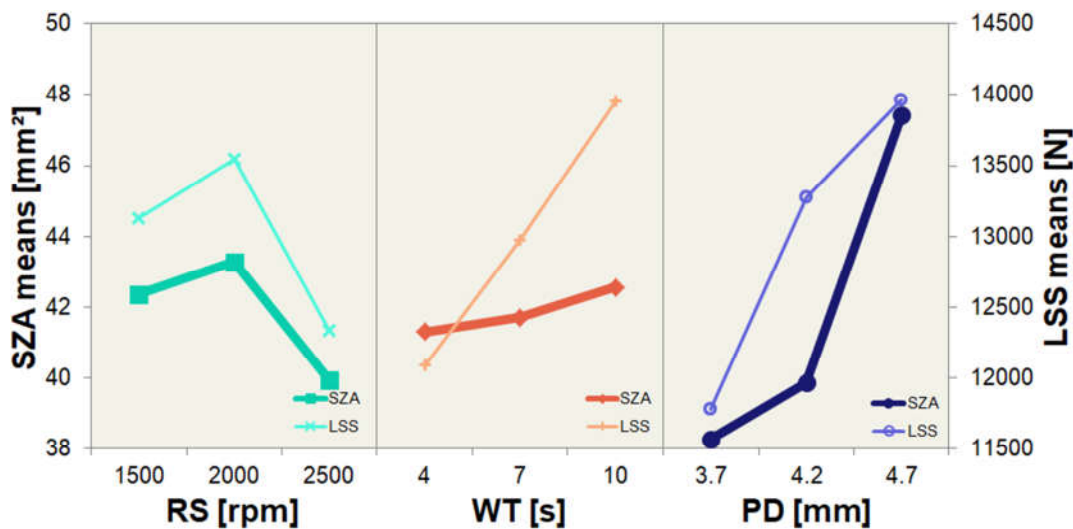


Figure 5.11 – Main effect plots of means for rotational speed (*RS*), welding time (*WT*) and plunge depth (*PD*) based on *SZA* and *LSS* for the thickness of 3.2 mm

The main effect plots for 3.2 mm-thick sheets presented on Figure 5.11 also indicate the effectiveness of the each factor in face of variations of its levels. It is interesting to note that, contrarily to the convergent response of *WT* variation on stir zone size and strength observed in 1.6 mm sheets, variations on *WT* levels produces different effects on *LSS* and *SZA*. For *LSS* responses, the variation of the levels associated to *WT* is ranked as the second most influent factor on *LSS* response based on the difference between highest and

lowest *LSS* means. Considering *SZA* responses, however, the variations on *WT* levels produces minor effect in welds' stir zone size according to the processing window selected in this study – variations from the 4 s to 10 s are indicated to increase only 1.26 mm² in *SZA*, versus 9.15 mm² increasing-in-area associated to the shift in *PD* levels. Although the already-described correlation between *SZA* and *LSS*, the discrepant behavior observed in these two responses for *WT* can be associated with several other factors which affects welds' strength, like geometric defects such as incomplete refill, bonding ligament and voids.

Like it was already observed on the 1.6 mm-thick sheets, *PD* is the factor responsible for the largest variation on *SZA* and *LSS* for both sheet thicknesses, producing the effect of incrementing the stir zone cross-section area in up to 9.15 mm² according to delta-values listed in Table 5.6. Furthermore, based on the steepness of the second portion of the slope of Figure 5.11, the variation of levels from 4.2 to 4.7 mm is the most influent effect on *SZA* response.

The main effect plots for joints' produced by 3.2 mm-thick sheets presented in Figure 5.11 also shows the intermediate effect of *RS* in comparison with *WT* and *RS* for both *LSS* and *SZA*. It is interesting to note the existence of a negative slope between 2000 and 2500 rpm – from levels 1 to 2 –, which indicates a considerable depreciative influence of *RS* on *LSS* and *SZA* responses. This limitation of rotational speed's positive contribution to the responses will be explored in the next section.

Figure 5.12 shows the influence of individual parameters (*RS*, *WT* and *PD*) given by ANOVA approach (analysis of variance) for welds produced by sheets with 1.6 and 3.2 mm of thicknesses. *PD* is remarkably the ultimate influencing factor in *SZA*, representing more than 80% of contribution percentage in welds of both thicknesses. Furthermore, it is noted that *RS* and *PD* are the two factors in control of *SZA* variance, representing altogether more than 95% of I% on welds' stir zone size for the two different sheets. On the other hand, *WT* is found as an irrelevant factor in welds' stir zone area since it represents the lowest and near-to-zero percentage of contribution (0.2% and 1.2% for thicknesses of 1.6 and 3.2 mm respectively). Besides, *WT*'s influence

in *SZA* variation is even smaller than the error (3.9% and 2.9%), which confirms the statistical insignificance of the factor.

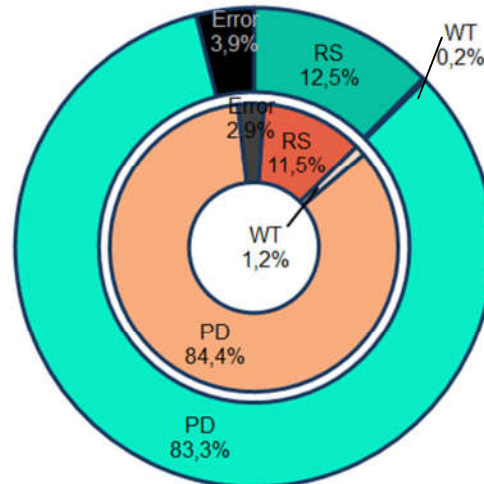


Figure 5.12 – Influence of individual parameters – rotational speed (*RS*), welding time (*WT*) and plunge depth (*PD*) – on the variance of *SZA* given by ANOVA for different sheet thicknesses: 1.6 mm (in teal) and 3.2 mm (in orange)

The analysis of variance for *SZA* (Figure 5.12) based on the welding conditions presented in Table 5.5 for both 1.6 and 3.2 mm-thick sheets indicate a very similar effect of each parameters regardless the thickness of the sheet. This fact can be evidence that the conditions which determine the metallurgical phenomena during the welding process are similar for sheets whose thickness are thin enough in order to guarantee a heat transport though this dimension which is not time-limited. According to these results, sheets up to 3.2 mm-thick present a similar dependence on each welding parameter – *RS*, *WT* and *PD* – on joints' microstructural development.

5.3.3 Effects of *RS* and *PD* on stir zone development

A close look to stir zone's geometrical aspects allows the understanding of the role played by *RS* and *PD* on the development of welds' stir zone – physical and metallurgical phenomena – and the influence on its size. In this manner, these geometrical features are highlighted on the colored stir zone region on the cross-section of a typical 3.2 mm-joint presented in Figure 5.13.

As demonstrated before, the influence of parameters in the welding of 1.6 mm and 3.2 mm sheets is the same, and the analysis of the SZ formation in joints produced by the thicker sheets can be assumed as analogous to the 1.6 mm sheets. Since the stir zone is defined as the portion of the sheets' material which experiences dynamical recrystallization due to deformation and heat caused by the friction welding process, it can be interpreted as a function of the product between its width (w) and height (h). Note that w corresponds to the sum of sleeve diameter (D_{sleeve} – constant and corresponding to 9 mm) and a delta value (Δw), defined as an indicator for the process-parameter-related (RS , WT and PD) fraction of SZA . Similarly, h is a function of the sum between the selected PD (process variable) and a height-related delta value (Δh).

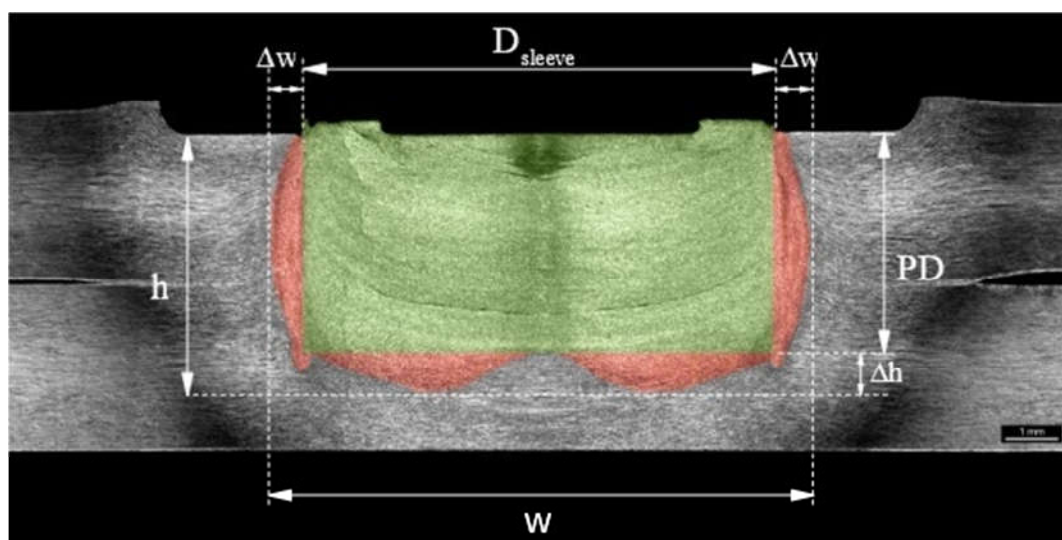


Figure 5.13 – Macrograph of a typical cross-section of a 3.2 mm-thick sheets joint with indication of geometrical variables of SZ. In green, portion of SZ determined by PD and sleeve diameter (D_{sleeve}). In red, SZ's region associated with metallurgical phenomena and ruled by rotational speed RS , WT and PD

The green area of Figure 5.13 represents the portion of SZ's material comprised between the sleeve path during the plunging and it is proportional to the PD and D_{sleeve} . According to previous discussion based in Figure 5.12, PD plays a major role on SZA variation in a manner that each variation on depth impacts both h and w dimensions. Variations on PD directly implicates in a proportional-to-sleeve-diameter variation in SZA simply for the plunge tool itself.

Besides the obvious impact of PD on the development of the green portion of the stir zone, each increment on the penetration produces a deformation much larger than PD in h , influencing the variation of the SZ's red area in Figure 5.13. The major influence of PD (87%) in the variance of height can be observed in Figure 5.14. Since the increasing of sleeve penetration in the bottom sheet produces a larger volume of plasticized material due to the larger frictional heat input – as a result of sleeve rotation and axial plunge –, PD variation also influences the Δh dimension and consequently SZA. Shen et al. [24] present macrographs of cross-sections of AlMgSi joints produced by the stop-action approach, where the evolution of the welding process in different steps can be observed. These are useful results to the understanding of the effect of PD in the evolution of h since even small increments on the plunging from step to step produces a notorious effect on SZ's height.

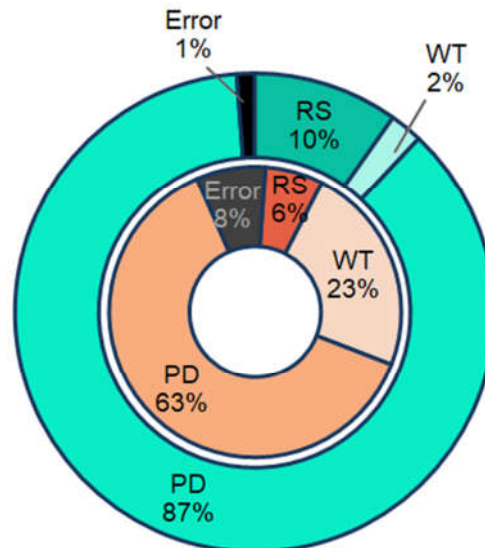


Figure 5.14 – Influence of individual parameters – rotational speed (RS), welding time (WT) and plunge depth (PD) – on the variance of h (in teal) and w (in orange) given by ANOVA

The great importance of PD in the SZA variation is also extended to its effects in w dimension – even if with a minor impact when compared to its contribution to height. According to ANOVA (Figure 5.14), the variation of PD is responsible for 63% of the stir zone's w -value. Similarly to the plunge depth influence observed for the h dimension, the macrographs presented by Shen et

al. [24] using the stop-action technique shows that the plasticized material from the bottom sheet is gradually extruded to the interface region between sleeve's outer interface and the sheet material as the sleeve penetrates into the workpiece. This material flow is a consequence of both rotational and axial displacement. The deeper the sleeve penetrates, the larger is the volume of plasticized material extruded to the sleeve's outer interface, leading to gradually larger values of w .

The influence of tool rotational speed in Δw and Δh can be directly associated to heat input since it is responsible for the high strain rate and high temperature at the fraction of stir zone area adjacent to the sleeve's outer surface, determining the dynamic recrystallization at the remarked-red region in Figure 5.13. Assuming a friction welding process with no energy loss, i.e., all mechanical energy input is transformed into thermal energy by the effect of torque, the heat input can be summarized as

$$Q_{app} = \sum_{n=1}^n T\omega\Delta t \quad (5)$$

where Q_{app} is the thermal energy resulted from the process, T is the torque associated with the tool, ω is the tool angular velocity and Δt is the process time [48].

In this manner, the increasing in RS – or ω – increments the temperature during the welding due to the frictional contact between sleeve and the material of the sheet. Since variations in temperature affects the viscosity of a material, temperature rise is responsible for a reduction in the plasticized material viscosity which leads to a decrease in torque and consequently a decrease in the heat input. This phenomenon is reported by Su et al. in FSSW of AA6061 and AM50 sheets [49]. Once high RS produces a critical condition of plasticity and torque, increments in RS produces an effect of reduction in heat input which produces diminished returns for the dynamical recrystallization occurrence. This phenomenon can be observed in the Taguchi analysis of 3.2 mm welds (Figure 5.11), where a reduction in SZA is expected in the

interval from 2000 rpm to 2500 rpm. Note that the same effect is found for *LSS*, since *SZA* and *LSS* presents some correlation as previously demonstrated. Similar effects of critical *RS* on refill friction stir spot welding joints' *LSS* are indicated by Campanelli et al. [26] and Tier et al. [48]: in both studies, higher values of *RS* produces a detrimental effect on heat input, implicating on joints' strength reduction.

5.4 Tool wear investigation

5.4.1 Lap shear strength along the welding cycles

The evaluation of the effects of tool wear on AA2198-Ti 1.6 mm-thick sheets welds' resistance along the cycles was based on lap shear strength tests executed in a number of welding cycles intervals. Figure 5.15 presents the plots of these *LSS* main values³ along the welding cycles in which each point represents a point of measure between intervals. The analysis of the influence of tool wear on *LSS* along its life-cycle was divided into three different stages according to the number of welds, determined by the points of tool disassembly from the machine for profilometry measurement of pin and sleeve.

³ *LSS* mean values and standard deviation (considering that the tests were carried out in triplicates) along the number of performed welds are listed in Appendix D.

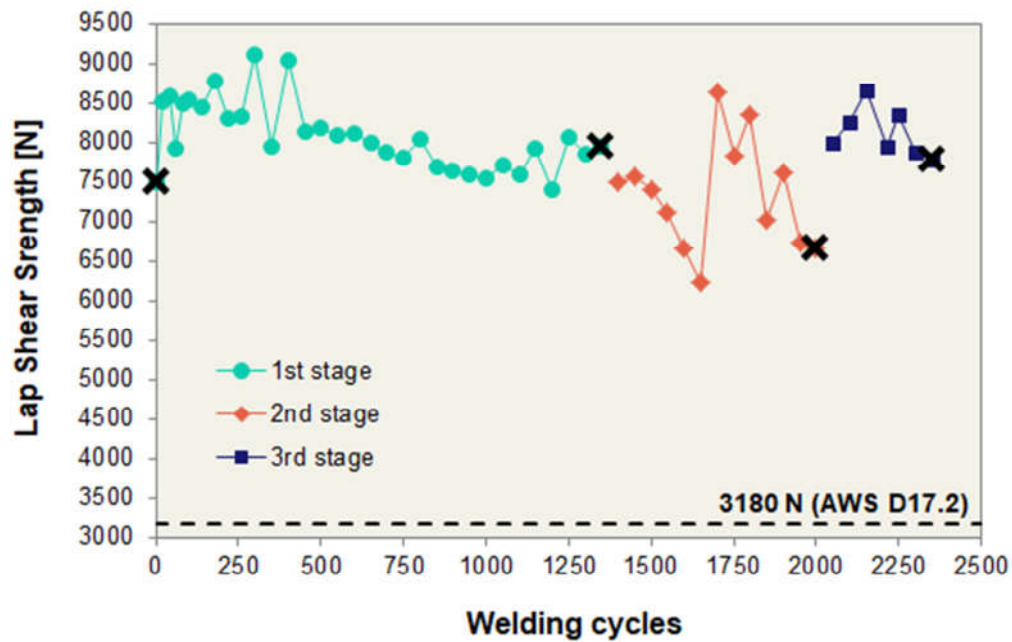


Figure 5.15 – Joints' strength behavior along welding cycles: *LSS* mean values measured between intervals along the welds, showing three different stages of the investigation and points of tool profile measurement (black-crossed points)

A trend pointing to the reduction in *LSS* means along the welding cycles can be seen in Figure 5.15. Nonetheless, all joints performed along the 2350 welding cycles were shown to greatly exceed AWS D17.2 [10] requirements for aeronautic applications (3180 N), since the minimum *LSS* mean value found in the study is 6231 N. This indicates that tool lifecycle could be significantly higher than the limits considered in this evaluation. However, other criteria – yet to be studied by the RFSSW community – must be considered in order to determinate tool lifecycle: not only the quality of produced welds along the cycles (fatigue resistance, in addition to *LSS* results presented in this work) but also the mechanical properties of the tool such as number of welding cycles before fracture.

First stage

The first stage of evaluation (Figure 5.16) is related to the 1350 initial welds. Because of the lack of research reports on the topic, the intervals of lap shear strength specimen production and testing were arbitrarily selected,

starting from a conservative number of welds which was progressively increased until an ideal measurement distance aiming the optimization of the experiment – considering a balance of productivity and data resolution. The initial *LSS* points of strength measurements were arbitrary defined between intervals of 20 welds (from the initial to the 100th weld), subsequently modified to 40 welds (between 101th and 300th welds) until the 50-welds-sized-interval was taken as the standard distance between the production and mechanical testing of specimens.

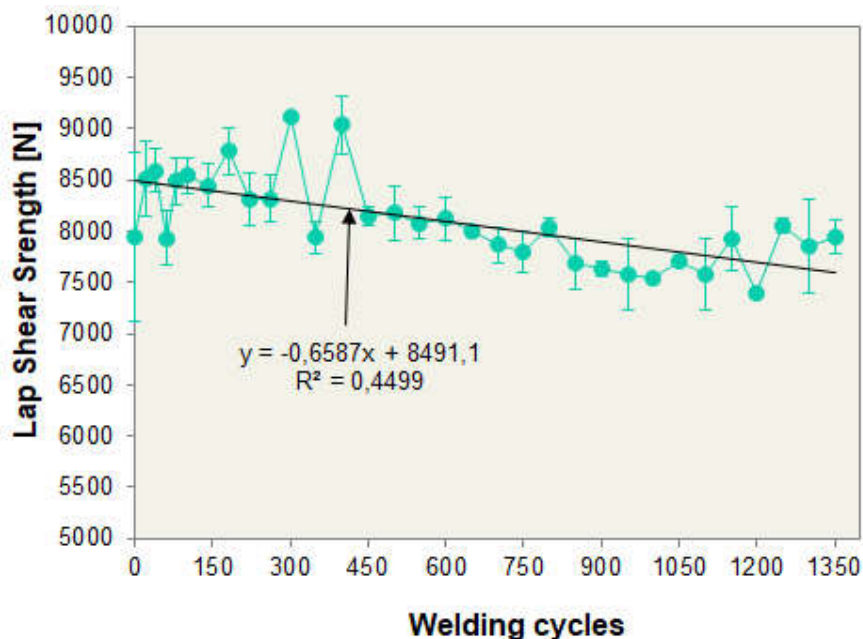


Figure 5.16 – *LSS* mean values with associate standard deviation and linear fit along the first stage of evaluation

The upper limit of the first stage was defined based on the statistical prediction of lap shear strength. The linear fit⁴ of the *LSS* mean values can also be observed in Figure 5.16, and it was the basis to estimate the trend of strength reduction for each new point added to the plot along the increasing of welding cycles. Based in this statistical prediction, the criterion for profile measurement of the tool was defined as a reduction of around 10% in *LSS*.

The linear regression model approach was initially idealized not only as a criterion for selecting the number of welding cycles for tool disassembly and dimensional characterization, but also to determinate tool's life cycle. Nonetheless, after analyzing the first stage's dataset, it was verified that the

linear fitting approach was not appropriate for this matter. The coefficient of determination (R^2) values associated with a particular dataset may be an indicative of the proportion of the variability explained by the fitted model, in a manner that it varies from 0 to 1.0 and $R^2 \approx 1.0$ represents a perfect fit [50]. The linear fit associated with the first stage of evaluation presents a $R^2 = 0.4499$, which is an indicative that the linear regression model is not effective statistical method to predict the behavior of *LSS* along the welds with the proper accuracy required for estimating the tool life cycle due to the considerable variability of the results.

Second stage

The second stage of evaluation is associated with the performance of 1351 to 2000th welding cycles. Figure 5.17 shows an enormous variance of *LSS* means – from the 6231 minimum to 8628 N maximum, almost 40% –, which denotes a very different variance behavior that the one found on the first stage. No obvious trend on *LSS* is observed: from 1400 to 1650 welds it is observed a tendency of strength reduction along the welds, followed by a great positive shift in *LSS* mean values around 1700 welds and again a trend in *LSS* reduction from 1700 to 2000 welds. Furthermore, considerably high standard deviation up to 30% the mean value of the sample (found on 1950th triplicate testing), which is, again, a very unlikely behavior when compared with the previous stage, as observed in Figure 5.18.

⁴ Linear fit values based on *LSS* means for the first stage of measurement are listed in Appendix E.

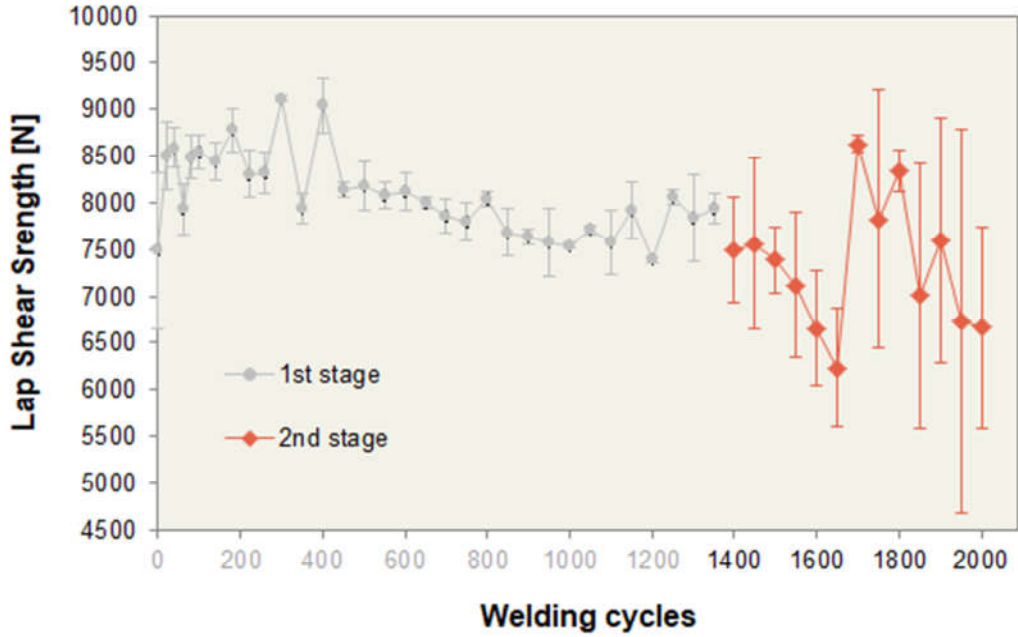


Figure 5.17 – LSS mean values with associate standard deviation for first and second stages of evaluation

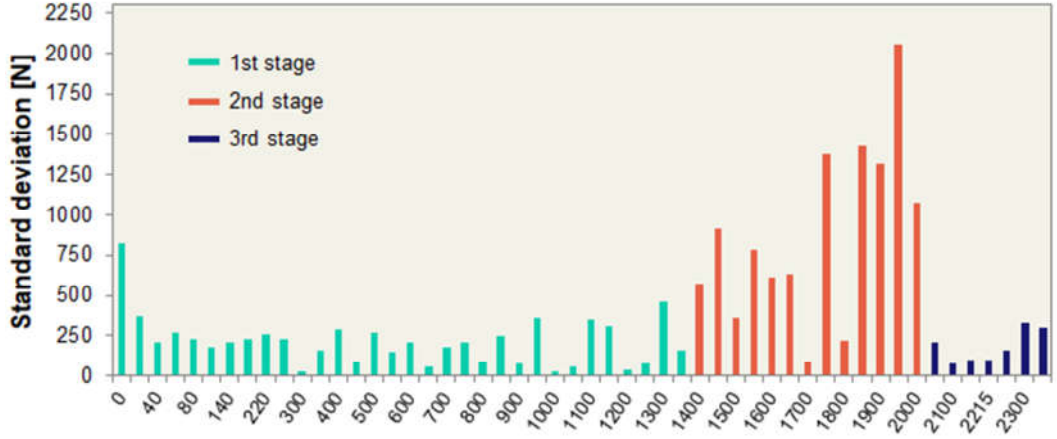


Figure 5.18 – Standard deviation of each LSS mean value

The strong discrepancies between the LSS behavior among the first two stages of evaluation was investigated in order to determinate their origins. Therefore, the second part of the experiments was interrupted after the completion of 2000 welds in order to evaluate the wear effects on the tool and correlate with this possibly errant behavior. The evidence of a new wear

mechanism not previously observed on sleeve at the first stage of evaluation is demonstrated in Section 5.4.2.2.

Third stage

The third stage of evaluation was performed to verify the hypothesis of external sources of problems that could lead to the great variance and standard deviation, such as the tool assembling issues.

The standard deviation plots of each *LSS* triplicate along the welding cycles presented in Figure 5.18 shows that from 2050 to 2350 weld cycles – bars identified as blue – standard deviation levels match the range found in the first stage of evaluation (teal bars). Furthermore, Figure 5.19 shows that the variance of the *LSS* mean values related to the 350 last welding cycles presents similarity with the variance of plots found in the first stage. These similarities indicate that the reassembly of the tool after the second stage was responsible for the return of the expected statistical behavior that matches the 1350 first results; hence, confirms that the errant behavior observed between the 1351 and 2000 welds are most probably associated to tool assembly issues.

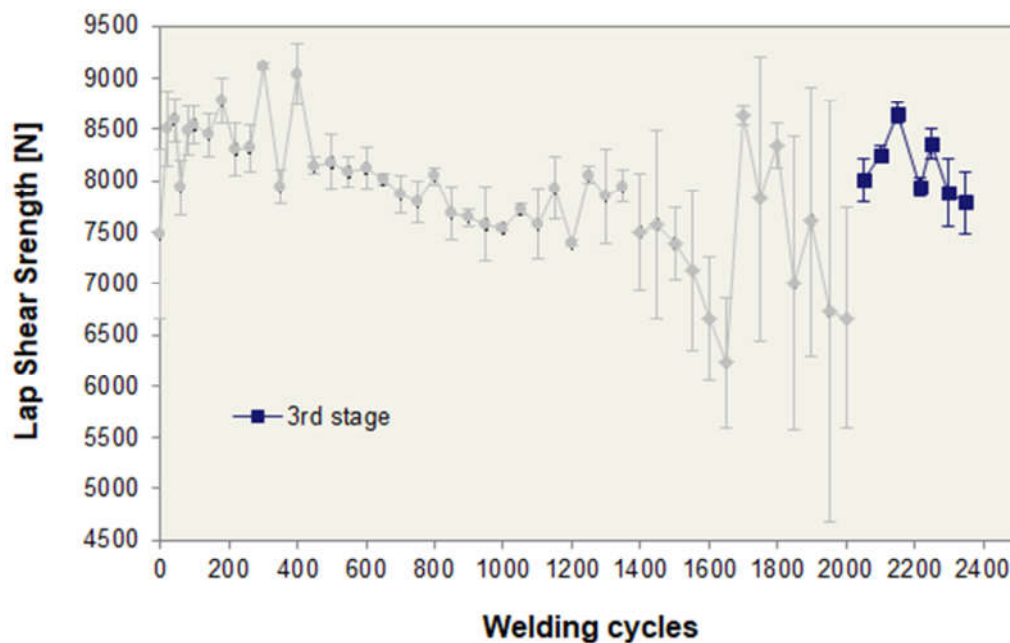


Figure 5.19 – *LSS* mean values with associated standard deviation highlighting the third stage of evaluation

5.4.2 Wear effects on tool dimension

The dimensional evaluation of the effects of wear on RFSSW tool was performed considering the frictional parts of the tool – sleeve and pin – in order to verify the modifications on their profiles and relate them to the effect of wear.

5.4.2.1 Pin wear

The wear on pin can be observed based on the visual aspect of the tool and profile dimensional analysis. Photographs (Figure 5.20) and profilometry-assessed measurement (Figure 5.21) were performed on the as-received pin (maiden tool) and after 1350, 2000 and 2350 welding cycles, as exposed in Section 4.6.

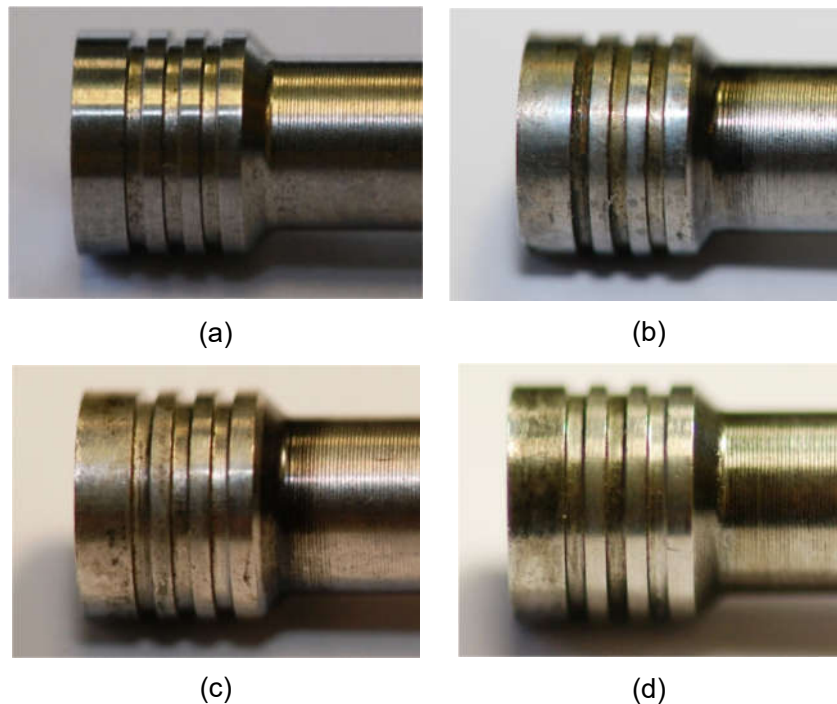


Figure 5.20 – Visual aspect of the pin along welding cycles: (a) as-received pin condition (b) after 1350, (c) 2000 and (d) 2350 welds performed.

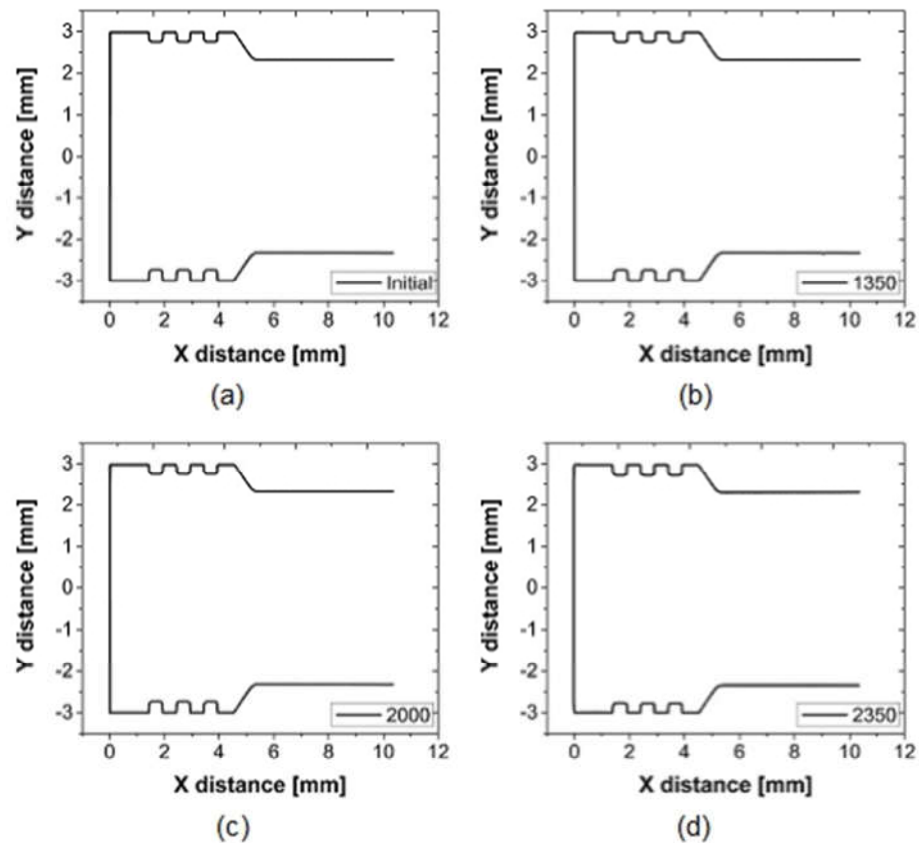


Figure 5.21 – Pin's profile along welding cycles: (a) as-received pin condition (b) after 1350, (c) 2000 and (d) 2350 welds performed.

It is possible to observe that the pin profile did not suffer considerable dimensional changes along all 2350 welding cycles analyzed in this study. Furthermore, in addition to the dimensional assessment, the weight measurement of the pin in each point of evaluation (Table 5.7) may allow inference that pin is not considerably affected by the wear effects: the pin weight reduction after 2350 welding cycles, in comparison with the before welding condition, was of 0.006 g or 0.028% wt.

Table 5.7 – Pin weight measurement at the different points of evaluation and their weight reduction relatively to the as-received pin condition (in mass and percentage)

	Pin weight (g)	Pin weight reduction (g)	Pin weight reduction (%)
As-received	21.3670	-	-
After 1350 welds	21.3643	0.0027	0.013
After 2000 welds	21.3603	0.0040	0.019
After 2350 welds	21.3543	0.0060	0.028

These results are in accordance with the expected absence of wear on the pin and is related to the sleeve-plunge process variant (Figure 3.3a) used in this analysis. Note that most critical frictional condition of the pin is achieved when pushing the displaced material – due to sleeve plunging – back into the sheets, which appears as a not severe enough condition for producing wear effects on the pin especially when compared with the high shear rates and tool temperature as those working on sleeve's surface.

5.4.2.2 Sleeve wear

Similarly as performed for the pin, the sleeve was disassembled from the welding machine and measured by the profilometer at the same four points of measurement presented before. Figure 5.22 presents photographs of the sleeve after cleaning procedure. Furthermore, the profile measurement at the referred points is shown in Figure 5.23.

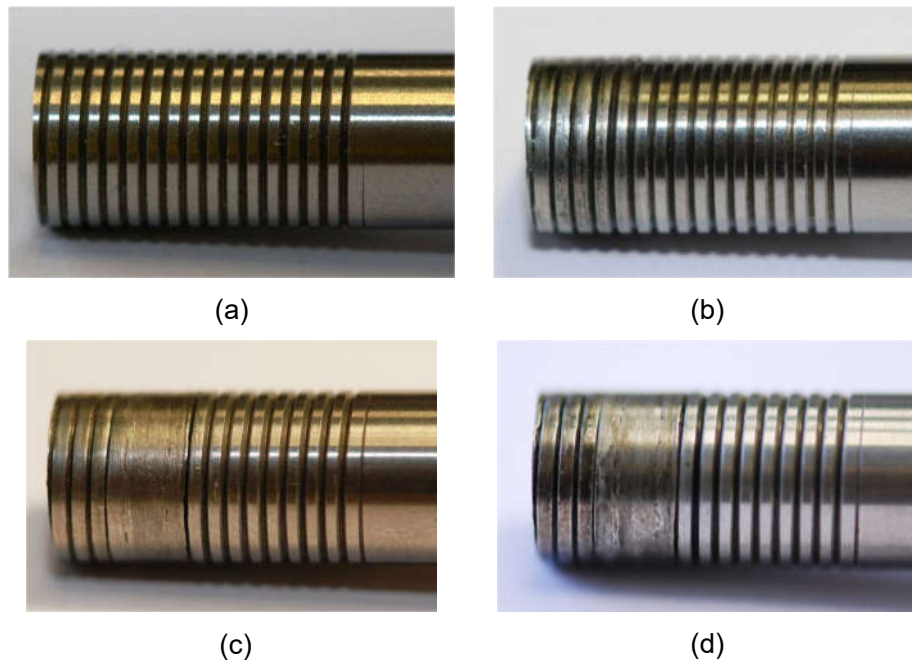


Figure 5.22 – Visual aspect of the sleeve along welding cycles: (a) as-received pin condition (b) after 1350, (c) 2000 and (d) 2350 welds performed.

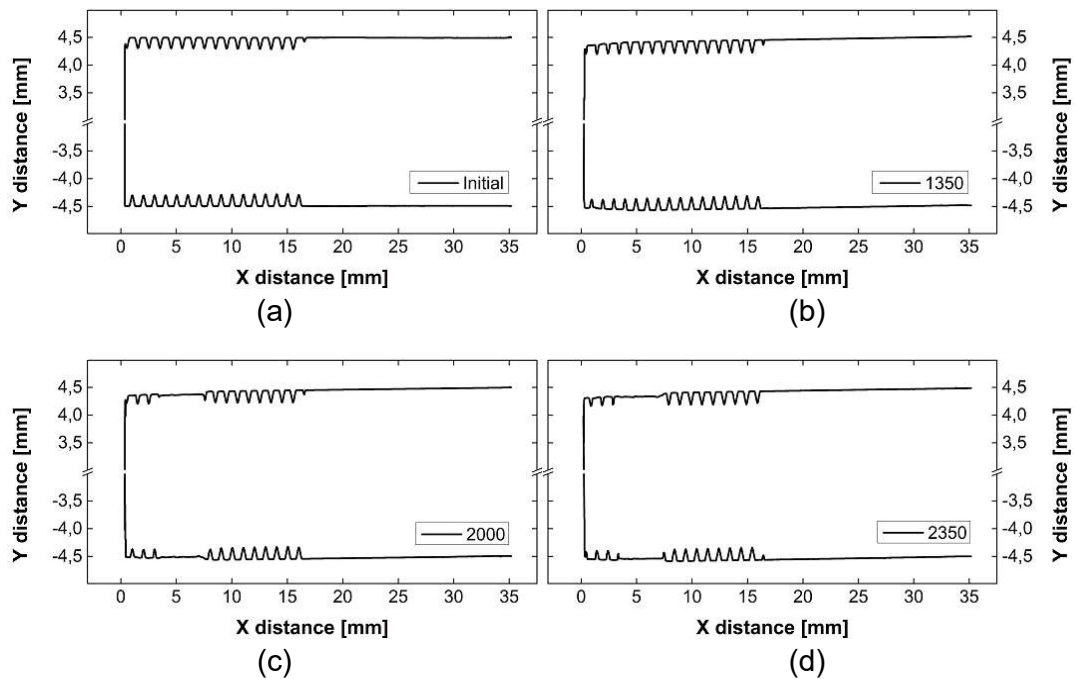


Figure 5.23 – Sleeve's profile along welding cycles: (a) as-received pin condition (b) after 1350, (c) 2000 and (d) 2350 welds performed.

Unlike what is identified on pin's aspect and profile along the welding cycles, it is noted that the threaded adjacent-to-the-tip region of the sleeve was impacted by wear along the number of produced welds. Figure 5.22 and Figure 5.23 show the development of two different types of wear effects according to the region of the tool and stage of investigation for the 2350 welding cycles evaluated.

Figure 5.24 remarks the result of wear effect on the sleeve at the first stage of the evaluation (between the initial and 1350th welds). It is possible to see the effects of wear: the external diameter at the tip of the tool suffered a reduction of 0.105 mm. Particles of tip were removed from the tool – a total of 0.0234 g according to Table 5.8 –, mostly at the main region in frictional contact with the plasticized sheet material considering the wear effect along around 3 mm from the tip, 0.9 mm further than the plunge depth (2.1 mm). Furthermore, as a result of the first stage of welding cycles it was verified a sleeve's material loss (0.109%, Table 5.8) almost nine times the pin weight reduction (0.013%, Table 5.7) in terms of percentage, indicating that the wear effects are considerably more relevant on sleeve rather than the pin. It should be noted that sleeve features such as threads groove depth and thread pitches did not suffer dimensional alterations, except for the outer diameter reduction at the edge of the tool.

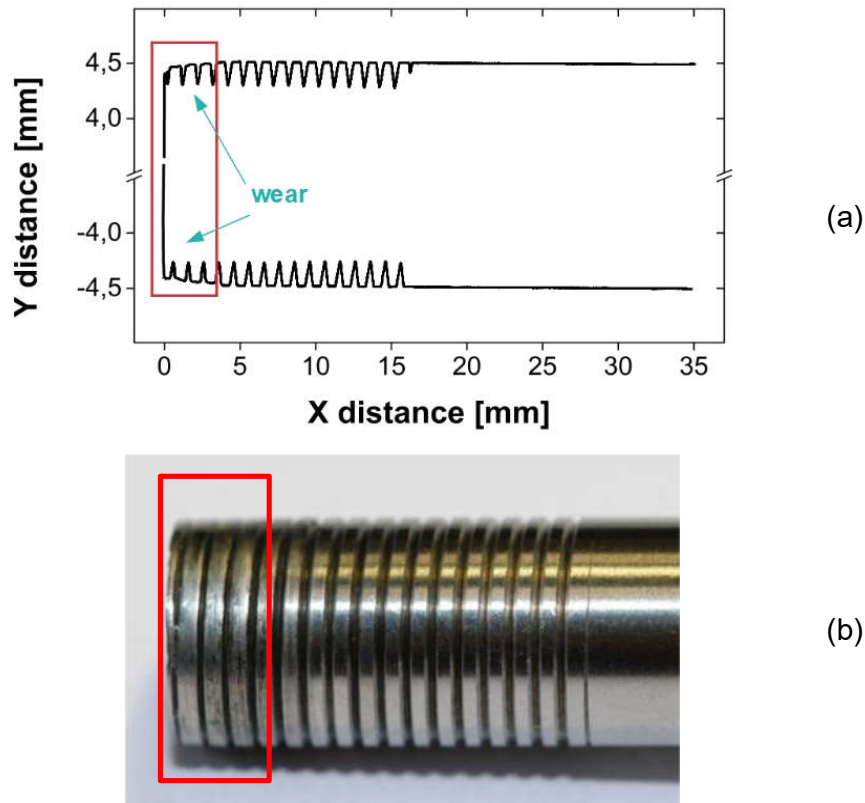


Figure 5.24 – Effects of wear on the sleeve: (a) sleeve profile and (b) visual aspect of the sleeve after 1350 welding cycles

Table 5.8 – Sleeve weight measurement at the different points of evaluation, weight reduction relatively to the as-received pin condition (in mass and percentage), and average rate of weight loss in each stage

	Weight (g)	Weight reduction (g)	Weight reduction (%)	Average rate of weight loss (10^{-4} g/weld)
As-received	21.4608	-		
After 1350 welds	21.4374	0.0234	0.109	0.173
After 2000 welds	21.3924	0.0684	0.319	0.692
After 2350 welds	21.3394	0.1214	0.566	1.514

A study of Wang et al. [51] investigate the wear mechanisms in friction stir welding tools. Using similar techniques as the applied in this current work, the authors indicate that this weight loss at the tip of the friction stir welding tool

is related to adhesive wear mechanism. This hypothesis can be endorsed by the presence of trapped-between-threads and adhered-to-H13-surface aluminum as showed in Figure 5.25. This Al/H13 adhesive junction can break under insufficient heat (at the start of the welding cycle), when the aluminum is not in a plasticized form. The succession of new Al/H13 adhesive junction formation and ruptures results in a worn sleeve surface. It should be noted that wear mechanisms in friction welding tools' studies are quite complex and are beyond the aims of this dissertation. Thus, future works for the investigation on this topic are strongly recommended.

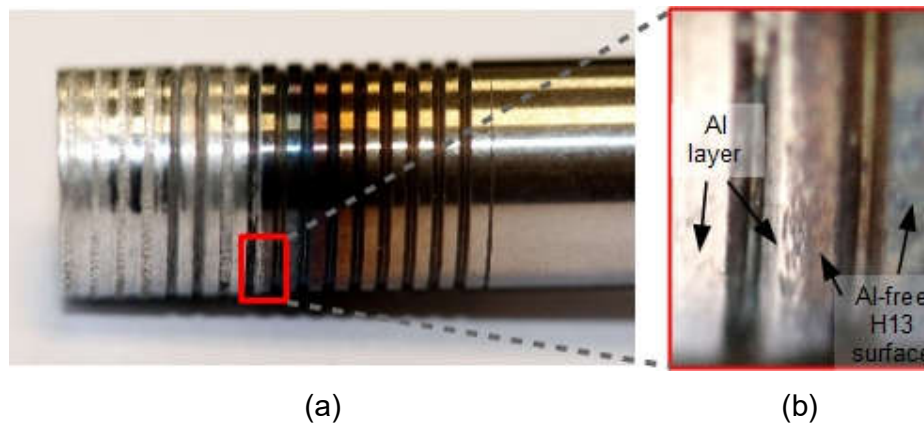


Figure 5.25 – (a) Visual aspect of sleeve after the first stage of evaluation showing the presence of aluminum adhered to H13 surface and trapped between the threads. (b) Detailed view of the sleeve's aluminum-covered region end (left) and start of the aluminum-free region (right).

The changes in sleeve profile and aspect associated to the second stage of the evaluation presented in Figure 5.26 indicate two different effects caused by the wear. The region highlighted in teal points to a similar behavior of material loss from the tip of the sleeve identified on the first stage of evaluation, the adhesive wear mechanism, which persists in the interval between 1350 and 2000 welds. At the end of the second stage, however, a different region also affected by the wear (with the orange contour) can be observed, adjacent to the eroded region. Furthermore, the sudden increasing in the average rate of weight loss (0.692×10^{-4} g/weld) compared to the first stage

(0.173×10^{-4} g/weld) may be an indication of adhesive wearing on this second worn surface of the tool.

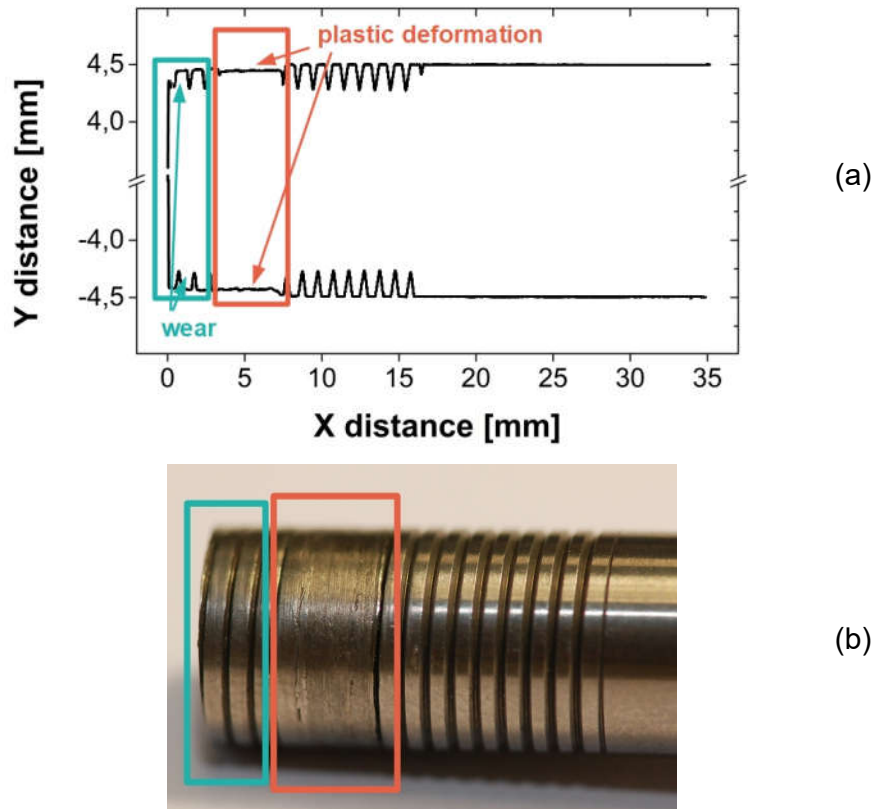


Figure 5.26 – Effects of wear on the sleeve: (a) sleeve profile and (b) visual aspect of the sleeve after 2000 welding cycles.

The effect of wear on the region pointed in orange is unmistakably distinct from the one caused exclusively by the frictional contact between the edge of the tool and the welding material. Note that this profile change appears at the same interval of welds in which the greatest variations on *LSS* means and considerably high-and-progressively-crescent standard deviation occur. First, it occurs in a different region, starting around 2.8 mm-distant from the tip and remaining through the length of approximately 5 mm. Moreover, the observation of Figure 5.26 indicates that in addition to the adhesive wear mechanism at the tip of the sleeve (region remarked in teal), another wear phenomenon involved in this profile modification can be interpreted as mostly associated to macroscopic plastic deformation evidenced by the reduction in sleeve outer diameter and the disappearance of threads in the region (indicated

in orange). Since this dimensional modification is observed after the first reassembly of the tool in the welding machine, the appearance of this new wear phenomenon might be related to issues on tool assembly, such as a possibly sleeve misalignment.

A correlation between the sleeve affected by wear after the second stage of measurement and the clamping ring (Figure 5.27) can be helpful to understand the cause of this second type of wear. The progressive wear in the tip of the sleeve allows the growing of a slack between clamping ring inner surface and the worn sleeve outer interface which traps the sheet material extruded upwards due to the sleeve plunging into the material. The evidence of this growing-in-size cavity can be observed along the presence of flash on the macrographs. A representative cross-section indicating the presence of the flash is presented in Figure 5.28. Note that the greater the dimensional alterations in sleeve, the higher the volume of trapped material and higher flow of plasticized material, which leads to progressive bigger surfaces affected by the wear – reaching sleeve regions away from the plunged surface and in contact with clamping ring.

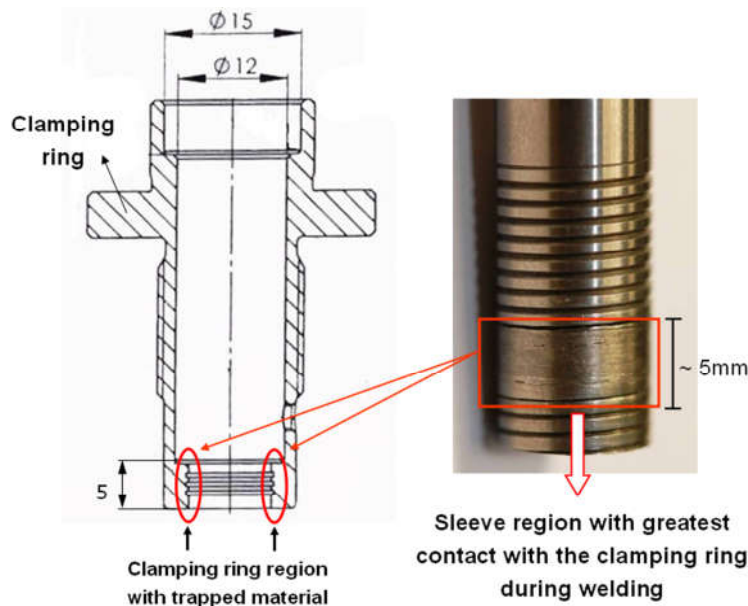


Figure 5.27 – Schematic representation of clamping ring indicating the region in frictional contact with sleeve matching the plastic deformed region of sleeve after 2000 performed welds.

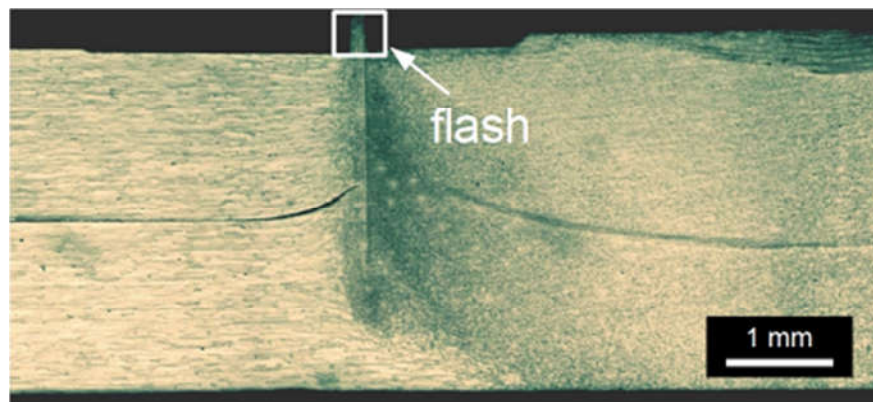


Figure 5.28 – Presence of flash in a typical weld indicating the increasing of a slack between clamping ring's inner surface and sleeve's outer surface

It should be mentioned that, additionally to the growing-in-size cavity effect associated to the wear on the sleeve, the presence of aluminum trapped on the inner surface of the clamping ring observed in Figure 5.29 indicates that this non-rotational component of the tool also experiences wear along the welding cycles and contributes to the progressive increase in tolerance between the parts. Unlike the pin, that suffers no wear due to the reduced frictional contact with the aluminum present between its interface and the sleeve (since both parts rotate with the same speed), the effect of wear on clamping ring can be much more aggressive since the relative velocity of the aluminum flow is proportional to sleeve's rotational speed considering that part is a stationary component. The study of wear on clamping ring in future works is strongly recommended.



Figure 5.29 – Trapped aluminum on the clamping ring inner surface

Finally, the effects of wear on tool profile and visual aspect resulting from the third stage of evaluation are presented in Figure 5.30. There is no evidence of further macroscopic plastic deformation likewise the observed in the second stage, since the shape of profile measurement after 2000 and 2350 welds are very similar – except for the increasing of wear effect observed in the tip of the sleeve. Furthermore, the absence of the second wear mechanism previously identified indicates that the *LSS* mean values along the third stage of measurement presented again a small variability and a decreasing-with-the-welding-cycles trend as observed in the initial stage, additionally to smaller standard deviation values comparatively with the previous stage.

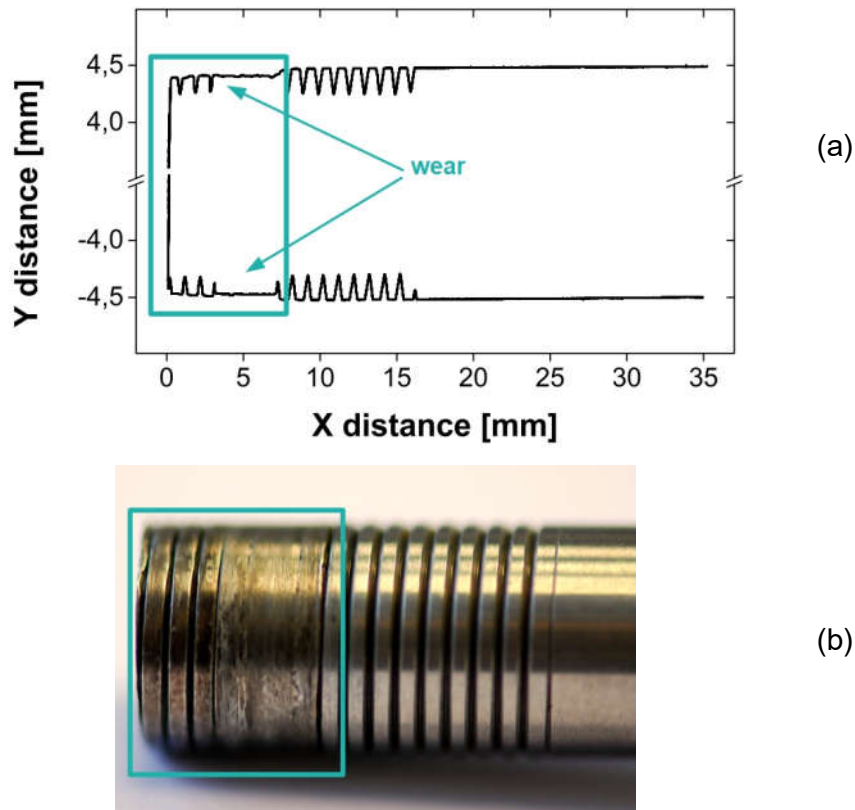


Figure 5.30 – Effects of wear on the sleeve: (a) sleeve profile and (b) visual aspect of the sleeve after 1350 welding cycles

Although no macroscopic plastic deformation was observed in this stage, the adhesive wear mechanism, continued to occur most probably at the whole worn surface, since the sleeve weight loss rate in this interval between 2000

and 2350 (1.514×10^{-4} g/weld) is considerably higher than the one observed in the first stage of measurement, when only the tip of the tool was affected by the erosion.

5.4.3 Effects of tool wear in welds' microstructural features

As previously discussed, the wear effects on sleeve are associated with a trend in reduction of *LSS* means along the welding cycles (Figure 5.15). In this way, an investigation about the modifications of welds' microstructural features – such as stir zone area and inclusions – along the welding cycles can be helpful to shed some light on the metallurgical effects of the tool wear on joints' and how it affects their mechanical strength.

The investigation of microstructural modifications of joints along welding cycles took place based on the cross-sections analysis of welds produced during the first stage of evaluation since the *LSS* results associated to the interval between 1 and 1350 cycles indicate a more consistent variance along the welding cycles as well as the presence of only the adhesive tool wear mechanism. In order to optimize the metallographic procedures, macrographs were prepared and analyzed in intervals of 40 welds for the first 80 welding cycles aiming a better resolution of these initial welds, and it was subsequently increased to the distance of 200 welding cycles between each macrograph preparation, resulting in representative images⁵ of 1, 40, 80, 220, 400, 600, 800, 1000 and 1200 performed welding cycles.

Stir zone area

In Section 5.3.1, the correlation between *SZA* and *LSS* was demonstrated for overlapped joints produced by the RFSSW of 1.6 and 3.2 mm-thick AA2198 sheets. The investigation based on *SZA* approach was performed in order to verify if the dimensional changes suffered by the sleeve

⁵ The cross-sections macrographs of samples along the welding cycles can be found in Appendix C.

are enough to induce any reduction in welds' SZA, and if these geometrical modifications in both tool and SZA are related to *LSS* reduction.

Table 5.9 lists the *LSS* and SZA means for the selected points of analysis. Figure 5.31 shows the plots of both SZA and *LSS* means representing the points of analysis of these welds' features along the welding cycles. A clear relation between area and strength is observed, which endorses the hypothesis that the modification of the external diameter in the tip of the sleeve produces an effect in stir zone area.

Table 5.9 – Mean of experimental results for lap shear strength test (*LSS*) and stir zone area (SZA) for selected points of measurement along welding cycles

Sample	Welding cycles	SZA	<i>LSS</i>
A1	1	27.89	7937
A40	40	28.31	8588
A80	80	29.10	8489
A220	220	28.92	8311
A400	400	28.90	9038
A600	600	28.79	8122
A800	800	28.83	8039
A1000	1000	28.78	7542
A1200	1200	28.61	7394

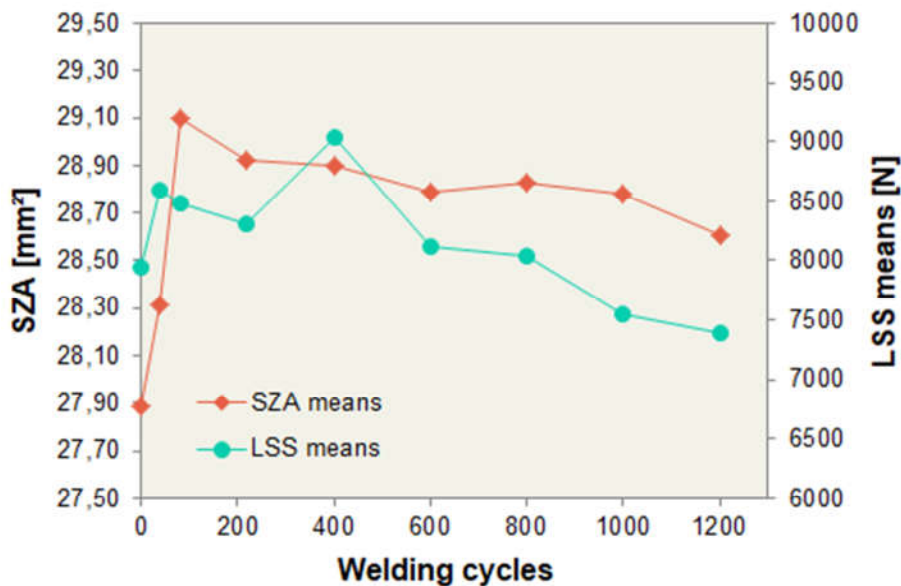


Figure 5.31 – Plots of lap shear strength (*LSS*) and and stir zone area (SZA) means of experimental results for selected points of measurement along welding cycles

The increasing in the number of uses of the sleeve produces a progressive wear in the tip of the tool, which results in a reduction of 0.105 mm in the external diameter at the tip of the tool. The effects of this decreasing-in-dimension trend of the sleeve implicates in a reduction of sleeve's volume, and consequently a reduction of the plasticized sheet material displacement which leads to a smaller dynamically recrystallized region. This effect is observed in welds from A80 to A1200.

An opposite trend in SZA, however, is noted in the interval from 1 to 80 welding cycles. The comparison of stir zone size of the initial samples (A1, A40 and A80) indicates a progressive increasing in SZA. In fact, this is a result of the material trapping effect described by Chen et al. [52], which is observed in friction stir welding tools: when the frictional contact between tool and sheet results in sufficient heat input for plasticizing this material, the threaded sleeve path is filled by the material flow, which remains trapped into the thread grooves. The observation of the first 80 welds in Figure 5.31 indicates that the increasing-in-area trend may be related to the progressive reduction of the transferred material from the sheet to sleeve grooves until a certain level of trapped material is reached. Once this limit volume of storage is reached, the trapped material is going to deposit in the weld while the new material being joined will be trapped into the groove, completing a balanced transference of mass with no further effects of SZA.

Microhardness

Figure 5.32 presents microhardness maps for samples A1, A80, A220, A600, A1000 and 1300. All microhardness maps indicate the stir zone as the region with higher $HV_{0.2}$ values, as a result of mechanical properties developed by the dynamic recrystallization of the region. Furthermore, it is observed a slight reduction in the joints' microhardness along the welding cycles, indicating a likely change in the strain rate that directly affects the dynamical recrystallization process. In general, hardness and strength of a particular material are directly related; thus, the reduction of welds' microhardness

associated to dimensional modifications of the sleeve due to wear matches the decrease in LSS mean values along the welding cycles.

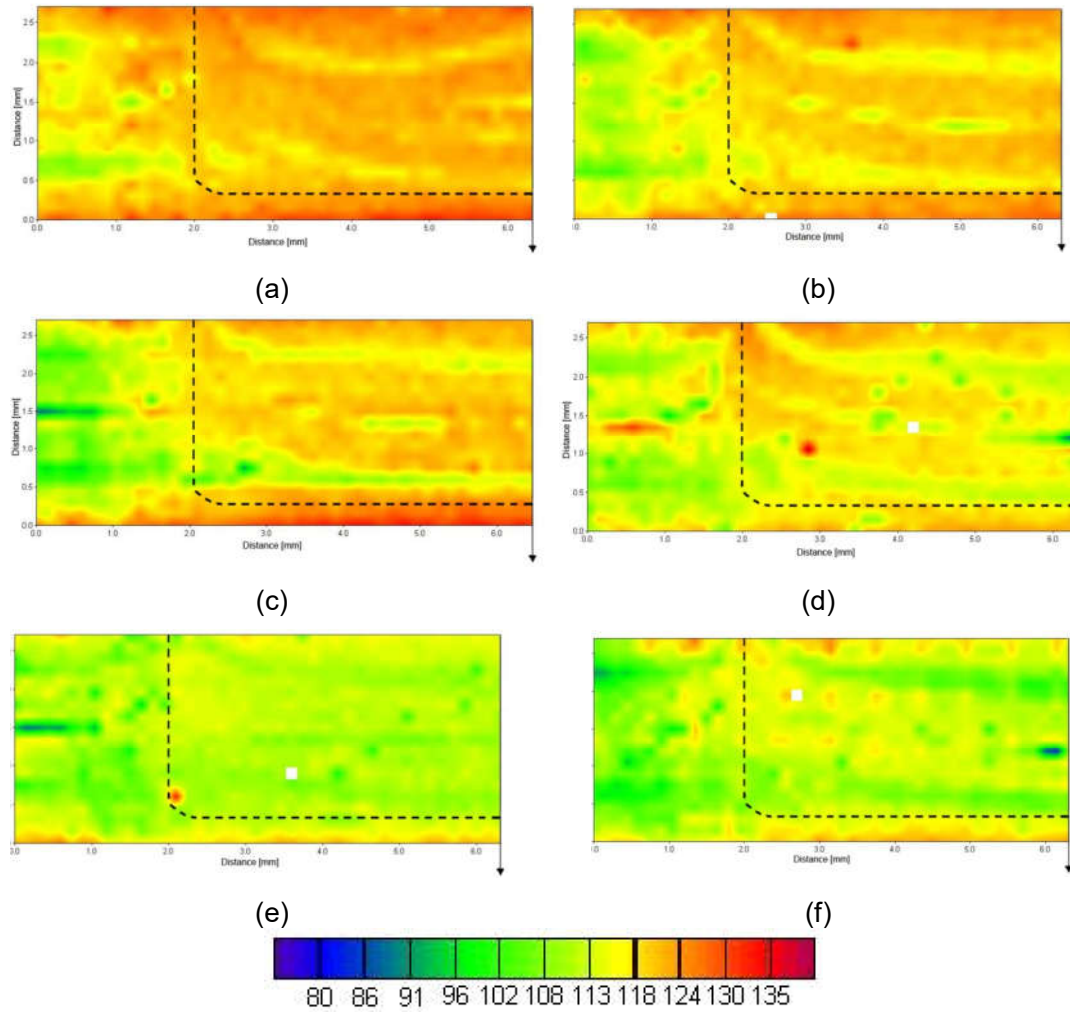


Figure 5.32 – Microhardness maps (HV_{0.2}) of selected welds: (a) initial welding, after (b) 80, (c) 220, (d) 600, (e) 1000, and (f) 1300 welding cycles

6 CONCLUSIONS

The feasibility of the refill friction stir spot welding of AA2198 1.6 and 3.2 mm-thick sheets based on joints' lap shear strength and their correlation with stir zone area were investigated using statistical and micrographic analysis. A preliminary study about the consequence of tool wear effects in welds' features were also performed considering dimensional modifications in tool profile and joints' macrographic analysis and mechanical testing. The following conclusions can be drawn based on experimental and analytical results.

- Microstructural development along the weld is determined by the combination of deformation and heat gradient caused by axial and rotational movement of the sleeve. Stir zone grain size variance along the interface between SZ and TMAZ results from SZ grain-refined material extrusion to sleeve-outer-interface adjacent areas caused by the towards-to-sheet-surface pin movement.
- All welds produced from 1.6 mm sheets with the welding conditions given by Taguchi L9 orthogonal array demonstrated to be suitable for aeronautical applications according to AWS D17.2 lap shear strength minimum requirements (3180 N), considering *LSS* mean values range from 4877 to 7947 N. For the selected range of parameters, analysis of variance indicates that *RS* (46%) and *PD* (40%) are the most influent parameters on these welds' resistance, with 86% percentage of contribution altogether. In contrast, *WT*'s percentage of influence was shown to be of no statistical significance, as an indicative of no significant influence of this parameter for this particular investigation.
- Considering technical, efficiency and economical matters, the parameter optimization for 1.6 mm-thick sheets has pointed *C7a* condition (*RS* = 1500 rpm, *WT* = 3 s, *PD* = 2.8 mm). Although Taguchi has indicated a different condition, *C10a* (*RS* = 1500 rpm, *WT* = 3 s, *PD* = 2.8 mm), *LSS* results endorses *C7a* as the optimum

set of parameters. *C7a* and *C10a* present similar *LSS* values identical levels of *RS* and *PD*, showing different *WT* levels – previously shown to be of no significant influence on joints' mechanical performance.

- For both 1.6 and 3.2-mm sheets, stir zone measured area values were observed to have a very close correlation with welds' lap shear strength. Furthermore, Taguchi analysis considering *LSS* and *SZA* means converges to the same combination of parameters for best and worst responses for both 1.6 and 3.2 thicknesses.
- *SZA* variations were demonstrated to be similarly affected by the variation of parameters for welds produced from 1.6 and 3.2 mm sheets. In both analyses, *PD* was ranked as the most influential factor in *SZA*, with a percentage of influence of 84%, followed by *RS* (around 12%). *WT* was shown to be statistically insignificant for *SZA*, especially when compared with ANOVA's error. The influence of *PD* variance is attributed to its larger-and-proportional-to-sleeve-diameter increase which leads to larger volume of material to be plasticized and recrystallized, resulting in *SZA* increments in both width and height dimensions.
- Mechanical testing of joints produced along 2350 welding cycles showed a trend of decreasing in welds' strength due to the tool wear effect. All welds greatly exceeded the minimum requirements of AWS D17.2 for lap shear strength in aeronautic applications (3180 N for AA2198-T8 1.6 mm-thick sheets against the minimum *LSS* of 6231 N).
- Pin did not suffer any considerable effect of wear along the 2350 welding cycles evaluation due to its minor frictional contact with sheet's material. The analysis of sleeve's profile in four different moments has indicated the presence of adhesive wear at the tip of the tool. Plastic deformation was also observed, but was probably related to assembling issues rather than wear effects caused by the process itself.

- The observation of welds' cross-section macrographs selected among the initial 1300 welding cycles along sleeve's profile changes indicated a trend in reduction in SZA along the reduction of the external diameter at the tool tip, which matched the LSS behavior. Furthermore, hardness maps performed in different points at stage one pointed to a decreasing-in-hardness trend with the increasing number of cycles, that could also be associated to the strength behavior.

7 SUGGESTIONS FOR FUTURE WORK

The RFSSW technique was shown to be a suitable method for spot-joining AA2198-T8 sheets according to lap shear strength criterion. However, further studies are required in order to guarantee the welds' performance especially for the critical application on structural components of aircraft industry. The recommendations for future works are summarized below:

- Optimization of RFSSW on AA2198-T8 sheets using the same parameter window defined in the current study considering other mechanical properties as response for the statistical analysis, such as fatigue.
- Investigate the mechanical behavior of AA2198-T8 joints produced by RFSSW under different loads conditions, such as *coach-peel* and *cross-tension* tests.
- Investigate the microstructure development considering heat input data for different combinations of *RS*, *WT* and *PD* using computational methods.

Furthermore, this preliminary investigation of tool wear on RFSSW opens new roads for the comprehension of tool's design and materials limitations to enable the development of optimized new instruments. The evaluation of tool lifecycle eliminating the steps of tool disassembling is strongly recommended, associated with further suggestion listed below:

- Evaluate *LSS* of produced welds considering standardized requirements for industrial application along tool lifecycle until sleeve failure.
- Tribological study of characteristics and wear mechanisms on affected sleeve and clamping ring along welding cycles.
- Evaluate the effects of surface modifications suffered by worn sleeve on heat input and strain rate and their impact on with welds' microstructural development (stir zone area, grain size) and hardness.

8 REFERENCES

1. Stocker, T. ed: Climate change 2013: the physical science basis: Working Group I contribution to the Fifth assessment report of the Intergovernmental Panel on Climate Change. Cambridge University Press, New York (2014)
2. OICA: Climate Change and CO₂: Automakers publish a comprehensive position paper. (2008)
3. Mishra, R.S., Ma, Z.Y.: Friction stir welding and processing. *Materials Science and Engineering: R: Reports*. 50, 1–78 (2005). doi:10.1016/j.mser.2005.07.001
4. Yang, C.-W., Hung, F.-Y., Lui, T.-S., Chen, L.-H., Juo, J.-Y.: Weibull Statistics for evaluating failure behaviors and joining reliability of friction stir spot welded 5052 aluminum alloy. *Materials Transactions*. 50, 145–151 (2009). doi:10.2320/matertrans.MRA2008341
5. Rioja, R.J., Liu, J.: The Evolution of Al-Li Base Products for Aerospace and Space Applications. *Metallurgical and Materials Transactions A*. 43, 3325–3337 (2012). doi:10.1007/s11661-012-1155-z
6. Amancio, S.T.: Joining of polymer-metal lightweight structures. *Lecture Notes*. , Helmholtz-Zentrum Geesthacht (HZG) and Technisch Universität Hamburg-Harburg (TUHH) (2015)
7. Schubert, E., Klassen, M., Zerner, I., Walz, C., Sepold, G.: Light-weight structures produced by laser beam joining for future applications in automobile and aerospace industry. *Journal of Materials Processing Technology*. 115, 2–8 (2001). doi:10.1016/S0924-0136(01)00756-7
8. Montag, T., Wulfsberg, J.-P., Hameister, H., Marschner, R.: Influence of Tool Wear on Quality Criteria for Refill Friction Stir Spot Welding (RFSSW) Process. *Procedia CIRP*. 24, 108–113 (2014). doi:10.1016/j.procir.2014.08.015
9. de Castro, C.C.: Tool wear evaluation and its influence in mechanical performance on FSpW. Helmholtz Zentrum Geesthacht, Geesthacht, Germany (2011)
10. American Welding Society: AWS D17.2/D17.2M:2019 - Specification for Resistance Welding for Aerospace Applications, (2019)
11. Starke Jr., E.A., Staley, J.T.: Application of modern aluminum alloys to aircraft. *Progress in Aerospace Sciences*. 32, 131–172 (1996). doi:10.1016/0376-0421(95)00004-6

12. Han, J., Zhu, Z., Li, H., Gao, C.: Microstructural evolution, mechanical property and thermal stability of Al–Li 2198-T8 alloy processed by high pressure torsion. *Materials Science and Engineering: A*. 651, 435–441 (2016). doi:10.1016/j.msea.2015.10.112
13. Mishra, R.S., Sidhar, H.: Friction stir welding of 2xxx aluminum alloys including Al–Li alloys. Butterworth-Heinemann, Oxford (2017)
14. Dursun, T., Soutis, C.: Recent developments in advanced aircraft aluminium alloys. *Materials & Design (1980-2015)*. 56, 862–871 (2014). doi:10.1016/j.matdes.2013.12.002
15. Gao, C., Zhu, Z., Han, J., Li, H.: Correlation of microstructure and mechanical properties in friction stir welded 2198-T8 Al–Li alloy. *Materials Science and Engineering: A*. 639, 489–499 (2015). doi:10.1016/j.msea.2015.05.038
16. Zhang, S., Zeng, W., Yang, W., Shi, C., Wang, H.: Ageing response of a Al–Cu–Li 2198 alloy. *Materials & Design*. 63, 368–374 (2014). doi:10.1016/j.matdes.2014.04.063
17. Higashi, A.L. de C., Lima, M.S.F. de: Occurrence of defects in laser beam welded Al-Cu-Li sheets with t-joint configuration. *Journal of Aerospace Technology and Management*. 4, 421–429 (2012). doi:10.5028/jatm.2012.04044212
18. Schilling, C., dos Santos, J.: Method and device for joining at least two adjoining work pieces by friction welding
19. Kubit, A., Kluz, R., Trzepieciński, T., Wydrzyński, D., Bochnowski, W.: Analysis of the mechanical properties and of micrographs of refill friction stir spot welded 7075-T6 aluminium sheets. *Archives of Civil and Mechanical Engineering*. 18, 235–244 (2018). doi:10.1016/j.acme.2017.07.005
20. Pieta, G., dos Santos, J., Strohaecker, T.R., Clarke, T.: Optimization of Friction Spot Welding Process Parameters for AA2198-T8 Sheets. *Materials and Manufacturing Processes*. 29, 934–940 (2014). doi:10.1080/10426914.2013.811727
21. Tier, M., Rosendo, T., Olea, C.W., Mazzaferro, C., Ramos, F.D., Bayer, M., dos Santos, J.F., da Silva, A.A.M., Mazzaferro, J., Strohaecker, T.R.: The influence of weld microstructure on mechanical properties of refill friction spot welding of 5042 aluminium alloy. 7th International Symposium on Friction Stir Welding. , Awaji Island, Japan (2008)
22. Amancio-Filho, S.T., Camillo, A.P., Bergmann, L., Dos Santos, J.F., Kury, S.E., Machado, N.G.: Preliminary investigation of the microstructure and

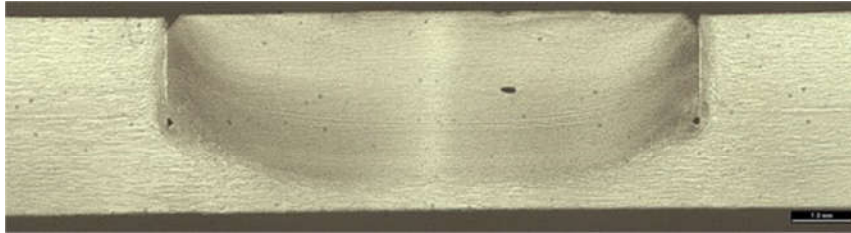
- mechanical behaviour of 2024 aluminium alloy friction spot welds. *Materials Transactions*. 52, 985–991 (2011). doi:10.2320/matertrans.L-MZ201126
23. Shi, Y., Yue, Y., Zhang, L., Ji, S., Wang, Y.: Refill Friction Stir Spot Welding of 2198-T8 Aluminum Alloy. *Transactions of the Indian Institute of Metals*. 71, 139–145 (2018). doi:10.1007/s12666-017-1146-2
 24. Shen, J., Lage, S.B.M., Suhuddin, U.F.H., Bolfarini, C., dos Santos, J.F.: Texture Development and Material Flow Behavior During Refill Friction Stir Spot Welding of AlMgSc. *Metallurgical and Materials Transactions A*. 49, 241–254 (2018). doi:10.1007/s11661-017-4381-6
 25. Lage, S.B.M.: Otimização dos parâmetros de soldagem a ponto por fricção (FSpW) da liga AlMgSc e avaliação das propriedades mecânicas estáticas e dinâmicas, (2018)
 26. Campanelli, L.C., Suhuddin, U.F.H., dos Santos, J.F., Alcântara, N.G. de: Parameters optimization for friction spot welding of AZ31 magnesium alloy by Taguchi method. *Soldagem & Inspeção*. 17, 26–31 (2012). doi:10.1590/S0104-92242012000100005
 27. Campanelli, L.C., Suhuddin, U.F.H., Antonialli, A.Í.S., dos Santos, J.F., de Alcântara, N.G., Bolfarini, C.: Metallurgy and mechanical performance of AZ31 magnesium alloy friction spot welds. *Journal of Materials Processing Technology*. 213, 515–521 (2013). doi:10.1016/j.jmatprotec.2012.11.002
 28. Plaine, A.H., Gonzalez, A.R., Suhuddin, U.F.H., dos Santos, J.F., Alcântara, N.G.: The optimization of friction spot welding process parameters in AA6181-T4 and Ti6Al4V dissimilar joints. *Materials & Design*. 83, 36–41 (2015). doi:10.1016/j.matdes.2015.05.082
 29. Plaine, A.H., Gonzalez, A.R., Suhuddin, U.F.H., dos Santos, J.F., Alcântara, N.G.: Process parameter optimization in friction spot welding of AA5754 and Ti6Al4V dissimilar joints using response surface methodology. *The International Journal of Advanced Manufacturing Technology*. 85, 1575–1583 (2016). doi:10.1007/s00170-015-8055-5
 30. da Silva, A., Tier, M., Bergman, L., Rosendo, T., Ramos, F., Mazzaferro, J., Mazzaferro, C., Strohaecker, T., Dos Santos, J.: Friction Spot and Friction Stir Spot Welding Processes - A Literature Review. *Bulletin of National R&D Institute for Welding and Material Testing*. 3, 36–44 (2007)
 31. Campanelli, L.C., Alcântara, N.G. de, Santos, J.F. dos: Soldagem por ponto no estado sólido de ligas leves. *Soldagem & Inspeção*. 16, 301–307 (2011). doi:10.1590/S0104-92242011000300011

32. The Welding Institute: Refill Friction Stir Spot Welding for Aerospace Applications. (2017)
33. Suhuddin, U., Fischer, V., Kroeff, F., dos Santos, J.F.: Microstructure and mechanical properties of friction spot welds of dissimilar AA5754 Al and AZ31 Mg alloys. *Materials Science and Engineering: A*. 590, 384–389 (2014). doi:10.1016/j.msea.2013.10.057
34. Reimann, M., Goebel, J., Gartner, T.M., dos Santos, J.F.: Refilling termination hole in AA 2198–T851 by refill friction stir spot welding. *Journal of Materials Processing Technology*. 245, 157–166 (2017). doi:10.1016/j.jmatprotec.2017.02.025
35. Bozkurt, Y., Boumerzoug, Z.: Tool material effect on the friction stir butt welding of AA2124-T4 Alloy Matrix MMC. *Journal of Materials Research and Technology*. 7, 29–38 (2018). doi:10.1016/j.jmrt.2017.04.001
36. Bist, A., Saini, J.S., Sharma, B.: A review of tool wear prediction during friction stir welding of aluminium matrix composite. *Transactions of Nonferrous Metals Society of China*. 26, 2003–2018 (2016). doi:10.1016/S1003-6326(16)64318-2
37. Gerlich, A., Su, P., North, T.H.: Tool penetration during friction stir spot welding of Al and Mg alloys. *Journal of Materials Science*. 40, 6473–6481 (2005). doi:10.1007/s10853-005-1568-9
38. Choi, D.H., Lee, C.Y., Ahn, B.W., Choi, J.H., Yeon, Y.M., Song, K., Park, H.S., Kim, Y.J., Yoo, C.D., Jung, S.B.: Frictional wear evaluation of WC–Co alloy tool in friction stir spot welding of low carbon steel plates. *International Journal of Refractory Metals and Hard Materials*. 27, 931–936 (2009). doi:10.1016/j.ijrmhm.2009.05.002
39. Yazdi, S.R., Beidokhti, B., Haddad-Sabzevar, M.: Pinless tool for FSSW of AA 6061-T6 aluminum alloy. *Journal of Materials Processing Technology*. 267, 44–51 (2019). doi:10.1016/j.jmatprotec.2018.12.005
40. Alcântara, N.G.: FSpW Valuation in the Automotive Industry. Helmholtz Zentrum Geesthacht, Geesthacht (2015)
41. Rosa, J.L., Robin, A., Silva, M.B., Baldan, C.A., Peres, M.P.: Electrodeposition of copper on titanium wires: Taguchi experimental design approach. *Journal of Materials Processing Technology*. 209, 1181–1188 (2009). doi:10.1016/j.jmatprotec.2008.03.021
42. International Organization for Standardization: ISO 14273:2016 - Resistance welding - Destructive testing of welds - Specimen dimensions and procedure for tensile shear testing resistance spot and embossed projection welds, (2016)

43. ASTM International: ASTM A681 - 08(2015) - Standard Specification for Tool Steels Alloy, (2015)
44. Villares Metals: Aços para trabalho a quente. Available at, <http://www.villaresmetals.com.br/content/download/28457/288071/file/VH13ISO-pt.pdf>. Accessed on 03/04/2019.
45. Prangnell, P.B., Heason, C.P.: Grain structure formation during friction stir welding observed by the 'stop action technique.' *Acta Materialia*. 53, 3179–3192 (2005). doi:10.1016/j.actamat.2005.03.044
46. Rosendo, T., Parra, B., Tier, M.A.D., da Silva, A.A.M., dos Santos, J.F., Strohaecker, T.R., Alcântara, N.G.: Mechanical and microstructural investigation of friction spot welded AA6181-T4 aluminium alloy. *Materials & Design*. 32, 1094–1100 (2011). doi:10.1016/j.matdes.2010.11.017
47. de Castro, C.C., Plaine, A.H., Dias, G.P., de Alcântara, N.G., dos Santos, J.F.: Investigation of geometrical features on mechanical properties of AA2198 refill friction stir spot welds. *Journal of Manufacturing Processes*. 36, 330–339 (2018). doi:10.1016/j.jmapro.2018.10.027
48. Tier, M.D., Rosendo, T.S., dos Santos, J.F., Huber, N., Mazzaferro, J.A., Mazzaferro, C.P., Strohaecker, T.R.: The influence of refill FSSW parameters on the microstructure and shear strength of 5042 aluminium welds. *Journal of Materials Processing Technology*. 213, 997–1005 (2013). doi:10.1016/j.jmatprotec.2012.12.009
49. Su, P., Gerlich, A., North, T.H., Bendzsak, G.J.: Energy Generation and Stir Zone Dimensions in Friction Stir Spot Welds. Presented at the SAE 2006 World Congress & Exhibition April 3 (2006)
50. Walpole, R.E. ed: *Probability & statistics for engineers & scientists*. Pearson Prentice Hall, Upper Saddle River, NJ (2007)
51. Wang, J., Su, J., Mishra, R.S., Xu, R., Baumann, J.A.: Tool wear mechanisms in friction stir welding of Ti–6Al–4V alloy. *Wear*. 321, 25–32 (2014). doi:10.1016/j.wear.2014.09.010
52. Chen, G., Li, H., Wang, G., Guo, Z., Zhang, S., Dai, Q., Wang, X., Zhang, G., Shi, Q.: Effects of pin thread on the in-process material flow behavior during friction stir welding: A computational fluid dynamics study. *International Journal of Machine Tools and Manufacture*. 124, 12–21 (2018). doi:10.1016/j.ijmachtools.2017.09.002

APPENDIX A

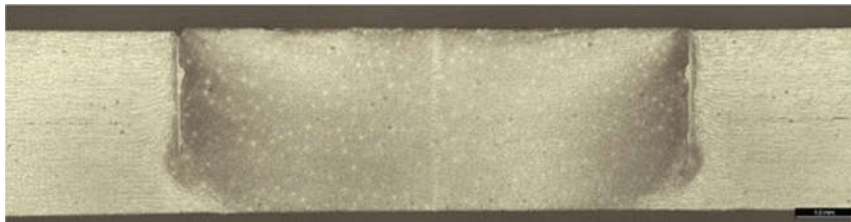
CROSS-SECTIONS OF WELDS PRODUCED BY THE WELDING OF
1.6 MM-THICK AA2198-T8 SHEETS



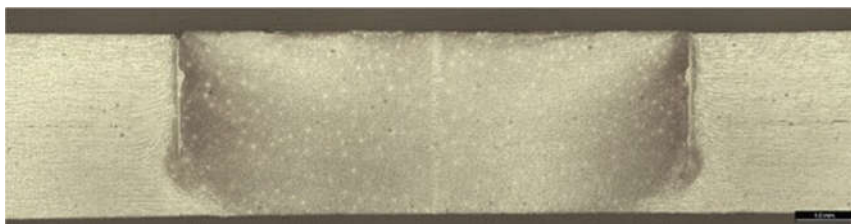
C1a



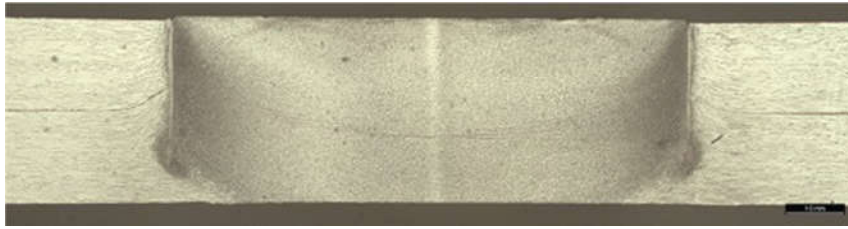
C2a



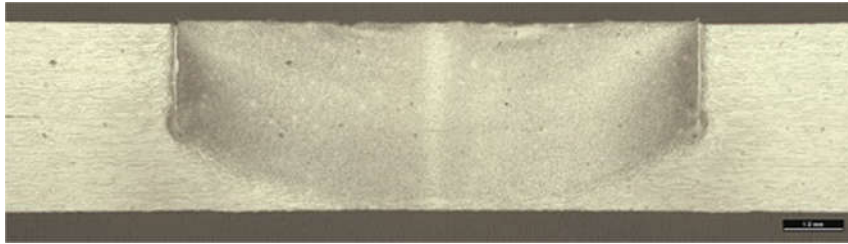
C3a



C4a



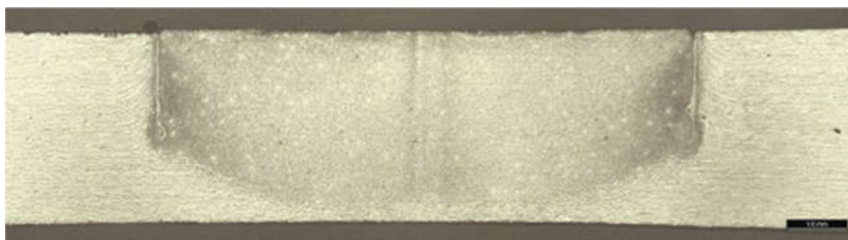
C5a



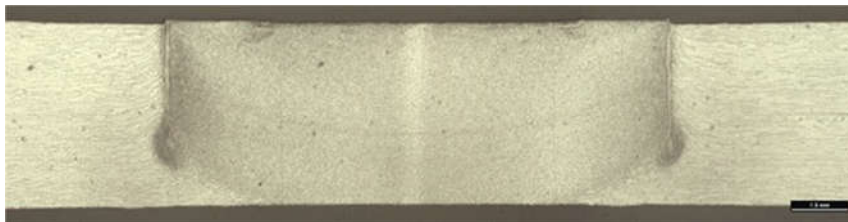
C6a



C7a



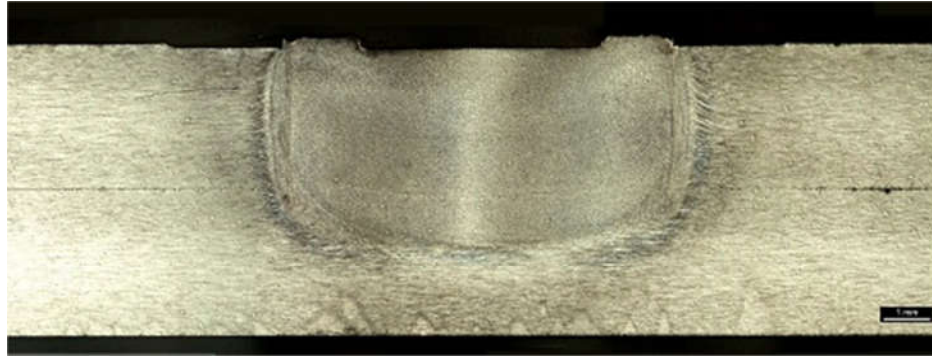
C8a



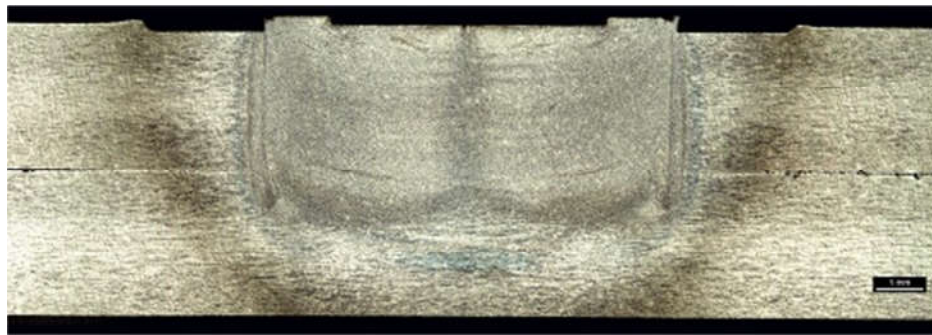
C9a

APPENDIX B

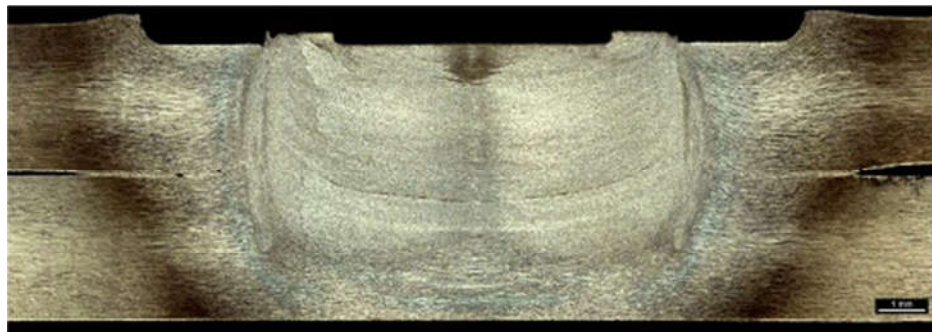
CROSS-SECTIONS OF WELDS PRODUCED BY THE WELDING OF 3.2 MM-THICK AA2198-T8 SHEETS



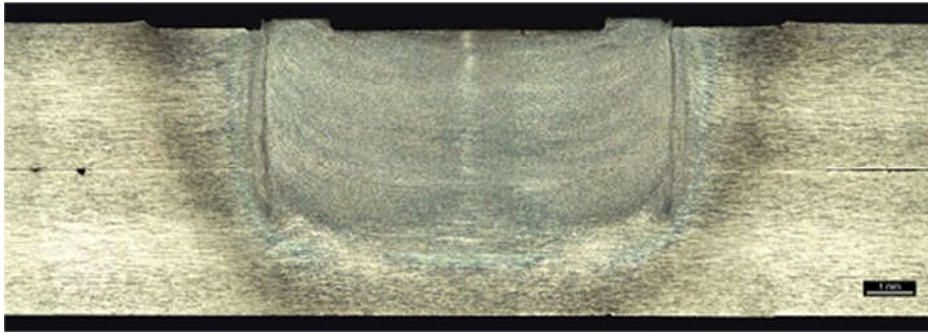
C1b



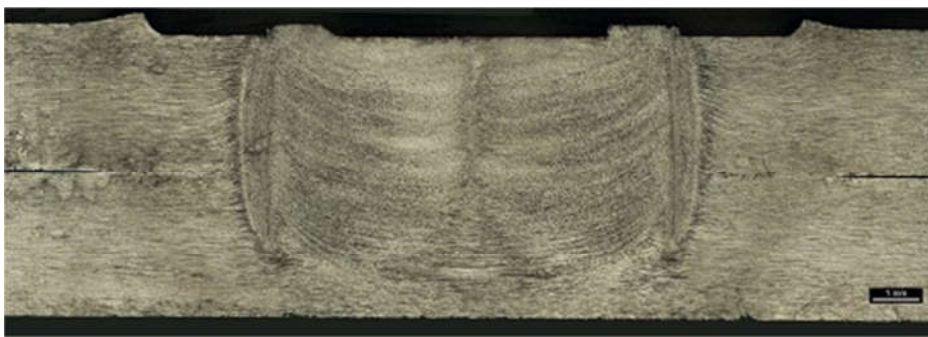
C2b



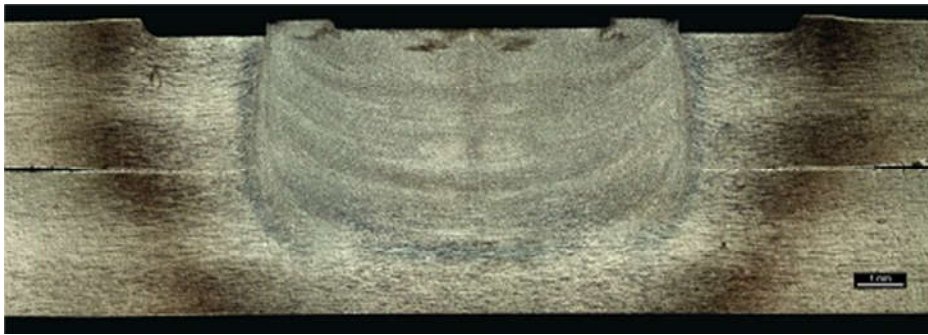
C3b



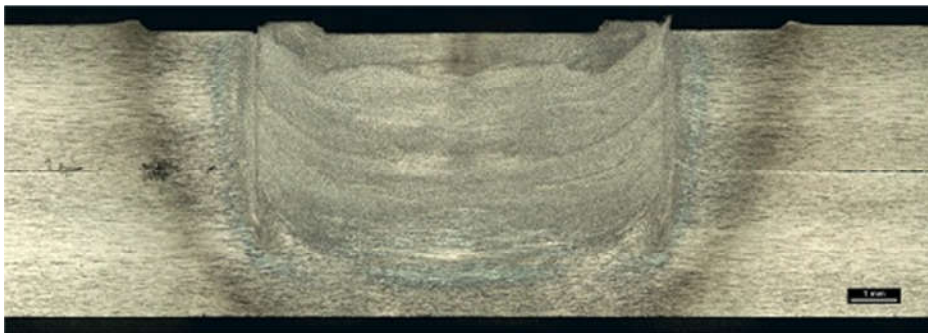
C4b



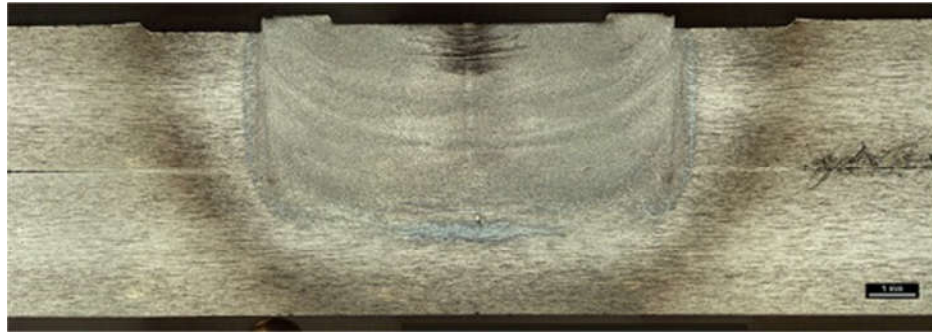
C5b



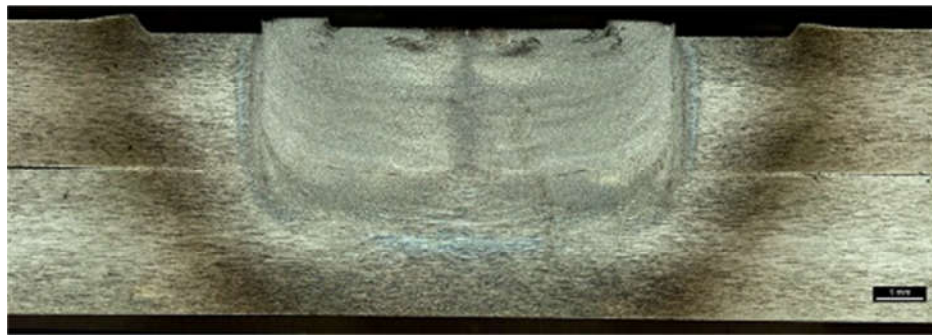
C6b



C7b

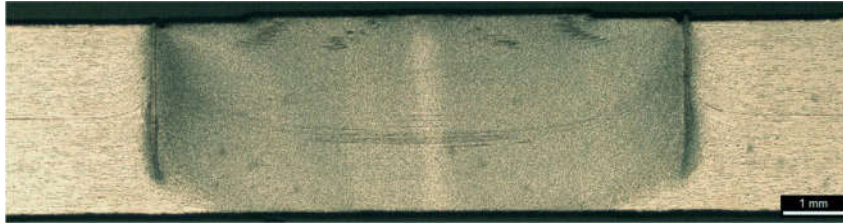


C8b

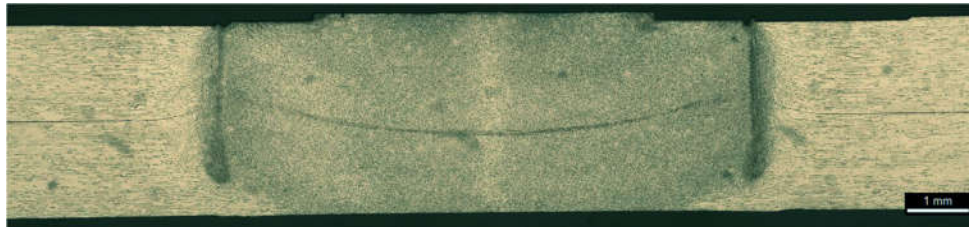


C9b

APPENDIX C

CROSS-SECTIONS OF SELECTED JOINTS PRODUCED BY RFSSW OF
1.6 MM-THICK AA2198-T8 SHEETS ALONG THE WELDING CYCLES

A1



A40



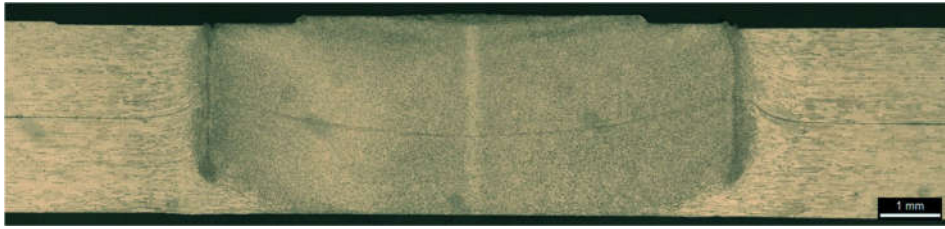
A80



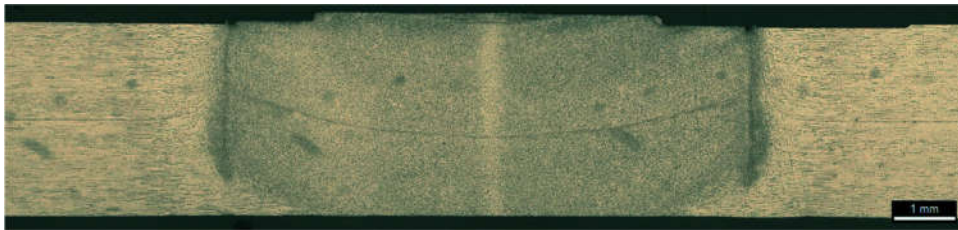
A220



A400



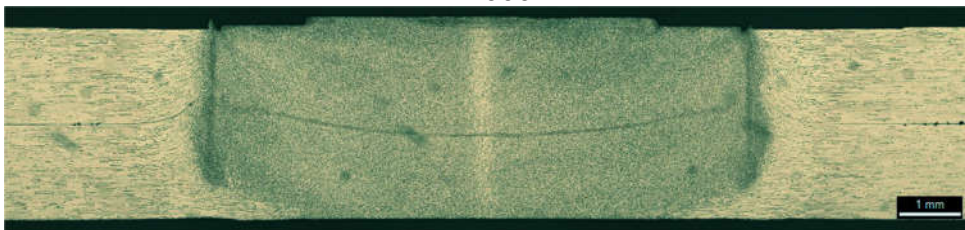
A600



A800



A1000



A1200

APPENDIX D

LAP SHEAR STRENGTH MEAN VALUES (*LSS*) AND THEIR STANDARD DEVIATION (σ) ALONG THE WELDING CYCLES

Table C.1 – First stage of measurement

WELDING CYCLES	<i>LSS</i>	σ	WELDING CYCLES	<i>LSS</i>	σ
0	7486	826	600	8122	208
20	8507	364	650	8004	57
40	8588	211	700	7862	181
60	7931	265	750	7793	203
80	8489	232	800	8039	90
100	8539	179	850	7680	252
140	8442	206	900	7637	76
180	8777	224	950	7577	355
220	8311	255	1000	7542	25
260	8318	226	1050	7713	53
300	9112	27	1100	7579	345
350	7935	162	1150	7924	305
400	9038	287	1200	7394	31
450	8145	85	1250	8056	79
500	8178	268	1300	7844	459
550	8080	149	1350	7943	158

Table C.2 – Second stage of measurement

WELDING CYCLES	<i>LSS</i>	σ
1400	7497	570
1450	7566	914
1500	7388	355
1550	7123	778
1600	6659	610
1650	6231	633
1700	8628	89
1750	7824	1380
1800	8346	217
1850	7006	1426
1900	7601	1313
1950	6733	2052
2000	6664	1071

Table C.3 – Third stage of measurement

WELDING CYCLES	<i>LSS</i>	Σ
2050	8003	203
2100	8256	79
2150	8658	97
2215	7936	98
2250	8358	155
2300	7876	328
2350	7783	298

APPENDIX E

**LAP SHEAR STRENGTH MEANS (LSS), LINEAR FIT VALUES (LSSLF) AND
PREDICTION OF LSS REDUCTION (%LFRED) ACCORDING TO THE
MODEL FOR THE FIRST 1350 WELDS (1ST STAGE OF EVALUATION)**

WELDING CYCLES	LSS	LSS_{LF}	%LF_{red}
0	7937	8491,10	0,00%
20	8507	8477,93	0,16%
40	8588	8464,75	0,31%
60	7931	8451,58	0,47%
80	8489	8438,40	0,62%
100	8539	8425,23	0,78%
140	8442	8398,88	1,09%
180	8777	8372,53	1,40%
220	8311	8346,19	1,71%
260	8318	8319,84	2,02%
300	9112	8293,49	2,33%
350	7935	8260,56	2,72%
400	9038	8227,62	3,10%
450	8145	8194,69	3,49%
500	8178	8161,75	3,88%
550	8080	8128,82	4,27%
600	8122	8095,88	4,65%
650	8004	8062,95	5,04%
700	7862	8030,01	5,43%
750	7793	7997,08	5,82%
800	8039	7964,14	6,21%
850	7680	7931,21	6,59%
900	7637	7898,27	6,98%
950	7577	7865,34	7,37%
1000	7542	7832,40	7,76%
1050	7713	7799,47	8,15%
1100	7579	7766,53	8,53%
1150	7924	7733,60	8,92%
1200	7394	7700,66	9,31%
1250	8056	7667,73	9,70%
1300	7844	7634,79	10,08%
1350	7943	7601,86	10,47%